Chapter 2

Active Tectonics and Earthquake Potential of the Myanmar region

Yu Wang[1,2], Kerry Sieh[2], Soe Thura Tun[3], Kuang-Yin Lai[4,5], Than Myint[3]

1. Division of Geological and Planetary Sciences, California Institute of Technology, Pasadena, U.S.A
2. Earth Observatory of Singapore, Nanyang Technological University, Singapore
3. Myanmar earthquake committee, Myanmar Engineering society, Myanmar
4. Department of Geosciences, National Taiwan University, Taiwan
5. Institute of Earth Sciences, Academia Sinica, Taiwan

Abstract

This paper describes geomorphologic evidence for the principal neotectonic features of Myanmar and its immediate surroundings. We combine this evidence with published structural, geodetic and seismic data to present an overview of the active tectonic architecture of the region and its seismic potential. Three tectonic systems accommodate oblique collision of the Indian plate with Southeast Asia and extrusion of Asian territory around the eastern syntaxis of the Himalayan mountain range. Subduction and collision associated with the Sunda megathrust beneath and within the Indoburman range and Naga Hills accommodates most of the shortening across the transpressional plate boundary. The Sagaing fault system is the predominant locus of dextral motion associated with the northward translation of India. Left-lateral faults of the northern Shan Plateau, northern Laos, Thailand and southern China facilitate extrusion of rocks around the eastern syntaxis of the Himalaya. All of these systems have produced major earthquakes within recorded history and continue to present major seismic hazards in the region.

Introduction

In the context of plate tectonics, the eastern margin of the Indian Ocean is a right-lateral convergent plate boundary (Fig. 1a). Along the entire plate boundary, the Sunda megathrust accommodates eastward subduction of oceanic under predominantly continental lithosphere. Right-lateral strike-slip faults traverse the entire margin, from Sumatra in the south to Myanmar in the north. The Sumatran fault accommodates most of the right-lateral component of oblique convergence along the 2000-km length of Sumatra (Fitch, 1972; Sieh and Natawidjaja, 2000; Chlieh et al., 2007; McCaffrey, 2009). An en-echelon spreading center carries a large component of the dextral component of deformation beneath the Andaman Sea (Curray, 2005). Farther north, the Sagaing fault plays a significant dextral-slip role along a 1400-km span centered on Myanmar (e.g., Win Swe, 1970; Vigny et al., 2003; Curray, 2005). Both the Sunda megathrust and the Sagaing fault systems terminate northward into the eastern Himalayan syntaxis.

The 1000- to 1300-km wide terrane bisected by the Sagaing fault is tectonically complex. On the west is the subducting oceanic Indian plate, and on the east are the predominantly continental Yangtze and Sunda blocks (Fig. 1b). Between the Indian plate and the Sagaing fault is an elongate tectonic block that is commonly called the Burma plate or the Burma sliver (Curray, 1979). Between the Sagaing fault and the Yangtze and Sunda blocks is a terrane that includes the Shan Plateau, characterized by a plexus of dextral and sinistral strike-slip faults (e.g., Lacassin et al., 1998).

Geodetic measurements show that the motion of the Indian plate relative to the Sunda block ranges from 2.7 to 4.3 cm/yr at the latitude of Myanmar (Sella et al., 2002; Prawirodirdjo and Bock, 2004; Kreemer et al., 2003; Socquet et al., 2006; DeMets et al., 2010). Geodetic and geologic measurements indicate that the Sagaing fault accommodates only about 2 cm/yr of the north component of this relative motion (Bertrand et al., 1998; Vigny et al., 2003; Socquet et al., 2006;

Maurin et al., 2010; Wang et al., 2011). The megathrust and related upper-plate structures also absorb some of the relative strike-slip plate motion (e.g., Nielsen et al., 2004; Socquet et al., 2006); the rest of the strike-slip motion may be partitioned into the interior of the Burma plate (e.g., Socquet et al., 2006). Except under southernmost Myanmar, the geometry of the subducting slab is well established from hypocenters of an east-dipping Wadati-Benioff zone (e.g., Ni, 1989; Richards et al., 2007). The 60-km isobath runs approximately beneath the eastern flank of the Indoburman range.

Historical records demonstrate that great and destructive earthquakes have occurred throughout much of the region (Fig. 2). These reports are sparse but informative (e.g., Halstead, 1842; Oldham, 1883; Milne, 1911; Brown, 1917; Brown et al., 1931 and 1933; Chhibber, 1934; Win Swe, 2006; Martin and Szeliga, 2010). Although they provide important information about the general locations and approximate sizes of the earthquakes, they reveal little or nothing about the character of the causative faults. In fact, until 2011, no post-earthquake investigations had involved mapping the surface trace of an active fault in the region. For example, only the pattern of seismic intensities (Oldham, 1883) supports the contention that the Mandalay earthquake of 1839, which killed more than 500 people in central Myanmar, resulted from rupture of a section of the Sagaing fault west of Mandalay (Le Dain et al., 1984 and Win Swe, 2006). A far more mysterious example is the earthquake of 1927, which was felt most strongly north of Yangon (Brown, 1930; Chhibber, 1934). Potential seismic sources in this region remain speculative, even though the earthquake was close to the region's largest city, which is home to more than four million people and continues to grow rapidly.

Methodology

The aforementioned geological, seismological and geodetic investigations do not constitute a systematic assessment of the neotectonic architecture of the Myanmar region and its seismic

potential. Here we present a new synthesis of regional kinematics that relies principally on a modern geomorphologic analysis of tectonic landforms. The last such geomorphological study appeared three decades ago (Le Dain et al., 1984). That study relied upon Landsat satellite imagery, whereas our principal data are from shaded-relief digital-elevation imagery. In recent years, modern geomorphologic analyses founded upon the use of digital elevation models and high-quality imagery have substantially improved understanding of the kinematics and seismic potential of many other regions. A few examples include work in Sumatra (Sieh and Natawijaya, 2000), Taiwan (Shyu et al., 2005), and the eastern Tibetan plateau (Densmore et al., 2007).

In this paper, we describe the geomorphologic expression of active faults and folds within and around Myanmar. We then discuss the implications of this analysis for understanding the active tectonics of the area, drawing also on geodetic analyses, local structural studies, historical earthquake accounts and other seismological data. Our goal is to construct a view of the neotectonic architecture of the region that provides a clear framework for understanding of the recent seismic activity and the potential for future large earthquakes.

Our geomorphologic analysis relies heavily on terrestrial shaded-relief maps constructed from the Shuttle Topography Radar Mission (SRTM version 2 to version 4 at 90-m resolution) (e.g., Jarvis et al., 2008) and offshore shaded-relief maps derived from ETOPO-1 (Amante and Eakins, 2009). We also use stereoscopic imagery constructed from the Advanced Spaceborne Thermal Emission and Reflection Radiometer (ASTER VNIR L1B at 15-m resolution) (an index appears in the Appendix-1 as Fig. S1). Together these data resolve topographic features far better than non-stereoscopic imagery and enable a broad but detailed survey of the region.

In places of particular interest, we also use aerial photographs at scales of about 1:50,000 and 1:25,000. Fig. S1 in Appendix-1 shows the coverage we used. Where available, we integrate the

high-resolution bathymetric data and structural geologic maps published by others to inform our interpretations.

Our reliance on geomorphic expression of tectonic landforms implies that our analysis is limited by their expression and preservation, which varies, of course, as a function of the type of deformation (Yeats et al., 1997, Burbank and Anderson, 2012). Strike-slip faults have a vastly different geomorphic expression than thrust faults and normal faults, and fast-slipping faults show up in the landscape more clearly than slow-slipping faults.

Modulating these expressions of active structures in the landscape is the degree of interaction of the solid earth with the atmosphere and hydrosphere. In particular, variations in rainfall play a major role in the variable expression of tectonic landforms. Figure 1c shows that average annual rainfall across the region varies by at least a factor of five. Rainfall in Bangladesh and the western Myanmar coast is two to three times greater than in the central Burma basin and farther east (Rudolf and Schneider, 2005; Rudolf et al., 2010). All else being equal then, erosion would reduce a young tectonic structure in the central or eastern regions less than if the same active feature were on the western flank of the Indoburma Range or in Bangladesh.

Another variable in the expression of tectonic landforms is the youthfulness of the landscape (Yeats et al., 1997). For example, the expression of active faults and folds on the young prograding river deltas of southern Myanmar will be limited to very youthful features not buried by rapid sedimentation. Older and more prominent tectonic landforms would be evident only on older landscapes.

For these two reasons, we must expect that our analysis of active tectonic features will not be uniformly sensitive to rates of activity across the entire region. Active features along the western coasts and on the southern deltas are less likely to be clearly expressed than features elsewhere in the region.

Neotectonics of the Myanmar region

Figure 2 is a simplified version of our neotectonic mapping of the Myanmar region, drafted at a scale of about 1:10,000,000. This scale is far smaller than the 1:50,000 to 200,000 scales at which we mapped structures using the SRTM and other topographic data and GIS software. We provide a more detailed neotectonic map in Appendix 1 (Fig. S2).

Figure 2 shows the division of Myanmar's three principal tectonic regimes into six domains, each defined by its particular geomorphological and structural expressions of tectonic activity. In the Indoburman range, along-strike variations in expression of convergence vary appreciably, so we have divided this system into four distinct structural domains. In the next section, we discuss each of these four domains separately, beginning in the south and ending in the north.

The Indoburman range

In its grand, arcuate northward sweep from southern Myanmar toward the Himalaya, the Indoburman range of western Myanmar evolves from narrow, low hills at 16°N to a very broad and high range near 24°N (Fig. 2). Farther north, on the south side of India's Assam valley, the mountains swing toward the east-northeast and narrow considerably.

In the far south, highly oblique convergence dominates within what we term the Coco-Delta domain. Its northern neighbor, the Ramree domain, represents a transition from oblique subduction to nearly orthogonal subduction that involves a thin accretionary wedge of sediment. The broadest portion of the Indoburman range comprises the Dhaka domain, in which a very wide belt of folded and faulted sediment mantles a very low-angle subduction megathrust. East of the Shillong plateau is the Naga domain, where the northern edge of the Burma plate overrides India's Assam block.

Coco-Delta domain

The 500-km span of the Sunda megathrust between the Andaman islands and the southern end of the Indoburman range trends decidedly more easterly than adjacent sections (Figs 1 and 2). In fact, the trend of the deformation front between about 14.2°N and 17°N is nearly parallel (within the uncertainties) to the direction of relative motion between the Indian plate and the Burma sliver plate (see Appendix-1 Fig S3 last column of row 5; Appendix-1 Table S1). This implies that subduction and accretion should be very slow here and that relative motion across the boundary should be predominantly right-lateral at a rate between about 8 and 28 mm/yr (see Appendix-1 Table S1). The lack of a Wadati- Benioff zone down dip of the deformation front between about 14°N and 17.8°N (Ni, 1989; Richards et al., 2007) lends further support to this thought. Other areas of highly oblique subduction are similar in this regard (for example, the Scotia arc and the Queen Charlotte Islands (e.g. Aristeo et al., 1989; Mazzotti et al., 2003; Bustin et al., 2007). Additional support for low rates of convergence across the Coco-Delta domain comes from seismic tomography, which shows only weak evidence of a slab extending downdip (Li et al., 2008).

The low relief of both the Indoburman range and the fore-arc in this region and their narrow (70- to 90-km) width imply low rates of uplift and little total accretion. The small sizes of Coco and Preparis Islands relative to the Andaman islands farther south also likely reflect lower rates of uplift and accretion (Fig 2 and 3). Between Preparis Island and the southern tip of the Indoburman range, rates of uplift are so low that erosion and sedimentation on the Ayerawaddy (Irrawaddy) Delta have kept pace with any ground rising above wave base (Fig. 3a). Additional support for low rates of uplift and scant accretion in the Coco-Delta domain is the fact that the Indoburman range is far narrower and lower in the Coco-Delta domain than in the next domain to the north. The precise coincidence of the southward diminishment of the Indoburman range with the northeastward extrapolation of the Coco-Delta section of the plate margin argues for an abrupt and sustained drop off of the uplift that has created the Indoburman ranges. This is clear evidence that the abrupt bend

in the plate margin at the northeastern end of the Coco-Delta domain coincides with a sharp and major change in accretion and uplift rates.

Despite the abovementioned evidence for minimal vertical deformation, bathymetry along the steep escarpment of the plate margin shows clearly that there is a convergent component to deformation within the Coco-Delta domain. Swath mapping of Nielsen et al. (2004) shows that the 2-km high slope rising from the flat floor of the Indian Ocean is much steeper than is typical for accreting sedimentary prisms but very similar to the slopes of highly oblique convergent margins. The right-stepping en echelon character of both the deformation front and of some anticlines just upslope prove that the sense of slip along the section from 14° to 15.5°N is dextral-reverse rather than purely dextral (Fig. 3b).

Strike-slip faults within the thin tail of the Indoburman range conform to the dextral-reverse nature of the Coco-Delta domain. Breaking the low topography of its eastern portion are several linear features that strike roughly parallel to the range front and to the nearby plate margin (Fig. 3a and Fig. 3c). One outlying block, partially surrounded by sediments of the Ayeyarwady River appears to have shifted right-laterally about ten km from the main body of the range along the Seindaung fault. Unfortunately, the resolution of the SRTM imagery is too coarse to tell whether or not the faults laterally offset small channels and ridges there, so we do not venture an opinion as to whether or not these faults are currently active. Their sharp geomorphic expression does, however, suggest that they have been active within the Quaternary Period. Farther north, where the Indoburman range widens and transitions to the next domain, drainages are larger and more developed. Some of these display right-lateral offsets of about 10 km. We discuss these further in the next section.

Coseismic and post-seismic displacements of the great 2004 Aceh-Andaman earthquake confirm and illuminate the dextral-reverse nature of slip across the Coco-Delta domain. Meltzner et

al. (2006) show that several decimeters of uplift occurred on Coco Island and that Preparis may have risen 20 to 30 cm. Horizontal deformations were measured as far north as about 13.5° (Chlieh et al., 2007). Whereas horizontal motions farther south along the arc were nearly perpendicular to the plate margin, the five stations on the Andaman Islands (between 12 and 13.5°N) experienced a marked dextral component as well. Their coseismic and post-seismic motions are nearly parallel to the strike of the Coco-Delta domain plate margin and imply up to 5 meters of purely dextral slip at the very southern end of the Coco-Delta domain and equal parts of dextral and thrust motion on the megathrust beneath the rest of the Andaman Islands.

Ramree domain

The Ramree domain is the northern neighbor of the Coco-Delta domain (Fig. 2). Sustained convergence and accretion along this 450-km section of the plate margin have produced a belt of deformation that increases in width from about 170 km in the south to about 250 km in the north (Fig. 4a). Further evidence of northward-increasing convergence through the Ramree domain is the pronounced rise in height of the Indoburman range, from less than 1000 m in the south to more than 2000 m in the north. Seismicity of the subducting Indian plate also becomes more pronounced from south to north. In the south, the deepest hypocenters of the Wadati-Benioff zone are about 70 km deep and 140 km east of the deformation front, whereas in the north, hypocenters reach depths of about 120 km and extend to about 300 km from the deformation front (NEIC catalog, 1976 to 2010).

Plate-vector diagrams that relate motion of the Indian plate to that of the Sunda block and ascribe about 20 mm/yr of dextral slip to the Sagaing fault imply dextral-oblique convergence rates between 7 and 23 mm/yr across this domain (see Appendix-1, Fig. S3, last row of columns 3 and 4). Taking the vector diagram at face value, one would expect the ratio of convergence to dextral slip to be as large as about 3:2.

With these broad attributes of the Ramree domain in mind, we now discuss geomorphologic evidence of recent neotectonic activity, moving from west to east, from the offshore and coastal regions to the interior of the Indoburman range and then to the plains east of the mountains. We begin with bathymetric evidence for the nature of deformation at the deformation front offshore and then proceed to document bathymetric and topographic evidence for activity on thrust faults within the accretionary prism nearer the coast. We then present evidence for an important dextral strike-slip fault within the mountains and a backthrust along the eastern flank of the mountains. Finally, we describe thin-skinned folds and faults to the east.

Deformation front and active structures in the accretionary prism

High-resolution bathymetry between 17° and 18.5°N displays clear evidence of tectonic shortening at and adjacent to the deformation front along the southern half of the domain (Nielson et al., 2004). Accretion of sediment is particularly clear along the salient that they call the Ramree lobe, between 17°40’ and 18°N (Fig. 4b).

East of the deformation front, along the coast, is abundant evidence for youthful folding. Flights of uplifted coastal terraces are clear even in non-stereographic, high-resolution satellite imagery, because vegetational differences differentiate flat terrace treads from steep terrace risers (Figs. 4c and 4d). Figure 4a shows that the number of terraces visible in this imagery varies throughout the region.

Thus far, Cheduba and Ramree Island, which appear to have the largest number of marine terraces, have yielded the most definitive data on uplift patterns and timing. Shishikura et al. (2009) and Aung et al. (2008) showed that these two islands and coastlines up to 100 km farther northwest have been rising incrementally throughout the late Holocene, presumably in association with large earthquakes. They also report that the terraces on the islands northwest of Ramree Island tilt northeastward.

Wang et al. (2013a) added substantial detail to this story. They demonstrated that the islands are the subaerial expressions of two doubly plunging antiforms. The long axes of these antiforms run parallel to the deformation front for more than a hundred km (Fig. 4a) and their southwestern flanks are far steeper than their northeastern flanks. They also demonstrate from field measurements and radiometric dating of mid- to late-Holocene terraces that each of the islands is tilting progressively and independently toward the mainland coast, rising most rapidly along their southwestern coasts. The pattern of uplift implies that the two asymmetric antiforms are rising on the backs of two contemporaneously active northeast-dipping faults (splay faults) within the accretionary prism.

Eyewitness accounts collected by a British survey team 80 years after the great Arakan earthquake suggest that the lowest terrace on Cheduba and Flat Island rose out of the sea during the great 1762 Arakan earthquake (Halsted, 1842; Mallet, 1878; Oldham, 1883). Wang et al. (2013a) demonstrate via U-Th disequilibrium dating of coral microatolls that the most recent large uplift of both Ramree and Cheduba Island did, indeed, occur during the great Arakan earthquake of 1762.

Dextral strike-slip faulting in the Indoburman range

Clear evidence for a 160-km long right-lateral strike-slip fault exists within the Indoburman range, from about 17.75° to 19°N (Fig. 4). All major rivers flowing to the southwestern coast exhibit sharp dextral deflections of many km along the trace of this structure, which we call the Thahtay Chaung fault (labeled TCf in Fig. 4), after one of the large river channels that it offsets (Fig. 5). Between 17.75°N and 18.5°N, the best fitting offsets for the major stream canyons are predominantly between 10.3 and 11.3 km. From 18.5°N to 19°N, the best-fit offsets diminish from about 11 to about 5 km. The fault may splay northwestward into two or more obscure structures before dying out, but the geomorphological evidence for this is not at all compelling.

The acute angle between the nearly north-south strike of the Thahtay Chaung fault and the northwesterly trends of the large offset streams suggest substantial dextral warping associated with dextral slip on the fault. Such dextral warping is especially clear within several kilometers near fault, where major channels are constantly flowing northwestward at the western flank of the Indoburman range.

We can speculate about the age of the cumulative ~10-km offsets and about the ratio of dextral slip to convergence across the Ramree domain. It is reasonable to assume that the Thahtay Chaung fault began to develop river-channel offsets once the turbidites of the regional bedrock rose above the sea and fluvial channels began to incise. The time of this emergence must substantially post-date the age of the beds, which are shown on the geological map of Brunnschweiler (1966) to be Miocene flysch. If the drainage system began to develop around 5 Ma in this part of Indoburman range, we then expect the average slip rate of the Thahtay Chaung fault would be about 2 mm/yr, given by the ~10-km offset of river channels. This would be about an order of magnitude less than the rate of convergence across the entire domain.

The Thahtay Chaung fault is the only active strike-slip fault that we could recognize from the SRTM topography. Even though the southwestern flank of the Indoburman range is remarkably straight between about 18.75° and 20°, and between 20° and 21°N a notably linear valley extends northwestward from the mountainfront, these features do not appear to reflect active strike-slip faulting. Careful inspection of these and other, lesser lineations in the Ramree domain revealed very little evidence for other young strike-slip faulting. We conclude that the Thahtay Chaung fault is the only clear manifestation of strike-slip faulting in the Ramree domain.

Active faults and folds east of the Indoburman range

The eastern flank of the Indoburman range is an impressive escarpment along the entire length of the Ramree domain, averaging slopes of ~ 3° from the crest of the range to the mountainfront.

This is far steeper than the average ~1° slope of the southwestern flank of the range. The morphology of the mountainfront suggests that it is rising along an active, west-dipping reverse fault. Along most of its length, however, there is scant evidence (at least at the resolution of the SRTM imagery) for fault scarps that would indicate a young fault breaking to the surface.

A more plausible explanation is that the escarpment has been produced by flexure. Bedding orientations and dips along the mountainfront would help us infer the underlying structure, but bedding is cryptic in the SRTM imagery, and few published works address this section of the range. Structural sections from Brunnschweiler (1966) and Bender (1983) suggest steep eastward dips of the bedrock along the escarpment, and that these beds have been overridden by the east-dipping thrust faults of the Central Basin. Our guess is that the mountainfront is mainly a fold scarp due to slip on a ramp beneath the mountain range that ruptures to the surface only locally, if at all. If this is the case, then young folds ten to a hundred km to the east, in Myanmar's Central Basin and the floodplain of the Ayeyarwady River (Fig. 4), may result from a décollement that emanates from the top of this blind structure and traverses eastward at shallow depth to a position beneath them.

Several short scarps and folds in the central valley are topographically obvious, and we propose that they are active. For example, near 18°N we observe a series of highly dissected lateritic terraces 10 to 20 km east of the mountain front that are 20 to 30 meters higher than the active floodplain of the Ayerawaddy. Many of these have fan shapes that suggest they represent alluvium originating from the Indoburman range. The linearity of the eastern edge of these terraces suggests that these are fault scarps rather than cuts into alluvial fans by a laterally migrating Ayeyarwady River. We do not see scarps on younger, unlaterized fluvial or alluvial deposits in the coarse SRTM imagery, so we have no clear evidence for latest Pleistocene or Holocene rupture.

Several other reverse faults east of the Indoburman range also have mild geomorphologic expressions that might indicate current activity in the central Burma basin. All of these are in the

hundred km or so east of the Indoburman range and most are associated with anticlinal folding. The West Bogo-Yoma fault (WBf, Fig. 4) and the Paungde Fault (PDf, Fig. 4) are two east-dipping reverse faults that show clear activity during the late-Quaternary Period. At least two of these folds and reverse faults cross the Ayerwaddy River, but the coarseness of the 90-m SRTM and 15-meter ASTER imagery preclude recognition of small river terraces that would confirm young anticlinal deformation.

Eyewitness accounts of a phenomenon associated with the Prome earthquake of 1858 support the hypothesis that this field of folds and faults is seismically active. The strongest shaking of this widely felt large earthquake was reported from the reach of the Ayerwaddy valley that encompasses the cities of Prome and Thayet-Myo (Fig. 4). Eyewitnesses report that in the several hours following the earthquake, the Ayerawaddy near Thayet-Myo flowed upstream (Oldham 1883). This could be explained by sudden uplift across the 30-km long, 10-km wide anticline that crosses the Ayerwaddy about 20 km downstream from the city. The river drops about 2 m between Thayet-Myo and the anticline, so if incremental uplift of a few meters occurred during the earthquake, the river gradient might have been impeded enough to cause the river surface to be instantaneously tilted upstream. A considerable amount of time would have been necessary for the river surface to re-equilibrate to an appropriate gradient. This explanation is identical to that advanced for the retrograde flow of the Mississippi river in the hours following the New Madrid earthquake of Feb-1812. During that event, a six-meter uplift of the Tiptonville dome, an anticline astride the river, caused the river to flow upstream and overflow its banks (Penick, 1981).

Dhaka domain

North of the Ramree domain, the Burma sliver plate collides with the thickest part of the great Ganges-Brahmaputra delta. The effect of this collision with a 20-km thick pile of Eocene to Holocene sediment (Fig. 1a) has been the formation and rapid westward growth of a great fold and

thrust belt within the sediments of the eastern side of the delta (Fig. 6a). The total width of this Chittagong-Tripura fold belt (CTFB) and the higher part of the Indoburman range approaches 400 km at 23°N. The crest of the Indoburman range increases in height northward from the Ramree domain to nearly 3000 m at 21.3°N, and retains a height of more than 2000 m for many hundreds of km northward. We refer to this ~500-km long section as the Dhaka domain, after the largest city within the fold and thrust belt.

In marked contrast to domains to the south and north, a well-expressed Wadati-Benioff zone illuminates the subducting Indian oceanic lithosphere in the Dhaka domain (e.g. Ni, 1989; Satayabala, 1998; Guzman-Speziale and Ni, 2000). Hypocenters occur as deep as 200 km and up to 450 km from the deformation front. Few of the focal mechanisms are consistent with either strike-slip or dip-slip on the megathrust; most reveal steeply dipping strike-slip and normal faulting associated with internal deformation of the down-going slab (e.g., Satyabala, 1998; Purnachandra and Kalpna, 2005). Beneath the Chittagong-Tripura fold belt, several moderate earthquakes show dextral or reverse faulting in the shallow part of the crust; however, their hypocenters are not well constrained by the global seismic network. The seismic silence of the megathrust raises an important question: Does the megathrust in the Dhaka domain slip only aseismically or is it capable of generating great megathrust earthquakes?

GPS-based vector diagrams suggest that modern relative motions between the Indian plate and the Burma plate at the latitudes of the Dhaka domain are similar to relative motions across the Ramree domain (Appendix-1, Fig. S3, rows 1 and 2). Relative motion between the Indian plate and Sunda plate, with 18-22 mm/yr of right-lateral slip on the Sagaing fault removed, yields oblique convergence between the Indian plate and Burma plate. At 21.25°N, estimated motions of 6 to 25 mm/yr are predominantly perpendicular to the deformation front, with a small component of dextral strike-slip. Further north, at 23.5°N, the dextral strike-slip motion increases significantly due to the change of megathrust fault's orientation. Relative motion of a station within the fold belt

(Aizawi, Fig. 6a) is about 10 mm/yr eastward toward Dhaka (Jade et al., 2007; Banerjee et al., 2008). Although GPS stations are too sparse to fully map strain accumulation across the Burma plate at this latitude, this measurement is consistent with a predominance of convergence and a minimal oblique component. Farther north and east, Imphal is converging southwestward toward Dhaka at between 11 and 20 mm/yr. This implies significant active right-lateral strike-slip faulting or clockwise rotations at this latitude.

With these broad attributes of the Dhaka domain in mind, we now discuss stratigraphic, geomorphologic, and seismic evidence of recent neotectonic activity, moving from west to east, as we did for the Ramree domain. We begin with a discussion of the history of deformation within the Chittagong-Tripura fold belt (CTFB) on the eastern flank of the Ganges-Brahmaputra delta. We then proceed to document topographic evidence for activity on faults within the higher parts of the Indoburman range. Finally, we discuss the significance of the steep eastern flank of the range and evidence for and against active faulting in the lowlands farther east.

Chittagong-Tripura fold belt (CTFB)

Relevant to our neotectonic analysis is a large body of work on the geological architecture and history of the Ganges-Brahmaputra delta and the CTFB. We begin with a summary of salient information.

The Ganges-Brahmaputra delta rests on lithosphere that is transitional between thick, buoyant Indian continental lithosphere on the west and north and dense Indian oceanic lithosphere on the east. (e.g., Alam, 1989; Curray, 1991). Sediment contributions to the delta began to arrive from the Himalaya and Indoburman range around the early Oligocene epoch (~35 Ma) and have been prograding southward to the present day (e.g., Curiale et al., 2002; Curray et al., 2003). The arriving mass of these sediments loaded and depressed the underlying lithosphere, leading to the creation of additional accommodation space for deltaic sediment. Additional lithospheric

depression and accommodation space has resulted from the southward thrusting of the Shillong Plateau over the delta through the past 5 million years and from the westward thrusting of the Indoburman ranges toward the delta (e.g., Johnson and Alam, 1991). Altogether, current thicknesses of the deltaic sediment now range from about 12 to 21 km on the western flank of the Dhaka domain (Curray, 1991; Brune et al., 1992).

The Chittagong-Tripura fold belt has developed within the upper parts of this thick deltaic sequence. Many folds are clearly visible in the SRTM imagery as north-northwest-striking anticlinal and synclinal hills (Fig. 6a). Through construction of a balanced cross section across the CTFB, Maurin and Rangin (2009) estimated a total east-west shortening of about 11 km in the past 2 million years, which implies a long-term shortening rate of about 5 mm/yr.

Various stratigraphic and structural studies show that the CTFB has not developed synchronously. In general the fold belt has grown progressively westward, toward the deformation front (Johnson and Alam, 1991; Uddin et al., 1999; Steckler et al., 2008; Maurin and Rangin, 2009). Many of the folds in the west have been active only from the late Pliocene or later. Many of the folds in the eastern part of the CTFB appear to no longer be active, even though they are clearly evident on the SRTM imagery. The rate of propagation of the deformation front has been about 100 mm/yr in the past 2 million years (Maurin and Rangin, 2009), far greater than the current rate of convergence across the fold belt.

This rapid propagation of the deformation front helps to explain the broad curvature of the CTFB between 24°N and the Shillong plateau. As the fold belt has propagated into the basin over the past 2 million years, it has not been able to propagate over the continental crust of the Shillong plateau, which has been rising and thrusting southward out over the basin through the past five million years. The sweep of the fold belt thus reflects the impediment to westward propagation imposed by the Shillong plateau.

Figure 6 shows in black those anticlines and related faults that do not appear to have been active recently. Those anticlines and related faults mapped in red have evidence for recent activity. In the case of the faults, evidence for activity consists of unusually steep flanks on the related anticline, which suggests that a fault has propagated to, or close to, the surface. In the following paragraphs we describe the evidence for recent activity of some of the anticlines.

Published seismic reflection profiles across several anticlines reveal growth strata that constrain the initiation of folding. In some places the age of the growth strata constrain the initiation of anticlinal growth to Pliocene or younger. The initiation of the Sylhet, Habiganj, Patiya, Jaldi, and two offshore anticlines (labeled S, H, P, and J in Fig. 6a) are so constrained (Johnson et al., 1991; Steckler et al., 2008; Maurin and Rangin, 2009).

Evidence of even more youthful activity exists for a few other folds. These include the Maheshkhali anticline, whose upper surface formed during the Last Glacial Maximum, when the fluvial plain extended many kilometers out onto the current seafloor but now sits far above the modern floodplain (M, Fig. 6a). Khan et al. (2005) interpret this to indicate uplift in the past 18,000 years. Possible support for activity of this anticline is a report of extensional cracks that developed atop this anticline during a small (mb 5.2) earthquake in 1999 (Ansary et al., 2000). Steckler et al. (2009) plausibly interpret these as an indication of "coseismic slip on a blind ramp-flat fault with extension in the hangingwall block as it moved through the kink." Khan et al. (2005) also propose that the nearby Jaldi anticline is active, as evidenced by the young age of the soil on its crest. Their luminescence date from the crestal surface of the anticline implies a rise in fluvial baselevel in the past 35,000 years.

Other clear evidence of youthful vertical deformation along the western portion of the CTFB is resolvable from the SRTM 90-meter digital elevation model and from optical satellite imagery. Sandwip Island, at the mouth of the Ganges is a good example (SW, Fig. 6a). A nearby radiocarbon

date (Goodbred and Kuehl, 1999) suggests to us that its upper surface is about 7,000 years old or younger. That surface displays an anticlinal warp of ~5 meters above sea level (Fig. 6b). This is likely representative of the entire Comilla Tract immediately to the north. The surface of this large tract at the front of the modern delta is three to four meters above the modern surface of the delta (Steckler et al., 2008) and appears to be very gently folded (CT, Fig. 6a). Another tract of the delta, Madhupur tract north of Dhaka (MT, Fig. 6a), sits well above the surrounding modern delta plain (Morgan and Mclntire, 1959, Coates and Alam, 1990; Steckler et al., 2008). Its westward slope raises the possibility that a fault has recently propagated beneath it and may even break the surface at its western edge (e.g., Steckler et al., 2008). The existence of both the Comilla and Madhupur Tracts suggest that the active deformation front has propagated as far west as the Ganges River.

Other evidence from SRTM topography and optical imagery are two uplifts farther south. The anticline at the southern tip of Bangladesh (Dakhinpara) uplifts a terrace ~ 5 to 10 meters above the current fluvial and coastal plain (Da, Fig. 6a). Farther south, St. Martin Island sports at least two marine terraces, which imply incremental uplift since the mid-Holocene (SM, Fig. 6a, and Fig. 4).

Although the earthquake history is mostly unclear throughout the Chittagong-Tripura fold belt, large, destructive earthquakes are well known and frequent in this area. One of the recent large events is the Srimangal Earthquake of 1918 (M ~7.5), during which the northwestern part of the CTFB and the adjacent Ganges-Brahmaputra delta were shaken strongly. Stuart's (1920) isoseismal map shows clearly that the highest intensity occurred just east of the Rashidpur anticline (R, Fig. 6a), where most of the buildings were leveled to the ground. The distribution of high intensities during the Srimangal Earthquake suggests the earthquake was caused by a fault beneath the northwestern fold belt, perhaps most likely the fault that is associated with uplift of the Rashidpur anticline.

Other large earthquakes within the Chittagong-Tripura fold belt may have resulted from slip on the megathrust itself. The area of Chittagong was so badly damaged by the Arakan earthquake of 1762 that some have suggested that the megathrust ruptured from the Ramree domain through the southern portion of the Dhaka domain (e.g., Cummins, 2007; Gupta and Gahalaut, 2009). Another earthquake in 1548 also wreaked havoc across nearly the entire Dhaka domain. Based on its widespread high seismic intensities, Steckler et al. (2008) suggests this earthquake resulted from rupture of the megathrust north of the 1762 rupture patch. However, paleoseismological investigations along the southern flank of the Shillong Plateau suggest that the earthquake was caused by slip on the north-dipping Dauki fault (Morino et al., 2011).

The high Indoburman range

A ~170-km long right-lateral oblique-slip fault is clearly evident in the topography of the high Indoburman range near Imphal (Fig. 6a). Along the western flank of the Imphal basin, many of the eastward flowing rivers and basins exhibit dextral deflections and warping along the Churachandpur-Mao fault (Fig. 6). This NNE-SSW-striking fault also shows a clear vertical component in the SRTM topography, as the range rises up steeply more than 1000 m from the basin floor to the mountain crest. We find the largest dextral geomorphic offset is about 3 km along the fault trace, whereas the vertical offset is likely more than 1.5 km (Fig. 7a and 7b). Both the vertical and right-lateral offsets diminish northward and southward, and the geomorphological evidence becomes less compelling north and south of the basin.

The latitudinal span of the Churachandpur-Mao fault is almost perfectly coincident with the span over which the CTFB narrows from south to north. This spatial correlation suggests that the fault resulted from the impediment posed by the Shillong block to westward motion of the Indoburman range. If the high Indoburman range is not moving westward as fast in the north as it is

in the south, then a dextral-slip fault with the orientation of the Churachandpur-Mao fault could be a consequence and manifestation of that differential motion.

This neotectonic scenario also suggests the initiation of the Churachandpur-Mao fault would have been much later than the formation of the high Indoburman range. Geomorphic features within the Imphal basin support this hypothesis. For example, wind gaps along the western flank of the basin suggest that the drainage basins west of the Imphal basin originally extended east into the basin. Moreover, the burial of highly eroded ridges in the eastern part of the basin indicates that it became the depositional center after formation of these ridges. Both of these observations support the hypothesis that initiation of the Churachandpur-Mao fault occurred long after initiation of uplift and erosion of the high Indoburman range.

We can speculate that lifetime-averaged slip rate of the fault is about 2 mm/yr, if we assume that the fault initiated about 2 Myr ago and that its total maximum offset is represented by the 3-km dextral and 1.5-km vertical geomorphic offset. This very long-term guess is much lower than the differential motion seen in geodetic measurements across the high Indoburman range. GPS vectors suggest modern motion across the Churachandpur-Mao fault is an order of magnitude higher and the horizontal motion is almost purely dextral (i.e., 1 to 1.6 cm/yr; Jade et al., 2007; Kumar et al., 2011; Gahalaut et al., 2013). This disparity implies that our calculation of a long-term rate may be grossly in error. It could be correct, however, if either the rate of slip has accelerated by nearly an order of magnitude or permanent dextral deformation across the high Indoburman range is distributed across a wider deformation belt rather than localized along the Churachandpur-Mao fault.

East flank of the Indoburman range and beyond

The tectonic morphology of the eastern flank of the Indoburman range in the Dhaka domain is very different than that throughout the Ramree domain. In addition to an impressive east-facing

escarpment, the eastern flank includes the basin of the Kabaw valley, which is flanked on the east by a narrow range of low hills (Fig. 6a). This implies that the east-dipping fault that traverses the eastern side of the Kabaw valley is raising the hills faster than sediment streaming out of the Indoburman range can bury the hangingwall block of the fault.

We call this the Kabaw fault system, as originally proposed by Win Swe et al. (1972). Others have used this name in reference to west-dipping thrust faults along the entire eastern flank of the Indoburman range (e.g., Hla Maung, 1987; Curray, 2005). In this work, we conform to the original use of the name.

The youthful appearance on SRTM and ASTER images of the eastern flank of the Kabaw valley between 22˚N and 24.8˚N suggests that the Kabaw fault system is active. Closer inspection of the southern half of the valley with 1:25,000-scale aerial photographs revealed no evidence for offset of an elevated erosion surface along a steeply dipping strike-slip fault in the center of the valley (Fig. 8). Moreover, evidence of thrust-fault scarps on the eastern side of the low hills was equivocal. We therefore believe that if the Kabaw fault system is currently active, its rate of slip is equal to, or lower than rates of sedimentation and erosion in this N-S running narrow basin.

Naga domain

A fundamental change in the Indian-Burma collision occurs at 25˚N, where the Dauki thrust intersects the western flank of the Indoburman range (Fig.1). As the folds of the Chittagong-Tripura fold belt approach the Dauki thrust from the south, they swing eastward and the width of the belt narrows from about 240 to about 160 km (Fig. 6a). North of the Dauki fault the CTFB is absent, and in its place along the steep western flank of the Naga Hills is a fold and thrust belt that is an order of magnitude narrower (Fig. 9a). We refer to this segment of the Indo-Burman collision as the Naga domain, after the eponymous mountains that span the 430-km distance between the Shillong plateau and the Himalayan syntaxis.

This dramatic change in the structural and topographic expression of collision at 25°N reflects the dramatic change in nature of the footwall block across the Dauki fault. As we have just described, collision south of the Dauki fault in the Dhaka domain is extending rapidly westward, out into the thick pile of Gangetic delta sediments that rest atop transitional and foundering oceanic crust (Fig. 1). North of the Dauki fault the Naga Hills override a very different footwall – recently uplifted continental crust of the Shillong Plateau and (farther east) the narrow continental shelf of the Assam block (e.g., Verma et al., 1976; Clark and Biham, 2008).

The stark geomorphologic contrast between Chittagong and Naga domains appears to reflect shallow crustal differences in collision rather than deep-seated ones. The nature of the higher Indoburman range does not change markedly across the domain boundary. Nor do isobaths drawn on the top of Wadati-Benioff zone beneath the mountains show any clear bend or tear across the domain boundary below depths of ~60 km. The narrower width of the shallow portions of the Wadati-Benioff zone beneath the Naga Hills is consistent with the lack of a wide, CTFB-like fold and thrust belt and underlying décollement.

Beneath the Naga Hills, the Wadati-Benioff zone extends to depths of ~160 km, as far as 150 km from the mountainfront. This implies subduction of at least a couple hundred km of oceanic lithosphere before the thrust faults of the Naga hills began to ramp up onto the continental shelf of the Assam block in the early Miocene (Kent et al., 2002).

The Naga Hills reflect convergence of the Burma plate and the Assam block across the 430 km that separate the Shillong Plateau from the Himalayan syntaxis. The narrowing of the hills from about 170 km in the southwest to 90 km in the northeast (Fig. 9a) may imply a northeastward diminishment in total shortening across the range.

Geomorphological expression of the Naga thrust is very clear along the front of the Naga Hills, and its presence there is well known from geological and geophysical surveys (e.g., Mathur and

Evans, 1964; Berger et al., 1983; Ranga Rao and Samanta, 1987). The fault trace appears as several arcuate lobes along the range front. Along its southwestern 100 km, a linear scarp clearly marks the location of the fault. An anticline and 5-km wide piggyback basin sit on the hanging-wall block, and nested terraces imply incremental uplift. The highest terrace projects ~200 m above the range front, suggesting late-Quaternary uplift of at least that amount (Fig. 9b). Younger terraces display uplifts ranging from 20 to 50 m.

Geological mapping and seismic reflection lines at ~95.5°E illuminate the nature of the fault system. The fault dips moderately to steeply and breaks the surface at the position shown on Figure 9a. It thrusts folded lower Miocene rocks over undeformed upper Pliocene to Quaternary beds (Kent et al., 2002). The geometry of the anticlinal fold implies that it developed as a fault-propagation fold that was eventually breached by propagation of the fault to the surface. The clear geomorphological expression of the anticline implies that it is still active and that the dip of the thrust fault decreases at depth (Fig. 9c).

The Naga thrust system terminates at 96° E where it appears to be cut by a NW-striking thrust fault and associated anticlines. This short fault appears to be the westernmost element in a system of thrust faults associated with westward thrusting of the Eastern Himalayan syntaxis over the Assam valley and Naga Hills. We infer from the topographic profile of the crest of the Naga Hills that slip on the Naga thrust dies out over ~100 km as it approaches this termination.

The Sagaing domain

The Sagaing fault system performs the classic role of a ridge-trench transform fault as it traverses the 1400-km distance between the Andaman Sea spreading center in the south and the eastern Himalayan syntaxis in the north (Fig. 1) (Yeats et al., 1997). Total dextral offsets since the Miocene, estimated from bedrock matches, river offsets across the fault and the total opening of the Andaman Sea, range from about 203 to 460 km (e.g., Mitchell, 1977; Myint Thein, 1981; Curray et

al., 1982; Hla Maung, 1987; Armijo et al., 1989). The central and the southern part of the Sagaing fault also approximated the western boundary of the Sunda block during its eastward and southward extrusion in an early (~34 to ~17 Ma) phase of the Indian-Asian collision (e.g., Leloup et al., 2007). It is recognized as the region's major tectonic divide, separating disparate rocks of the Burma plate from those of the Sunda plate (e.g., Mitchell, 1977; Curray et al., 1982).

Seismicity and both geomorphologic and structural evidence confirm that it is a dextral-slip fault system (e.g., Myint Thein, 1991; Hla Maung, 1987; Guzman-Speziale and Ni, 1993). Its recent slip rate, assessed from an offset Pleistocene basalt and from GPS measurements, is about 20 mm/yr (Bertrand et al., 1998; Vigny et al., 2002, Socquet et al., 2006, Maurin and Rangin 2010). Given its high slip rate, it is no surprise that the fault is well expressed geomorphically – the most notable exception being where it traverses the rapidly aggrading and prograding young delta north of and beneath the Andaman Sea. Isoseismal maps and seismic analyses of historical earthquakes show that about half of the Sagaing fault has ruptured during many large earthquakes over the past nine decades (e.g., Brown and Leicester, 1933; Hurukawa and Phyo Maung Maung, 2011, Table 1).

Like the San Andreas Fault, but in contrast to the Sumatran fault, the Sagaing fault system is unbroken by large stepovers or complications along most of its length. This unbroken geometry is probably due to the fault's large accumulation of slip. The northern 400 km of the fault system, however, is very complex. It comprises several distinct faults arranged in a complex horsetail pattern that fans out northward to a width of about 100 km. This complex geometry likely reflects both the lengthening of the fault system to accommodate India's northwards motion and the extrusion of Asia around the eastern Himalayan syntaxis.

Between about 18˚N and the Himalayan syntaxis, the Sagaing fault forms a broad concave-eastward arc (Fig. 1). The fact that the arc mimics the curvature of the eastern flank of the Indoburman range to the west and coincides with the belt of sinistral-slip faults to the east intimates

a shared cause – likely the westward extrusion of the Sichuan-Yunnan block around the syntaxis. The fast slip rate of the Sagaing fault overwhelms erosional and depositional activity along most of its trace, so abundant tectonic landforms enable us to map and characterize most of the fault well. This geomorphic evidence, in addition to historical seismicity, inspires us to divide the fault into various segments. We begin with segments along the southern subaerially exposed and relatively simple portion of the fault and then proceed to the complex horsetail of the northern few hundred km.

The southern section of the Sagaing fault

Although a synoptic view of most of the Sagaing fault leads one to think that its geometry is simple, careful geomorphic mapping justifies its division into five distinct segments between 16.5˚ and 23.5°N (Fig. 10). What distinguishes these segments are bends, splays and distinct secondary features, as well as the terminations of historical ruptures.

Bago segment

The Bago segment extends northward at least 170 km from the Myanmar coast, across the young, southward-propagating delta of the Sitong River (Tsutsumi and Sato, 2009, Wang et al., 2011). We do not know how much further it extends southward on the submarine portion of the Sitong River delta. However, regional structural maps show that the Bago segment connects to a series of E-W running normal faults several tens of km south of the current coastline (e.g., Replumaz, 1999; Pubellier et al., 2008). Its northern limit coincides with an abrupt 10˚ westward bend at 18˚N (Fig. 10). Tsutsumi and Sato (2009) and Wang et al. (2011) mapped in detail the tectonic landforms of this segment, from the aerial photos and satellite imagery. The last major earthquake produced by the Bago segment was the Mw 7.2 Pegu earthquake of May 1930 (Table 1; Pacheco and Sykes, 1992). Measurement of small offsets led Tsutsumi and Sato (2009) to suggest that the maximum offset during this earthquake was at least 3 meters. Wang et al. (2011) suggest a

rupture length of about 100 km, extending from the southern coastline to ~20 km north of Bago city, based on the field investigations and their interpretation of isoseismals published by Brown et al. (1931). Measurements of an offset ancient wall and related paleoseismic work north of Bago led Wang et al. (2011) to propose an earthquake recurrence scenario for the Bago segment.

Pyu segment

The Pyu segment extends ~130 km, from the sharp bend at 18°N to a bifurcation at 19.1°N. Along this reach, the main trace of the Sagaing fault skirts the base of the escarpment of the Bago-Yoma range (Fig. 10). SRTM imagery clearly shows that most fluvial channels and alluvial fans from the Bago-Yoma range are offset right-laterally at the mountain front (for details see Appendix-1 Fig. S2). Close to the central part of this segment, an elongate terrace borders the Pyu segment on the east. The terrace is rising on the hangingwall block of a west-dipping reverse fault that crops out on the east flank of the ridge (Replumaz et al., 1999). This reverse fault and the escarpment are manifestations of a minor component of transpressional shortening across the Pyu segment (Replumaz et al., 1999; Wang et al., 2011). This transpression is consistent with the 10˚ counterclockwise deviation of this section of the Sagaing fault from its overall more northerly strike.

The last major earthquake generated by the Pyu segment is the Mw 7.3 Pyu earthquake, which occurred in Dec 1930, just a few months after the similar-sized rupture of the Bago segment to the south (Table 1). The relocated epicenter of the Pyu earthquake is close to the segment's southern boundary (Hurukawa and Phyo Maung Maung, 2011). The isoseismals drawn by Brown and Leicester (1933) clearly show that the highest intensities of the earthquake span the entire Pyu segment. Thus it is appears that the entire Pyu segment ruptured during the Dec 1930 earthquake.

Nay Pyi Taw segment

At 19.1°N the Sagaing fault splays into two parallel fault traces that span the entire ~70 km length of the Nay Pyi Taw segment (Fig. 10). The relief across the fault along this segment is much more subdued than it is along the Pyu segment. This indicates lesser vertical motion during the Quaternary Period. Both traces of the Nay Pyi Taw segment offset channels and alluvial fans, so slip is significantly partitioned between these two branches. In the north, both traces traverse the ~30 km long basin in which the new capital, Nay Pyi Taw, was established in 2005. The western trace cuts through the eastern edge of the new capital, and sports a ~5-m high east-facing scarp.

This segment does not appear to have produced a large earthquake in recent times. The moderate Swa earthquake of August 1929 (Table 1) severely damaged the railroad and bridges about 40 km south of the new city (Brown, 1932; Chhibber, 1934). The highest intensities of the earthquake occurred along the eastern branch of the Nay Pyi Taw segment south of Myanmar's new capital city (Brown, 1932). But because the earthquake does not appear in the early global seismic catalog and was only felt in a limited area, we believe its magnitude is likely not to have been larger than Mw 7.

Meiktila segment

The Meiktila segment traverses a ~220 km reach of the fault between Nay Pyi Taw and Mandalay. Its very simple trace runs almost uninterrupted from just north of Nay Pyi Taw to the southern side of the Irrawaddy river. Our choice for the northern boundary of the Meiktila segment is a bit arbitrary, but is coincident with a greater prominence of transpressional secondary features north of the river.

Unlike the Pyu and the Nay Pyi Taw segments, the Meiktila segment does not run along the eastern base of the Bago-Yoma Range; instead it traverses a broad valley (Fig. 10; Appendix-1 Fig. S2). Narrow linear ridges are common along the fault trace as it traverses the fluvial valley fill.

These probably reflect shallow shear dilatation of the faulted sands and gravels of the floodplain (e.g., Gomberg et al., 1995). The utter lack of elevation differences across the fault shows that along this segment the Sagaing fault has no vertical component of slip. The largest clear right-lateral offset is ~2.4 km across a channel at 20°N.

There is no clear historical record of rupture of the Meiktila segment. The most recent plausible such event would be the Ava earthquake of 1839, so named for the ancient capital that straddles the fault on the southern bank of the Ayeyarwady River. Records written by British officers in nearby Mandalay indicate that the earthquake caused catastrophic damage and liquefaction east and south of the Ayeyarwady River, especially in Ava (Oldham, 1883, Chhibber, 1934).

Sagaing segment

The namesake of the Sagaing segment is a small city on the fault just north of the Ayeyarwady River. It is the tectonic morphology of this section of the fault that led to the fault's discovery by Win Swe (1970). The northern limit of the Sagaing segment is at 23.5˚N, where the fault steps left approximately 2 km from the eastern bank to the western bank of the Ayeyarwady River (Fig. 10; Fig. S2). The northern limit of the Sagaing segment also marks the location where the fault splays into multiple traces. Further to the south, in the low Sagaing hills, east of the fault and north of the Ayeyarwady crossing are the southernmost outcrops of metamorphic rocks on the eastern flank of the fault.

Like the Meiktila segment, the Sagaing segment is relatively straight and simple. However, along its southern extent, the elongate ridges that comprise the Sagaing hills are larger than the ridges in the young fluvial sediments of the Meiktila segment and display more structural relief. Perhaps this greater relief is an indication that the formation of the Sagaing hills began well before the fault-zone ridges to the south, where they involve disruption only of young sediment and rocks.

Between 21.9˚N to 22.6˚N, the Sagaing segment runs along the western bank of the Irrawaddy River and offsets a series of post-Pliocene alluvial fans along a 20-km reach (Myint Thain et al., 1991).

North of the Singu basalt, SRTM topography suggests that the Sagaing fault comprises two parallel fault traces, west and east of the Ayeyarwady River. Farther north, the western trace becomes what we term the Tawma segment, after it splits to two northward-diverging faults. A 5- to 10-meter high east-facing scarp on a fluvial surface attests to the recent activity of the eastern trace.

The northern two-thirds of the Sagaing segment may have produced the magnitude 7.6 earthquake of September 1946 (Fig. 10; Table 1). The relocated epicenter of the earthquake implies that the event initiated south of the Singu basalt (Hurukawa and Phyo Maung Maung, 2011) (Fig. 10). A field investigation after the Shwebo earthquake of 11 November 2012 located ground cracks along the youthful-looking small scarps that we mapped from SRTM (Soe Thura Tun, personal communication). We therefore suggest that that part of the fault may have ruptured during both the September 1946 earthquake and the most recent event. The southern third of the segment may have ruptured during a smaller, Ms 7.0 earthquake in July 1956, which caused severe building damage in the Sagaing-Mandalay area (Win Swe, 2006). Unfortunately, no field investigations were conducted or isoseismal maps made after the 1946 or 1956 events. Based on the historical records of shaking, however, we speculate that the part of the Sagaing segment that runs along the western flank of Sagaing hills ruptured during the 1956 Sagaing earthquake.

The Northern section of the Sagaing fault

Beginning at 23.5˚N, the Sagaing fault system fans northward as four distinct active fault zones that terminate sequentially from west to east between about 25˚ and 27˚N (Fig. 11). Geomorphological evidence for the westernmost fault zone ceases at about 25˚N, whereas evidence

for the easternmost one extends as far north as ~27˚N and nearly connects to active structures between the Sagaing fault system and the Naga thrust. Because slip is distributed among these four sub-parallel fault traces, their geomorphic expressions are not as clear as those of the southern strands. The four fault zones of the northern Sagaing fault system comprise six discrete segments, distinguished by their geometries and discontinuities. In the paragraphs below, we describe each, starting with the southern and western ones and moving north and east.

Tawma and Ban Mauk segments

The Tawma segment extends northward from a complex of faults at 23.5°N (TMs in Fig. 11). The Tawma segment is the northward continuation of the western fault trace of the northern part of the Sagaing segment (see Fig. S2 for details). The Tawma segment strikes northward nearly along the base of an east-facing escarpment. Some of the drainages flowing across the escarpment show right-lateral deflections across the fault.

The geomorphic expression of the segment disappears at ~24°N, at a left stepover to the Ban Mauk segment, which is 10 km farther west (BMs, Fig. 11). The stepover between the two segments is complicated. SRTM imagery shows an array of NE-SW striking faults across a 10-km wide transpressional ridge. Some of these faults may have a normal component of slip. The lengths of these secondary faults are mostly less than 20 km, and their subtle expression suggests they have low slip rates, compared to the rates of the main traces of the Sagaing fault.

A Mw 6.9 earthquake in 1991 may have resulted from rupture of the Tawma segment. Its relocated epicenter is near the segment's southern termination (Hurukawa and Phyo Maung Maung, 2011) (Fig. 11). The CMT solution is consistent with dextral slip on a nearly N-S striking fault. This orientation is more consistent with the strike of the Tawma segment than the strike of the active In Daw segment to the east (IDs in Fig. 11). Moreover, the length of the Tawma segment is

comparable to typical rupture lengths for an earthquake of this magnitude (Wells and Coppersmith, 1994).

The Ban Mauk segment extends ~150 km northward from approximately 23.8˚N (BMs in Fig. 11). It separates Neogene volcanic rocks on the west from Miocene sedimentary rocks on the east (Bender, 1983). Geomorphological expression of the Ban Mauk segment is more muted than along segments to the south and east; clear geomorphic evidence, such as offset channels and offset drainage basins are rare. Thus, we posit that the right-lateral slip rate of the Ban Mauk segment is significantly lower than the rates of neighboring faults. The northern terminus of the Ban Mauk segment is east of Taungthonton volcano, at 25˚N. It appears that the fault trace there is covered by the apron of clastic deposits from Taungthonton volcano. This is another indication of the low rate of slip of the Ban Mauk segment at least through the late Quaternary period.

The scant evidence of youthful activity along the Ban Mauk and Tawma segments is consistent with recent analysis of geodetic data, which implies that most strain across the Sagaing fault system is accumulated on fault segments farther east (Maurin et al., 2010).

In Daw and Mawlu segments

The In Daw and Mawlu segments extend northnortheastward 170 km from the Sagaing segment. They form the eastern boundary of the fault system between ~24˚ and ~25˚N (Fig. 11). The In Daw segment separates from Tawma segment on the northern bank of Ayeyarwady River at 23.7°N, striking 7˚ more easterly than the Tawma segment. Farther north, at 24.25°N, a 3-km wide pull-apart basin, holding In Daw Lake, separates the In Daw segment from the Mawlu segment, which continues northnorthwestward another 90 km. The northern limit of the Mawlu segment coincides with several fault traces that cut Cretaceous to Eocene ultramafic rocks.

The InDaw and Mawlu segments are much more clearly expressed geomorphically than their western neighbors, the Tawma and Ban Mauk segments. We find the largest dextral

geomorphologic offset across the In Daw/Mawlu segments to be about 4 km, four to five times larger than the largest geomorphologic offset across the Tawma and Ban Mauk segments. Furthermore, recent geodetic analysis implies strain accumulation equivalent to ~2 cm/yr of dextral slip across the InDaw and Mawlu segments (Maurin et al., 2010). These two independent observations imply that the slip rate across these eastern segments has been substantially higher than the slip rates of the western segments through at least the past few thousand years.

Although their epicenters were separated by 200 km, the In Daw segment produced a Mw7.3 foreshock three minutes before the Sagaing segment's Mw 7.7 earthquake of September 1946 (Pacheco and Sykes, 1992; Table 1; Figs. 10 & 11). The size of the 7.3 earthquake is consistent with the 80-km length of the In Daw segment, so we suspect that the entire In Daw segment ruptured during this foreshock.

Shaduzup, Kamaing and Mogang segments

The northern termination of the Mawlu segment is at ~ 24.8°N, where the fault system trifurcates and fans northward in the shape of a horse's tail (Fig. 11). From west to east, we call these strands of the horse's tail the Shaduzup, Kamaing and Mogang segments (SZs, KMs and MGs in Fig. 11).

The obscurity of geomorphic evidence for activity along the westernmost of these suggests that it accommodates less strain than its two neighbors. Although the Shaduzup segment truncates Tertiary geological units and structure, we did not find clear evidence of drainages offset across the fault. The northern termination of the Shaduzup segment is not well defined in the coarse SRTM topography north of 26°N, so it appears that its total length is no more than 120 km.

The Kamaing segment traverses the western flank of a ridge composed of Precambrian and Miocene rocks (Bender, 1983) and displays clear geomorphologic evidence of youthful activity along its middle reach. The Kamaing segment extends much farther north than the Shaduzup

segment, well into the eastern border of the Naga Hills, north of 26.7°N. Several drainages along the eastern side of the Naga Hills show clear dextral offset near the northern termination of the Kamaing segment. Farther northwest, the northwestern extension of the Kamaing segment connects to the thrust fault system that bounds the eastern margin of the Assam valley (Fig. 11).

The Kamaing segment has been seismically active over the past four decades, but no earthquakes larger than M 6 appear in the global catalogue. A cluster of moderate (M 5 to 6) earthquakes forms a lineation parallel and almost beneath the fault trace between 26˚ and 27.4˚N. Another set of earthquakes clusters along it around 25.4˚N. If generated by this segment, these clusters may indicate partial decoupling of this reach of the Kamaing segment, a notion supported by a modern geodetic analysis that implies very shallow locking of this segment (Maurin et al., 2010).

The easternmost of the active horsetail faults is the Mogang segment. It extends in a broad arc from ~24.8˚N to ~26.8˚N. Northward from 24.8˚N, it forms an arcuate boundary between hills of Precambrian and Miocene rocks on the west and a broad valley on the east. Along the eastern flank of the hills, deflections of a series of drainages that incise the Miocene formation suggest up to 10 km of dextral offset. This implies that the Mogang segment has also been active during the late Quaternary Period. The Mogang segment terminates at 26.8°N, east of the Naga domain, along strike of a NW-SE running thrust fault that bounds Precambrian and Cretaceous units of the eastern Himalayan syntaxis (Fig. 11).

Unlike the Kamaing segment, the Mogang segment has been seismically silent in the past several decades. The last major earthquake to originate near these segments is the Ms 7.5 earthquake of January 1931 (Pacheco and Sykes, 1992; Table 1). Its relocated epicenter is within kilometers of the arcuate Mogang segment (Table 1). The magnitude of the earthquake suggests a surface rupture of about 100 km, short enough to be associated with either the Mogang or the

Kamaing segment (Fig. 11). The lack of a reliable isoseismal map for this earthquake precludes us from confident assignment of the earthquake to either of the two segments. We favor the Kamaing segment as the source, however, because earthquake intensities were higher near the Kamaing segment than along the Mogang segment (Chhibber, 1934). However, we cannot rule out the possibility of a Mogang source of this event, as the seismic intensity records were sparse for this event.

The Shan-Sino domain

The Shan-Sino domain embodies a plexus of active predominantly left- and right-lateral faults between the Sagaing and Red River faults (Fig. 2). North- to north-northwest-striking dextral-slip faults dominate the western and central eastern parts of the domain. West- to northeast-striking sinistral-slip faults dominate the central corridor of the domain, from its northwestern corner, near the northern Sagaing fault, to the arcuate Dien Bien Phu fault, about 750 km to the southeast (Fig. 1). The geometry of these faults and GPS vectors drawn relative to the Sunda block (e.g., Simons et al., 2007) show that these faults accommodate southwestward rotational extrusion of the northern part of the Sunda block at rates that increase northwestward, toward the eastern Himalayan syntaxis. This extrusion appears to be driven by the ongoing extrusion of eastern Tibet's Sichuan-Yunnan block, which is bounded on the east by the Xiaojiang fault system (see Tapponnier et al., 1982) (Fig. 1). In the past 4 to 5 million years, the Xiaojiang fault has experienced about 60 km of left-lateral motion, which is consistent with the broad 40- to 60-km bend of the Red River fault (e.g., Allen et al., 1984; Wang et al., 1998). The presence of significant dextral-slip faults and a few normal faults within the region southwest of the Red River fault imply that the Shan-Sino domain is also extending slightly in an east-west direction (Fig. 12).

The Sunda block has an earlier Cenozoic tectonic history involving its eastward and southward extrusion during an earlier phase of collision of India into Asia (e.g., Tapponnier et al.,

1982; Leloup et al., 2007). Many of the structures related to this earlier collision remain visible in the topography of the Shan-Sino domain, but by and large appear to be inactive. Some of these earlier structures served as dextral-slip faults in the earlier phase of extrusion, but have been moving left-laterally throughout at least the past 5 million years (Lacassin et al., 1998).

In the paragraphs below we describe evidence for activity of the faults of the Shan-Sino domain, beginning with the larger left-lateral faults and then the larger right-lateral fault systems.

The left-lateral faults

Summary

The large left-lateral faults form the core of the Shan-Sino domain (Fig. 12). In general, these left-lateral faults (like the GPS vectors) arc around a pivot point near the eastern Himalayan syntaxis, with fault curvature decreasing away from the syntaxis.

Many of these left-lateral faults distinctly offset the major river courses of Southeast Asia, including the Salween and Mekong Rivers and their tributaries. These sharp offsets imply a long and ongoing history. Some of these offsets have a hairpin shape that implies a regional reversal of slip from right- to left-lateral sometime between 5 and 20 Ma (Lacassin et al., 1996).

To facilitate a structured discussion, we separate these left-lateral faults into four geographical subgroups. The first group including the Daying River, Ruili, Wanding and nearby smaller faults slice through the northwestern corner of the Shan-Sino domain. These exhibit left-lateral shear and have associated west-northwest normal faults. The second group includes the Nanting, Lashio and Kyaukme faults, which are farther southeast and show almost purely westward left-lateral motion. The third group is still farther southeast and much shorter. The southeastern limit of the domain is defined by the long Dien Bien Phu fault zone.

Daying River, Ruili and Wanding faults

The Daying River fault, Ruili fault and Wanding fault cut the northwesternmost portion of the Sunda plate (Fig. 12). Two common characteristics are that each connects to a N-S striking normal-dextral fault in the northeast and that each has a clear normal-slip component in the southwest. These characteristics show that this corner of the Shan-Sino domain is extending roughly east-west.

The **Daying River fault** is the northwesternmost of these three principal left-lateral faults. It courses southwestward about 135 km from the Tengchong Volcanic field in Yunnan (TCV, Fig. 12) to the western escarpment of the Shan plateau in northern Myanmar. Along its traverse of the southeastern margin of the Yingjiang basin, it shows well-developed triangular facets indicative of a normal-slip component and clear left-lateral channel deflections (Fig. 13a).

A field survey along the Daying River fault that enabled thermoluminescence (TL) dating determination of 10 and 20 ka ages for alluvial surfaces showed that left lateral slip rates are ~1.2 to 1.6 mm/yr (e.g., Guo et al., 1999a; Chang et al., 2011).

A Mw 5.5 earthquake that struck the region in March 2007 also indicates that the Daying River fault is active (Table 1). Both the focal mechanism and relocated aftershocks are consistent with the strike and sense of slip on the Daying River fault (Lei et al., 2012). Judging from the lateral extent of the aftershock sequence, the 2007 earthquake may have resulted from rupture of an approximately 12-km long section of the fault.

The **Ruili fault** (aka Longling-Ruili fault) parallels the Daying River fault to the south. It roughly follows the highly sheared Gaoligong metamorphic belt and extends more than 140 km from Yunnan to northeastern Myanmar (Fig. 12; Socquet and Pubellier, 2005; Wang et al., 2008; Huang et al., 2010). We map the fault splitting in the east into several northward-striking faults and

connecting to N-S striking normal-dextral faults (Fig. 12; Fig. S2). The Ruili fault merges southwestward with the E-W striking Wanding fault.

Figure 13b illustrates some of the complexity of the Ruili fault in the east, at the north margin of the Luxi basin. There the fault comprises at least two major active fault traces. These parallel faults cut the highly sheared Goligong metamorphic belt and offset a series of incised drainages that are separated by wind or water gaps (W, Fig. 13b). Left-lateral channel deflections along the southern of the two faults range from 2 to 3.6 km, but the wind and water gaps along the trace allow for a plausible offset as large as 11 km. The northern of the two faults could accommodate an additional km of slip and a lesser fault nearer the mountain front could have slipped 0.5 km. The down-to-the-southeast steps across these faults implies a normal-slip component to the fault zone here, as well.

The geomorphic features in the west are not as clear as those in the east. Perhaps slip is transferred to a normal fault at the left step of the fault across the Ruili basin. This 60-km long normal and left-lateral Namkham fault (NKf, Fig. 12) forms the southern margin of the Ruili basin and dies out near the western escarpment of the Shan plateau.

An alluvial fan surface offset near the eastern end of the Ruili fault and shown to be 33 kyr old by luminescence dating has been offset about 70 m (Huang et al., 2010). This and a nearby channel deflection of about 20 m on a 10-kyr old alluvial fan suggest the left-lateral slip rate of approximately 2 mm/yr.

The 170-km long **Wanding fault** is southeast of the Ruili fault. It bends northward near its eastern end and terminates at a N-S striking normal fault. The Wanding fault connects with the Ruili fault at its western end. Topographic relief across the Wanding fault is small, perhaps because its strike is not oblique to the direction of regional extension.

Lacassin et al. (1998) and Wang et al. (1998) report 9- and 10-km left-lateral offsets of the Salween River across the Wanding fault. Tributaries of the Salween River are offset similar amounts (Figure 13c). This observation indicates the horizontal displacement along the entire Wanding fault is roughly constant.

Field investigations and a survey of aerial photography shows that the Wanding fault offsets a series young fluvial terraces of the Salween River (Chang et al., 2012). They derive an average left-lateral slip rate of about 2 mm/yr based on the thermoluminescence (TL) ages from the offset sediments. This confirms the earlier estimate of Lacassin et al. (1998), which was based upon the assumed age of incision of the Salween River.

On May 29, 1976, two Mw 6.7 and Mw 6.6 earthquakes struck the region between the Ruili and Wanding fault in quick succession, causing severe destruction in local villages (Table 1; Fig. 12). Focal mechanisms match the strike of the Ruili fault, but no fault surface ruptures were found along the fault trace. An isoseismal map of the second earthquake centers on the intersection of the Ruili fault and a normal fault (Compilation Group of China Seismic Intensity Zoning Map SSB, 1979). We speculate that the Mw 6.6 event resulted from rupture of the easternmost portion of the Ruili fault. The isoseismal contours of the first earthquake focus close to the Wanding fault. One of the high intensity is coincident with a secondary normal and left-lateral fault of the Wanding fault system, so we suspect it to be the cause of this earlier event.

Nanting, Lashio and Kyaukme faults

These faults comprise an arcuate 400-km long system of left-lateral faults that cuts across nearly the entire width of the Shan plateau. SRTM topography and LANDSAT imagery show that this system terminates near, but slightly east of the western escarpment of the plateau. The fault traces sport geomorphological features typical of strike-slip faults without a large component of dip

slip: linear ridges, narrow and localized pull-apart basins, laterally offset stream channels and alluvial fans and the like (Yeats et al., 1997).

The longest of these faults, in fact the longest within the entire Shan-Sino domain, is the **Nanting (Nan Tinghe) fault**. An abundance of offset features demarcate its trace. Within the Yunnan area, two traces mark the eastern section of the fault. Both traces clearly exhibit large channel offsets. The southeastern of the two is the less linear, less continuous and shorter of the two, which indicates that the northwestern branch is structurally more mature; that is to say that it has accommodated more slip. This is supported by the fact that most of the young depositional basins align along the northwestern trace (Zhu et al., 1994). Along the western margin of the Shan Plateau, geomorphically obvious fabric within the Mogok metamorphic belt shows clear sinistral warping near the termination of the Nanting fault, indicating its left-lateral fault slip has been accommodated by diffuse deformation within the metamorphic belt, and that the fault does not extend as far west as the Sagaing fault.

The geomorphic evidence for recent activity of the Nanting fault has been long recognized (e.g., Zhu et al., 1994; Wang and Burchfiel, 1997; Lacassin et al., 1998; Wang et al., 1998; Socquet and Pubellier, 2005; Wang et al., 2006), but the total slip across the Nanting fault is not agreed upon. Lacassin et al. (1998) suggest that left-lateral offset is greater than 8 km, based on the offset of the channel of the Salween River. Wang and Burchfiel (1997) suggest the northeastern part of Nanting fault offsets the Mengliang ophiolitic suture about 40 to 50 km, five to six times greater than the Salween River offset along the central section of the fault. A later study from Wang et al. (1998) suggests that the southern branch of the Nanting fault may accommodate 17 km of left-lateral offset, based on the left-lateral warping of a major river.

In an attempt to resolve the dispute between the proponents of the 8-km and the 40-km offsets, we re-examined the geomorphic evidence for offset of the Salween River. We note that a wide

wind gap east of the 8-km measurement would permit an offset as great as at least 15 km (Fig. 14a). This wind gap is wide enough to have accommodated the Salween River before it migrated to its current channel south of the fault. Moreover, a plausible restoration of channels at the eastern end of the fault implies a left-lateral offset as large as 21 km across the Nanting fault (Fig. 14b and c). This 21-km offset estimation magnitude of left-lateral offset could also apply to the Salween River offset. Nonetheless, this value would still be no more than half the 40- to 50-km bedrock offset suggested by Wang and Burchfiel (1997).

The last major earthquake in the vicinity of the Nanting fault is a M ~7 event in May 1941 (Figure 12; Table 1). The eastern part of the Nanting fault intersects the zone of highest intensities (Compilation Group of China Seismic Intensity Zoning Map SSB, 1979). Wang et al. (2006) argue from the historical earthquake reports that surface rupture of an at least 12-km long section of the fault is plausible. No other sections of the 370-km long fault can be associated with large earthquakes of the 20th century. Indeed, for that eastern part of the fault within Yunnan province, Chinese historical data reveal no other destructive events in their written history (Wang et al., 2006), which for this region extends at least prior to the Qing dynasty (~17th century).

South of and parallel to the western part of the Nanting fault are the left-lateral Lashio and Kyaukme faults. The two faults also exhibit clear geomorphic evidence of activity, but not to the degree that the Nanting fault does. This comparison suggests comparatively lower slip rates.

The 85-km long **Lashio fault** lies 30 km south of the Nanting fault (Fig. 12). The match of bedrock ridges, channel deflections and the width of a transtensional basin suggest a plausible total left-lateral offset of about 6.5 km. The eastern part of this E-W fault curves to the northeast and splits into a group of southeast-dipping normal faults. Along the Lashio fault's western span, geomorphic evidence of horizontal displacement gradually diminishes westward, which suggests

that left-lateral slip may disperse into secondary faults that we cannot identify in the SRTM and ASTER imagery.

The Kyaukme and Nanting fault have an en echelon relationship to each other, whereby the former runs parallel to, but lies to the south and west of the latter (Fig. 12). Like the shorter Lashio fault, the Kyaukme fault curves northward along its eastern part.

The approximately 210-km long **Kyaukme fault** does not show any clear horizontal deflection of the current channel of the Salween River, although the river does have a gentle left-curving channel south of an ~300-m high fault scarp. A series of small beheaded channels at the base of this scarp suggests left-lateral offsets greater than one km. The western portion of the fault traverses the northern margin of two large basins and there shows left-lateral deflections of rivers flowing into the basins. The largest geomorphic offset that we see in SRTM topography is approximately 2.5 km, along the central and western parts of the fault (for locations see Table 2).

With one possible exception, both the Lashio and the Kyaukme fault were seismically quiet throughout the 20th century. An Mw 7.2 earthquake on June 22, 1923 may have resulted from failure of one of these faults, as the epicenter from global earthquake catalog falls southeast of the Kyaukme fault (Fig. 12; Table 1). However, the lack of an isoseismal map or a damage report impedes assignment of a likely source.

Menglian, Jinghong, Wan Ha and Mengxing faults

Still farther southeast, a group of left-lateral faults occupies the central part of the Shan-Sino domain (Fig. 12). The most prominent of these are the Menglian, Jinghong, Wan Ha, Mengxing, Nam Ma and the Mae Chan faults. All of these faults are more limited in their eastern and western extent that the large fault systems just discussed. Three features in common are that they strike NE-SW, their lengths range from roughly 100 to about 200 km, and they terminate to the northwest just shy of a prominent NW-SE striking fault. In this section, we will discuss together the

geomorphic evidence for the Menglian, Jinghong, Wan Ha and Mengxing faults, the smaller of the six.

The 120-km long **Menglian fault** straddles the border between China and Myanmar and shows clear geomorphic evidence for activity (Mf; Fig. 12). On the east, it terminates before reaching the major NW-SE running dextral Lancang fault. On the west, the fault ends near where it crosses the Salween River.

The total left-lateral offset of the Menglian fault is approximately 5 km. Lacassin et al. (1998) suggest that it offsets the Nam Hka River about 2.5 km at the hairpin loop that led them to propose an earlier 5 km offset as well (Fig. 15a). However, a tributary of Nam Hka River, west of the Nam Hka's hairpin, shows a left-lateral deflection of about 5 km (Fig. 15a). At the eastern part of the Menglian fault, a tributary of the Nam Loi River (Nanlei River) shows approximately 5.5 km left-lateral deflection (for location see Table. 2). Smaller left-lateral deflections and warps are also evident in the drainage networks traversed by the fault.

The Menglian fault is the likely source of an Mw 5.9 foreshock and Mw 6.8 earthquake mainshock in the Chinese-Myanmar border region in July 1995. Both epicenters and the aftershock cluster are ~20 km south of the Menglian fault. Both focal mechanisms are consistent with left-lateral slip on the Menglian fault. The mapped region of highest intensity roughly coincides with the fault near the border (Chen et al., 2002). Thus, we suggest the western part of the Menglian fault produced the mainshock.

Eighty km southwest of the Menglian fault is a very similar structure, the 110-km long **Jinghong fault**. As with the Menglian fault, the Jinghong fault terminates just before reaching the dextral-slip Lancang fault (Fig. 12). Coincident with the intersection of these two active faults is a triangular shaped basin. Beyond the Jinghong's western termination is a normal fault that may relate to the termination of the Jinghong fault.

The Jinghong's largest geomorphic disruption is an 11-km sinistral deflection along its central part. There the Taluo River, which flows along the China-Myanmar border, bends left-laterally along the fault (Fig. 15b). Both upstream and downstream, its channel is deeply incised into bedrock, so this likely represents an offset. Further support for this hypothesis is the fact that a nearby contact between granitic intrusive rocks and Paleozoic rocks displays a left-lateral offset that is similar to that of the nearby river (Bureau of Geology and Mineral Resources of Yunnan, 1993). Smaller offsets of fans and channels indicate that the Jinghong fault continues to be active.

A Mw 7.1 earthquake on Feb 2, 1950 was most likely caused by rupture of the Jinghong fault. The epicenter of mainshock is very close the central part of the fault and several Chinese cities north of the Jinghong fault were damaged (Xie and Tasi, 1983). Unfortunately, though, Chinese intensity data are too sparse to enable construction of an isoseismal map that might confirm the source. Two more recent and more moderate earthquakes (Mw 5.6 and Mw 5.4) on June 23, 2007, may also have resulted from failure of the Jinghong Fault. Their GCMT focal mechanisms are consistent with the fault's strike.

Further southeast, the Wan Ha and Mengxing faults form a complicated left-lateral fault system. They come within about 10 km of each other in their central reaches, but diverge toward the southwest (Wf & MXf; Fig. 12). Both curve southward near their southwestern termini and transform into southeast-striking normal faults. To the northwest, the nexus of these and the dextral-slip Lancang fault zone are series of extensional basins.

Two major river channels that flow across the ~140-km long **Wan Ha fault** show left-lateral deflections of several km. Lacassin et al. (1998) suggest that the Nam Loi River, which flows across the central part of the Wan Ha fault, is left-laterally offset about 5 km. Farther east, the Mekong River has a similar sized left-lateral curve along the easternmost trace of the fault (Fig.

15c). Matching the shape of these two river channels and the crest of a bedrock ridge, we derive a 5- to 6-km geomorphological left-lateral offset of the Wan Ha fault. Along its northeastern part, where the Wan Ha fault strikes nearly NNE-SSW along the eastern margin of a transtensional basin, SRTM topography shows clear left-lateral bends and deflections of channels. These small tectonic landforms imply activity of the fault during the Quaternary period.

The **Mengxing fault** traverses more than 180 km from near the Lancang fault to the Myanmar-Thailand border region, where both the Mekong and Nam Loi Rivers display a large left-lateral offset (Fig. 15c). Lacassin et al. (1998) noted the hairpin shape of the Nam Loi River and suggested that the sense of slip reversed from right- to left-lateral about 20 to 5 Myr ago. We estimate the left-lateral deflection of the Mekong River to be between 7 and 11 km and that of a small tributary just to the southwest to be ~11 km. This small tributary and the Mekong River are separated by a wind gap at the Mengxing fault (Fig. 15c). The Nam Loi River hairpin loop, however, shows 23 to 24 km of left-lateral deflection 56 km farther southwest. Both upstream and the downstream sections of the Nam Loi River are deeply incised into bedrock, so it is reasonable to surmise that the river has had little space to meander from its ancient to its current course. Moreover, there seems to be little possibility for this deflection to have been caused by river capture. The 23- to 24-km bend may be the largest geomorphological left-lateral offset on the Mengxing fault. This would imply that the smaller 11-km offset of the Mekong River and its tributary result from river capture after the initiation of left-lateral slip.

Nam Ma and Mae Chan faults

We now consider two larger left-lateral faults farther to the southeast in the central Shan-Sino domain (Fig. 12). The **Nam Ma fault** appears as a narrow 215-km long fault zone in the region of the Lao-Myanmar border, with a 12-14 km left-lateral offset of the Mekong River channel at the central part of the fault (Lacassin et al., 1998). The hairpin geometry of the Mekong River channel

here implies that a larger 30-km right-lateral offset preceded this left-lateral phase (Lacassin et al., 1998). Left-lateral offset across the 310-km long Mae Chan fault is smaller; landforms visible in SRTM topography suggest an offset of about 4 km (Table 2).

The Nam Ma fault terminates on both ends in transtensional basins. Consistent with the fault's left-lateral sense of slip, the basin at the northeastern terminus is in the block north of the fault, whereas the basin at the southeastern terminus is in the block to the south.

Two-hundred to 400-m left-lateral deflections of small river channels crossing the fault that we identify from SRTM and LANDSAT imagery imply that the fault is still active. Rupture of the westernmost 30 km of the fault during the Mw 6.8 Tarlay earthquake in March 2011 proved that the fault is still active (chapter 5 and 6).

Tectonic landforms along the **Mae Chan fault** are less clear than those along the Nam Ma fault. Perhaps this implies that the fault is slipping at a lower rate, as its smaller total geomorphic offset also implies. SRTM topography suggests that the fault has multiple traces west and south of the Mekong River. Farther west, the fault cuts through a Quaternary basin, within which it exhibits a ~50-m high north-facing scarp.

The epicenter of the Mw 6.3 earthquake of May 16th, 2007 is mid-way along the Mae Chan Fault, and the focal mechanism of the earthquake is consistent with the strike of the fault. A larger, M 6.8 earthquake in 1925 may have resulted from rupture of the eastern part of the Mae Chan fault (Table 1). However, neither an isoseismal map nor earthquake reports are available to constrain better the 1925 earthquake source.

Dien Bien Phu fault

The Dien Bien Phu fault forms the southeastern boundary of the Shan-Sino domain (Fig. 2 and Fig. 12). It is the southeasternmost active left-lateral fault between the right-lateral Red River and Sagaing faults. The fault is nearly but not quite co-linear with the left-lateral Xiaojiang fault system

on the opposite (north) side of the Red River fault and is southeast of the 40- to 60-km left-lateral bend of the Red River fault that has resulted from extrusion of the Sichuan-Yunnan block (e.g., Wang et al., 1998). Along its southern reaches, the Dien Bien Phu fault exists within the much older (Triassic) Nan Suture zone and multiple linear valleys imply that it fans into multiple left-lateral faults within a wide deformation belt.

Tectonic landforms are prominent along the southwestern and northern thirds of the 370-km long Dien Bien Phu fault. The central section of the fault may, in fact, not be active. SRTM topography along the northern (Vietnam) segment and the southern (Mekong) segment clearly shows river channel and alluvial fan offsets. The largest left-lateral geomorphological offset along the Vietnam segment is about 12.5 km (Lai et al., 2012). Numerous kinks in the Mekong River canyon parallel the Mekong River segment and may indicate large left-lateral offsets there as well. However, we are not confident that these left-lateral bends reflect left-lateral motion because we cannot restore small drainages and regional geomorphic or bedrock patterns in any consistent way.

The central (Nam Hou) segment of the Dien Bien Phu fault separates the Vietnam and Mekong segments by a 110 km stretch, along which evidence of young fault activity is weak. Young fluvial landscapes dominate the low-relief topography and the best evidence for the fault seems to be contrasts of bedrock. We find only weak geomorphic evidence of fault activity. Moreover, the Nam Hou River shows no evidence for tectonic warping where it crosses the fault. We suggest that the Nam Hou segment has experienced only very small left-lateral motions and that what deformation has occurred is distributed across a wide zone.

Some historical earthquakes may have been caused by the Dien Bien Phu fault. The Mw 6.8 earthquake of Nov 1935 occurred near the southern end of the Vietnam segment (Figure 12). Moreover, the Mw 6.2 earthquake of June 24, 1983, has a focal mechanism that is consistent with the strike of the fault.

The right-lateral faults

Summary

Two right-lateral fault systems define the western and northeastern flanks of the Shan-Sino domain (Fig. 2; Fig. 12). The western of these systems is nearly parallel to the Sagaing fault and extends about 200 km into the Shan-Sino domain (Fig 10). The northeastern set of faults is subparallel to the Red River fault and extends nearly 300 km into the Shan-Sino domain. These systems extend along most of the western and northeastern flank of the domain, but notably terminate northward near the Nanting fault system (Fig. 12).

Wuliang Shan fault zone

The Wuliang Shan fault zone is a diffuse, dextral shear zone 50 to 100 km southwest of the Red River fault. It extends nearly the entire 400-km length between the Nanting and Dien Bien Phu fault zones as a set of discontinuous dextral and normal faults. The strand that courses along the eastern flank of the Wuliang Shan range shows very large and significant dextral offset of the river channels. Dextral offsets there range from 300 m to more than 3 km. The largest dextral offset in SRTM topography is approximately 6 km, along the central part of the fault (Fig. 16a). Field investigations and interpretations of aerial photography supports our observation, suggesting right-lateral offsets of several hundred meters on several NNW-running faults within the Wuliang Shan fault zone (e.g., Guo, et al., 1999b).

The Wuliang Shan fault zone was very active in the 20th century. The last of five moderate earthquakes along the fault zone was an Mw 6.1 on June 2, 2007, near the city of Ning'er (Table. 1). Both the GCMT focal mechanism of the mainshock and the distribution of the relocated aftershocks (Lu and Zhou, 2011) are consistent with the general strike of and sense of slip on the Wuliang Shan faults. Other recent earthquakes, such as the Mw 6.0 of March 15, 1979 and the Mw

5.6 of January 26, 1993, also show GCMT focal mechanisms that are consistent with the strike and the slip sense of the Wuliang Shan fault.

Lancang fault zone

The right-lateral Lancang fault zone traverses a distance of about 210 km, between the left-lateral Nanting and Mengxing faults (Fig. 12). It forms the boundary between set of left-lateral and right-lateral faults. The fault is a simple strand in the north but a complex set of anastomosing faults in the south. Although a regional geological map shows that the Lancang fault offsets the Lincang batholiths 30 km left-laterally (e.g., Wang and Burchfiel, 1997), geomorphic offsets are clearly right-lateral. This implies a history of slip inversion as previously hypothesized for currently left-lateral faults in this region (Lacassin et al., 1998).

We estimate right-lateral slip across the Lancang fault system to be about 17 km, based on a series of right-lateral bends of the Nanguo River valley (Fig. 16b). If this offset began to accrue around 5 Ma, in concert with initiation of right-lateral slip on the Red River fault and left-lateral slip on the Xiaojiang fault (e.g., Lacassin et al., 1998; Wang et al., 1998; Leloup et al., 2007), then the average fault slip rate of the Lancang fault system is approximately 3.4 mm/yr. This rate is close to the higher bound of the 2 ± 2 mm/yr dextral rate estimated in the geodetic study of Shen et al., (2005).

The best seismic confirmation of the activity of the Lancang fault is a Mw 7.0 earthquake that occurred on Nov 6, 1988 (Table 1). An approximately 45-km long rupture occurred along the northern part of the fault accompanied the earthquake (Yu et al., 1991). A post-earthquake field survey found clear dextral slip at least at two locations along the main trace of the fault. At one of these locations, offset reached 1.4 m (Yu et al., 1991; Wang et al., 1991).

Kyaukkyan fault zone

The Kyaukkyan fault zone is a complex 500-km long right-lateral fault zone that lies within the western Shan plateau between ~18˚ and 22.5˚N, 100 to 150 km east of the Sagaing fault (Fig. 10). Its northern terminus nearly coincides with the western terminus of the left-lateral Kyaukme fault. The fault zone includes a 40-km wide right step with prominent active normal faults in the vicinity of Taunggyi. At 18˚N it intersects the Mae Ping fault zone, which arcs southeastward into Thailand (e.g., Morley et al., 2007). We separate the Kyaukkyan fault zone into three distinct segments, based primarily on its stepovers and geomorphic expression.

Myint Nge segment

The northern 160 km of the Kyaukkyun fault is east of Mandalay and north of Taunggyi, the capital of the Shan states (Le Dain et al., 1984). Tectonic landforms along this reach demonstrate clearly that it is an active dextral-slip fault (Fig. 17; Fig. S2). The largest of these is the offset of the Myint Nge River (Fig. 17a). This deeply incised river flows westward from the Shan plateau and down the Shan escarpment. At the fault crossing, it has a hairpin geometry that implies initial sinistral motion of 8 to 10 km followed by dextral offset of approximately 5 km (Fig. 17a & b).

The Northern segment of the Kyaukkyun fault produced one of the largest earthquakes in Myanmar's history on 23 May 1912 (Brown, 1917; Chhibber, 1934). Earlier reports assign it a magnitude of 8 (Gutenberg and Richter, 1954), but later studies re-assess its magnitude and revise it downward to Ms 7.7 to 7.6 (e.g., Abe and Noguchi, 1983; Pacheco and Sykes, 1992). The area of highest intensities encompasses the entirety of the Northern segment but does not extend close to Taunggyi (Brown, 1917; Wang et al., 2009; Fig. S4). The distribution of highest intensities and the size of the earthquake are consistent with rupture of the entire northern segment.

Taunggyi segment

Geomorphological expression of the Kyaukkyun fault zone becomes obscure as it extends southward toward Taunggyi, likely because it splays into several less-rapidly slipping traces (Fig. 10; Fig. 12). From 21.5°N the fault zone widens into several obscure strands that extend southward into a 50-km wide transtensional basin. This basin extends 100 km from north to south, to 20.3°N. The most obvious active faults associated with the basin are the two normal faults that bound it – the Pindaya fault on the west and the Taunggyi fault on the east.

Both of these two bounding normal faults show clear, youthful vertical displacements. The steep limestone escarpment of the east-facing Pindaya fault is at least 350 m high and the west-facing Taunggyi escarpment is about 400 m near the city of Taunggyi. Farther south, Inle Lake shows an asymmetric geometry that suggests eastward tilt of the basin associated with motion of the Taungyi fault. The western side of the lake is significant shallower than the eastern side (Fig 17c).

Although the limestone escarpment that extends from Taunggyi to Inle Lake is steep and rugged, we were unable in the field to find any small scarps along its base that might have indicated rupture within the past few centuries or millennia. Nonetheless, triangular facets and faulted alluvium indicate activity in the late Quaternary Period (Fig. 17c).

Salween segment

The Southern segment of the Kyaukkyun fault extends from the southern end of the transtensional basin southward ~220 km to the Mae Ping fault zone at the Salween River (Fig. 10). The maximum offset we found at this segment is ~4.7 km from the offset bedrock ridge and ~5.4 km from the offset Salween River, almost identical to the maximum offset we found at the northern segment of the Kyaukkyan fault. The major fault trace passes through the western bank of the Moybe dam (Fig. 10) and was covered by the young fluvial deposits south of the reservoir. Further

south, the fault trace bends nearly 20° westward at 19.2°N, and create a narrow transtentional basin along the Salween River. The southern segment of the Kyaukkyan fault connects to the Mae Ping fault zone at about 18.2°N. After merge with the Mae Ping fault zone, it continues runs ~170 km southeastward along the Thai-Myanmar border and may later entering the Mekong basin north of the Bangkok (e.g., Morley et al., 2007).

Mae Ping fault zone

We also find clear geomorphic evidence along the northwestern part Mae Ping fault that suggests the dextral slip along its fault trace. However, comparing to the Sagaing fault and the Kyaukkyan fault, the amount of dextral motion is smaller based on the maximum channel offsets we found along its fault trace. Between the Sagaing fault and the southern Kyaukkyan fault, we only find ~1.2 km dextral offset along the Mae Ping fault from the SRTM data. East of 97.5°N, the maximum dextral offset on the Mae Ping fault is ~2.5 km after the southern Kyaukkyan fault connects the Mae Ping fault system (Fig. 17d).

Partially reactivated faults of the Shan escarpment

A dramatic linear valley that parallels and lies between the Sagaing fault and the Kyaukkyun fault within the Shan escarpment, suggests the presence of a large strike-slip faults there (Fig. 10). The question for us is whether or not this large fault is active. The lack of disruption of small landforms along most of its trace implies that most of it is inactive. Perhaps it was an active element of the early to mid-Cenozoic extrusion of the Sunda block. In those few places where small drainages show right-lateral deflections, we show the fault as active on Figure 10.

Earthquakes past and future

The two principal motivations of our neotectonic study of Myanmar have been to understand the past occurrences of and future potential for large earthquakes in the Myanmar region.

Throughout the previous pages, we have accomplished the former by constructing a new neotectonic map that helps to make sense of many of the large earthquakes of the past century or so.

Looking to the future, public seismic safety will depend to a large extent on understanding the potential for other large earthquakes throughout this region. Our neotectonic map assists in this goal, as well. Many of the active faults within the region have not produced large earthquakes during the past century or more of human record-keeping, so what is their potential for the future?

Although what we have presented is by no means complete, our geomorphologic mapping augmented by seismic, geodetic and other relevant geological data, provides a fundamental basis for a simple evaluation of the predominant seismic sources for each of the three active tectonic domains of Myanmar and its neighboring countries. In this section we utilize our neotectonic understanding of these active faults to assess their potential for future rupture. The current scarcity of published structural information, high-quality seismological and geodetic data and paleoseismological information limits this effort to a pretty basic level. Nonetheless, we provide below a synoptic, first-order estimate of plausible earthquake scenarios within each domain.

Wells and Coppersmith (1994) (W&C) provide equations that relate rupture length to earthquake magnitude. Blaser et al., (2010) improved upon these scaling relationships by using a enlarged historical earthquake database. They also incorporated thrust fault ruptures in subduction environments, thus enabling better estimates of earthquake magnitude for such faults. Length-magnitude scaling relationships for subduction megathrusts have also been given by Strasser et al. (2010). These two independent scaling relationships help us to estimate the uncertainties in estimation of maximum earthquake magnitude produced by the megathrust along the western Myanmar coast. Table 3 lists the parameters that we used to calculate potential earthquake magnitude.

Although we used structural discontinuities, jogs and kinks to define structural segments and assumed that these segment boundaries delimit plausible future fault ruptures, we are well aware that fault ruptures sometimes propagate through such structural complications and thus produce larger earthquakes (e.g., Wesnousky, 2006). Currently, however, paleoseismological and historical documentation of rupture lengths in the Myanmar region are too sparse to warrant a sophisticated consideration of multiple–segment ruptures. In this first effort, we simply estimate magnitudes associated with single-segment rupture for the mapped faults. In some cases, we also use estimates of fault slip rate and published geodetic analyses to offer plausible average earthquake recurrence-times for these full-segment ruptures. These simplistic average recurrence intervals provide a useful starting point for future hazard analyses.

Table 4 summarizes the potential earthquake magnitudes we have calculated for all of the major structures. Below, we explain these results for the faults of each domain, starting in the west with the four domains of the Indoburman range and ending in the east with the Shan-Sino domain.

The Indoburman range

We will assess the seismic potential of the four domains of the Indoburman range from south to north, in the same order that we described them in the preceding section. In addition to the surface manifestation of these domains that appear in the maps of Figures 3a, 4a, 6 and 9a, we utilize four schematic cross-sections (Fig. 18 and 19), based upon available geological and seismicity data. Together the maps and cross-sections allow us to estimate the preliminary three-dimensional geometry of the megathrust and its relationship to large secondary structures. At this stage of our understanding of the geometries and kinematics of the region's active faults, it seems unwarranted to conduct a statistical analysis of plausible rupture areas, widths and slip amounts. We attempt here merely a crude first cut at assessing earthquake potential of the region. So for example, we do not attempt to include the range of uncertainty in the depth of down-dip

rupture limits for the megathrust; instead, we mainly use the length of fault mapped from the surface to assess the plausible maximum earthquake magnitude on the subduction zone interface.

Coco-Delta domain

We have described above a Coco-Delta domain dominated by a highly oblique plate interface that dips about 20° to 30° eastward (Dasgupta et al., 2003) (Fig. 18a). The orientation of this section of the megathrust (early parallel to the vector of relative plate motion), its steep dip and secondary features imply predominantly right-lateral slip across this oblique-reverse fault. A predominance of dextral slip within the domain, on the very northern part of the 2004 megathrust rupture (Chlieh et al., 2007), is consistent with this interpretation. The down-dip limit of its seismic rupture is likely shallower than the ~50-km down-dip limit of the adjacent megathrust farther south (Chlieh et al., 2007; Heurent et al., 2011), as its motion contains a large component of strike slip. However, the down-dip limit of the locked patch may still extend to about 20 or even 30 km, as the subducting oceanic lithosphere here is old and cold (> 80 Ma; Müller et al., 1997). We use the reverse fault and megathrust equations from both Blaser et al. (2010) and Strasser et al. (2010) of to estimate a Mw 8.6 to 8.9 range for the maximum earthquake that could be produced by this 480-km long segment (Table 4).

The fact that the southernmost part of this domain ruptured during the great 2004 earthquake (Meltzner et al., 2006), supports the suspicion that this section of the megathrust can accumulate tectonic strain and slip seismically. Moreover, large submarine landslides mapped by Nielsen et al., (2004) within this domain could well be evidence that the megathrust has produced high ground accelerations in the past. However, a complete rupture of the Coco domain megathrust segment would be very rare, because the ten or more meters of slip during such an event would take a millennium or longer to accumulate at the average slip rate of the fault, which could well be lower than 1 cm/yr.

In addition to the megathrust, we suggest that at least three other structures along the eastern flank of the Indoburman range may be capable of generating significant earthquakes (Table 4; Fig. 2 and Fig. 20). From their lengths, we estimate that Mw 7.6 to 7.7 earthquakes are plausible. Lacking reliable estimations of their fault slip rate, however, it would be speculative to estimate average return periods of such earthquakes.

Ramree domain

The Arakan earthquake of 1762 may represent the maximum earthquake within the Ramree domain, because it appears to have resulted from failure of the megathrust in combination with large splay faults in the upper plate (Wang et al., 2013a). If the megathrust ruptured across the entire length of the domain, from near Fouls Island to Chittagong (Figure 4), as Cummins (2007) suggests, then the magnitude would likely have been within the range Mw 8.5 and 8.8, based on the average coseismic fault slip on the megathrust fault plane (Wang et al., 2013a). This range of magnitudes is consistent with our estimation of the maximum earthquake magnitude based upon fault length (Blaser et al., 2010 and Strasser et al., 2010; Table 4).

Terrace- and coral-uplift records yield recurrence intervals ranging between about 400 to 1000 years for earthquakes that involve uplift of Ramree and Cheduba Islands (Shishikura et al., 2009; Wang et al., 2013a). This range is about twice as long as the 190- or 550-year recurrence interval calculated for Mw 8.6 to 8.8 earthquakes if the 23 mm/yr oblique plate convergence is fully taken up by slip on the 450-km long megathrust. This discrepancy implies either that the megathrust is not fully coupled or that the oblique Indian-Burman plate motion is partitioned between the megathrust and upper plate faults, such as the Thahtay Chaung fault within the Indoburman Range.

Upper-plate structures may fail separately from the megathrust and generate smaller, but nonetheless destructive earthquakes along the western Myanmar coast. The 1848 earthquake of

northern Ramree Island (Oldham, 1883) may be one of these events. It caused moderate damage to the city of Kyaukpyu, but the felt area was much more limited than that of the 1762 earthquake.

The great length of the right-lateral strike-slip Thahtay Chaung fault, within the Indoburman Range (Fig. 4a and 5) implies that this fault could generate the earthquake as large as Mw 7.6 (Wells and Coppersmith, 1994; Blaser et al., 2010). The lack of reliable written history in this mountainous region precludes knowing whether such an event has happened within the past 250 years. Moreover, a lack of constraints on the slip rate of the fault precludes us from saying anything meaningful about an average recurrence interval. Nevertheless, the existence of this large strike-slip fault within the Indoburman range gives good reason to hypothesize that large, destructive shallow earthquakes are plausible within the range.

The lengths of the west-dipping East Limb faults that crop out along the eastern flank of the Indoburman Range (Fig. 4a and 18b) imply that they are capable of generating Mw 7.8 and 7.3 earthquakes (Table 4). It is likely that these two faults may be connected in the subsurface by a blind thrust. If so, combined rupture could generate an even greater earthquake. The average recurrence interval of such an event along the eastern Indoburman Range would be greater than a thousand years, though, as GPS analysis shows the shortening rate across the eastern Indoburman Range and the central Burma basin is < 9 mm/yr (Socquet et al., 2006).

Several active reverse faults between Thayet-Myo and Yangon could generate large earthquakes along the floodplain of the Ayerawaddy River. Within the Ramree domain, the southernmost of these is the West Bogo-Yoma fault, on the eastern flank of the Ayerawaddy flood plain. The fault is likely a high-angle reverse fault that dips northeastward beneath the western flank of the Bago-Yoma Range. The length of the western Bogo-Yoma fault implies a maximum magnitude of Mw 7.2 to 7.3 for earthquakes near the Ayerwaddy flood plain north of Yangon. The Paungde fault, farther north along the Ayerwaddy flood plain, is longer, so we estimate that it is

capable of producing a Mw 7.3 to 7.4 earthquake in the vicinity of Prome. A related fault farther north likely produced the earthquake of 1858 and may have disrupted temporarily the flow of the Ayeyarwady River.

Before we leave the discussion of the Ramree domain, we should also note that rupture of faults within the downgoing slab could also produce damaging earthquakes in the region. Such hidden faults would not be manifest in our mapping of surface features, so we can say little more than that the existence of these should be contemplated in making a comprehensive seismic assessment of the region. The mb 6.5 Bagan earthquake of 1975 was an event of this type. Its hypocentral depth was about 120 km (Engdahl and Villasenor, 2002). The earthquake ruined several temples in the ancient capital of Burma that are believed to have been built in about the 12th century.

Dhaka domain.

The Dhaka domain is defined by the length and width of the broad belt of folds of the Chittagong-Tripura fold belt. As such it extends nearly 600 km along strike from south to north and more than 200 km from west to east. If the blind megathrust underlying this entire domain were to fail at once, the resulting earthquake would likely have a magnitude of about Mw 8.9 (Blaser et al., 2010; Table. 4).

Whether such a large event is plausible is currently a matter of some debate. Recent GPS studies above the megathrust show that the Indoburman Range is moving westward at least 5 mm/yr relative to the Indian plate (Steckler et al., 2012; Gahalaut et al., 2013). Whether this E-W shortening is reflects aseismic creep on or strain accumulation across the megathrust remains unclear. Gahalaut et al. (2013) argue the seismic risk from the underlying plate interface event is low because the E-W shortening on the N-S running megathrust is so low and they find no earthquakes in the history were sourced from the plate-interface. Steckler et al. (2008) argue from

comparison with other megathrusts with sediment-rich accretionary prisms that this section of the megathrust may well be capable of producing large earthquakes, even through the prism's internal strength and basal friction are weak.

The lack of large historical earthquakes in the past 400 to 500 years for this portion of the megathrust does not mean the risk of such large megathrust event is low. In fact, if elastic E-W shortening is indeed only 5 mm/yr, it would take nearly 1000 years to accumulate enough slip potency for an Mw 8.9 earthquake on a fully coupled 520-km long and 350-km wide megathrust. If the megathrust is semi-coupled, as many megathrusts are (e.g. Chlieh et al., 2008; Hsu et al., 2012), the recurrence interval of such events would be even longer.

Regardless of whether the megathrust/décollement is capable of producing a giant earthquake, many upper-plate structures associated with actively growing young anticlines (Fig. 6) are undoubtedly capable of producing earthquakes, either in association with failure of the megathrust or individually. Using the lengths of young anticlines as indicators of the lengths of the underlying faults, we calculate plausible maximum earthquake magnitudes ranging from Mw 6.3 to 7.7 (Table 4). The 1918 Mw 7.5 earthquake near the Rashidpur anticline may be an example of such an event. The 1999 mb 5.2 earthquake near the Maheshkhali anticline may be an example of partial failure of one of these faults.

Several other moderate but destructive earthquakes have struck within the fold belt during the pre-instrumental historical period. From the records of shaking alone, however, one cannot be certain that these were produced by failure of secondary structures above the megathrust. They could also have been caused by rupture of faults within the descending plate, beneath the décollement. Speculating about the recurrence intervals of these earthquake sources is not particularly useful because so little is known about the rate of slip on these structures or how their ruptures relate to ruptures of the subjacent megathrust/decollement.

Ruptures of faults within the down-going Indian Ocean lithosphere farther east are another plausible source of destructive earthquakes. One example is the Ms 7.4 earthquake of 1954, which struck east of the Indoburman Range. Its hypocentral depth is 180 km (Engdashi and Villasenor, 2002), clearly within the Wadati-Benioff zone of the downgoing slab. Fortunately, sources deeper than about 50 km within the Wadati-Benioff zone pose relatively low seismic hazard, because such ruptures are far from human infrastructure at the Earth's surface. Shallower sources, however, within the subducting Indian Ocean lithosphere west of the crest of the Indoburman range, could cause destructive earthquakes within the populated regions of Bangladesh. Destructive earthquakes in Bangladesh in 1842 and 1885, for example, are reasonable intraslab candidates, as there is no geomorphic evidence of surface deformation near their proposed epicenters.

As in the Ramree domain to the south, the Dhaka domain has seismic faults within and east of the high Indoburman range. The Churachandpur-Mao fault is the most prominent of these. Judging by its 170-km length, wholesale failure of this right-lateral fault could produce an Mw 7.6 earthquake. The geodetic analysis of Gahalaut et al. (2013) suggests, however, the fault may be slipping aseismically. Aseismic slip along active strike-slip faults is usually associated with minor to moderate earthquakes (Lienkaemper et al., 1991). However, we did not find any historical events that could be related to the Churachandpur-Mao fault in the earthquake catalog of Szeliga et al. (2010), nor does the instrument catalog show a high level of seismic activity along the fault.

The ~280-km length of the eastward dipping Kabaw fault implies that it could generate an Mw 8.4 earthquake if it were to fail all at once (Table 4). The average interval between such earthquakes would be a millennium or longer, since geodetic analysis suggests the fault slip rate must be lower than 9 mm/yr (Socquet et al., 2006).

Naga domain

The southeastward-dipping Naga thrust fault is the principal seismic source within the Naga domain (Fig 9). The 400-km length of the fault implies a maximum earthquake of Mw 8.5 to 8.7 (Table 4). The structural cross section from Kent (2002) suggests the dip of the Naga thrust fault is about 23°, higher than the dip angle of the megathrust of the Dhaka and Ramree domains. In addition to being distinguished by a steeper dip, the fault is also distinguished by the fact that it is the interface between two pieces of continental lithospheres (Fig. 19b; Fig. 1a), rather than the convergent boundary between oceanic lithosphere and the continental lithosphere.

Using the equations from Blaser et al. (2010) and Strasser et al. (2010), we estimate that the Naga thrust fault is capable of producing an Mw 8.5 to 8.7 earthquake, similar in size to the great Assam earthquake of 1950, which resulted from rupture of the Himalayan Frontal Thrust, just to the north. On the other hand, it is plausible that each of the three 100- to 150-km long arcuate lobes we have mapped commonly fail individually. In such a case, the magnitude of the largest Naga thrust earthquakes would be in the Mw 7.7 to Mw 8 range.

The slip rate of the Naga thrust fault is constrained neither by GPS vectors spanning the fault nor by vectors from plate-motion models. GPS vectors on either side of the western part of the Naga thrust are similar, so it appears that there is no shortening across this thrust fault system (Jade et al., 2007; Maurin et al., 2010). This ostensibly conflicts with recent field investigations that show the Naga thrust overrides Quaternary alluvium at the mountain front (Aier et al., 2011). Clearly, additional work will be needed to resolve this important question about the seismic potential of the fault.

Although we did not find any evidence of active faults along the southeastern flank of or within the northern Indoburman range (Fig. 9a), some intraslab earthquakes occur within the down-going Indian plate beneath the range. Although the intraslab events in the Naga domain were

not as frequent as those in the Dhaka domain, failure of faults within the subducting plate poses a potential hazard within the Naga domain. In addition, several earthquakes greater than magnitude 6 have occurred along the southeastern margin of the northern Indoburman range. These include a magnitude 7 earthquake in 1932 and an Mw 7.2 earthquake in 1988 (Engdashi and Villasenor, 2002). Both of these two events originated at depths greater than 90 km. Although their hypocenters are deep, the 1988 earthquake still caused some damages to the nearly regions.

The Sagaing fault

The 60- to 260-km range of segment lengths along the right-lateral Sagaing fault imply a range of maximum magnitudes from Mw 7 to 8 (Table 4; Fig. 20). This is consistent with the observation that during the first half of the 20th century, more than half of the fault appears to have ruptured in several earthquakes with magnitudes in the mid-7 range (Brown and Leicester, 1933; Hurukawa and Phyo Maung Maung, 2011) (Fig. 21). This historical behavior of the Sagaing fault appears quite similar to that of the more-highly segmented Sumatran fault through the first half of the 20th century (Daryono et al., 2012). The early-20th century clustering of large ruptures is also similar to the behavior of the North Anatolian fault, which produced several low- to high-7 earthquakes in the 20th century (e.g., Stein et al., 1997).

One notably (and perhaps ominously) quiet section of the fault is the 220-km long Meiktila segment, between the large city of Mandalay and the new capital of Naw Pyi Daw. This long quiet section separates the southern set of ruptures of 1929 and 1930 from the northern set of ruptures between 1931 and 2012. The length of the Meiktila segment implies it is capable of producing an earthquake as large as Mw 7.8 to 7.9, if it ruptures all at once (Wells and Coppersmith, 1994; Blaser et al., 2010; Table 4).

We speculate, on the basis of sparse historical records of shaking, that the 1839 Ava earthquake may have resulted from the failure of Meiktila segment, in conjunction with the Sagaing

segment, its neighbor on the north. If the Meiktila segment has been dormant since then, and the fault is fully coupled down to 12 to 15 km at depth, as Vigny et al. (2003) and Socquet et al. (2006) suggest, then we estimate the slip potency that has accumulated on the Meiktila segment to be enough to generate a Mw 7.6 earthquake.

We further estimate the average interval of an Mw 7.8 to 7.9 earthquake on the Meiktila segment to be about 330 to 460 years, based on the 18 mm/yr slip accumulation rate on a 220-km long vertical fault that is locked to 15 km at depth, as modeled from GPS data by Vigny et al. (2003). The estimated recurrence intervals of the Pyu and Bago segments, farther south, are much shorter, no more than 200 to 300 years, because slip per event for these shorter segments is much less. Paleoseismological investigations along the southern Sagaing fault suggest even shorter recurrence intervals, just 100 to 150 years (Tsutsumi and Sato, 2009; Wang et al., 2011). This even lower range of intervals results from even shorter rupture lengths (e.g., Wells and Coppersmith, 1994; Blasser et al., 2010).

The earthquake histories and complicated fault geometry of the northern half of the Sagaing fault imply a more complex behavior than that of the southern half of the fault. The segment lengths of the northern half of the fault yields a range of maximum earthquake magnitudes from about Mw 7.0 to 8.0 (Table 4; Fig. 21). These estimates may be high, however, because a recent geodetic analysis suggests the locking depth of the northern Sagaing fault is just ~5 to 7 km (Maurin et al., 2010), far more shallow than for most of the faults used in the global length-magnitude scaling relationships.

We have chosen in our analysis of plausible earthquakes to assume that each segment will rupture completely during future earthquakes. Nonetheless, it is clear that this is not always the case. The recent earthquake of a short portion of the Sagaing segment in November 2012 is an example of the partial failure of a segment. This Mw 6.8 earthquake took place along just part of a segment

that most likely ruptured wholly during a larger Mw 7.7 earthquake in 1946 (Fig. 21). Perhaps coincidentally, the slip potency accumulated on the 40-km long 2012 fault-rupture in the years between 1946 and 2012 roughly equals the potency of the 2012 event, if the rupture extended to 12 km. The 180-km long Sagaing segment illustrates well that our assumption of whole-segment rupture is a gross simplification of reality. One could calculate return periods of just decades for Mw 6.8 to Mw 7.0 partial failure events or Mw 7.7 whole-segment failures about every 350 years.

The historical record of the northern half of the Sagaing fault may illustrate another complexity as well – multi-segment rupture. One plausible example of this is the combined rupture of Meiktila and the Sagaing segment during the great 1839 earthquake. The boundary between these two segments is less well defined than other segment boundaries along the fault, so it may be that our assignment of that segment boundary is a bit tenuous. If the fault rupture propagates through both the Meiktila and the Sagaing segment, its length would be about 400 km. The earthquake produced by such a long rupture could have a magnitude between Mw 8.1 and 8.3 (Wells and Coppersmith, 1994; Blaser et al., 2010). The slip associated with such a long rupture would be so large that its return time would be longer than 500 to 1000 years.

Shan-Sino domain

We have identified 27 active faults systems within the Shan-Sino domain. The lengths of these faults range from about 30 to more than 480 km (Table 2). Our mapping suggests that maximum geomorphically expressed offsets range from approximately one to more than 20 km for these strike-slip fault systems (Table 2; Fig. 22).

From length-magnitude relationships, we estimate maximum earthquake magnitudes that range from about Mw 6.5 to 8.4 (Wells and Coppersmith, 1994; Blaser et al., 2010 Table 4; Fig. 22). For comparison, the earthquake catalogue for the past century shows the largest magnitude is 5.5 to

7.7 (Table 1; Table 4; Fig. 12). The difference between the estimated and actual maximum magnitudes suggests that most historical events involved partial failure of the fault.

The 1988 Mw 7.0 Lancang earthquake is one example of partial failure. The highest intensities (MMI ≥ VIII) and a ~45-km long surface rupture occurred along the northwestern part of the 200-km long dextral-slip fault (Yu et al., 1991; Fig. 12).

The 2011 Mw 6.8 Tarlay earthquake is another example of partial failure of one of these strike-slip faults. Measurements of the surface rupture from satellite imagery and field measurements show clearly that only the westernmost 30 km of the Nam Ma fault ruptured during this earthquake. The rupture spanned the entire length of a segment of the fault that terminates eastward in a pull-apart basin (Wang et al., 2013b). Other examples include partial failures of the Kyaukkyun fault during the 1912 Mw 7.7 earthquake and of Nanting fault during a magnitude 7 earthquake in 1941. Although the surface ruptures of these early 20th-century earthquakes were not mapped in the field, isoseismal maps in both cases imply that rupture of the faults was partial (Brown, 1917; Compilation Group of China Seismic Intensity Zoning Map SSB, 1979; Fig. 12). These examples and the commonly moderate size of earthquakes along the strike-slip faults of the Shan-Sino domain show that partial rupture of these faults is typical.

We now use the maximum geomorphically expressed offset and estimated ~5 Ma age of these offsets (Lacassin et al., 1998; Wang et al., 1998) to calculate fault-slip rates for the strike-slip faults of the Shan-Sino domain. These first-order slip rate estimations (Table 4) allow us to speculate about the average frequency of whole-fault or partial ruptures by estimating the seismic moment accumulation rate on the given fault plane. Most of the average fault-slip rates are lower than 4 mm/yr. Two exceptions are the 4 to 5 mm/yr rates of the Nanting fault and the Menglian fault. These estimated low fault slip rates imply recurrence interval > 1000 years for each of the slower-slipping faults. For example, we estimate an average recurrence interval of 3000 years for

the maximum (Mw 7.5) earthquake on the Daying River fault. The 180-km long Mengxing fault is one of the fastest moving faults, but its maximum (Mw 7.7) earthquake would recur only about every 1300 years.

Although the low fault-slip rates of these faults means long recurrence intervals for complete rupture of any one fault, the large number of faults and their common partial rupture mean that earthquakes are still very frequent throughout the domain. In fact, about 14 moderate to strong (Mw 6.7 to Mw 7.7) earthquakes occurred within the Shan-Sino domain during the past century – on average about one every eight years. If we assume that an average partial failure of these faults produces a Mw 7.0 earthquake, which is slightly smaller than the averaged earthquake magnitude of these 14 destructive earthquakes in the past century, we calculate a recurrence of about 15 years for the whole domain.. This recurrence interval is, however, about half the average interval of the past century. This implies that throughout the past century the Shan-Sino domain has been experiencing an episode of activity than is higher than its average level over the millennia. This speculation is supported by the observation that total seismic moment released during these historical earthquakes is about three times higher than the seismic moment that would have been accumulated based on their fault slip rates.

Conclusions

Geomorphologically evident active faults and folds of the Myanmar region comprise three majors systems, which accommodate the northward translation of the Indian plate into the Eurasian plate and the extrusion of crust around the eastern syntaxis of the Himalaya. The western of these three systems comprises four distinct neotectonic domains, each distinguished by a unique geometry of the Sunda subduction/collision megathrust. Distinct active hangingwall structures within each of these four domains include large strike-slip faults and both blind and surface-rupturing thrust faults. The Sagaing fault comprises the second of the three systems.

Second-order structural characteristics of this ~1200-km long domain suggest division into 12 segments. Historical seismicity confirms that to a large degree these structurally defined segments constrain seismic ruptures. The third of the neotectonic systems is the Shan-Sino domain, a large region of conjugate left- and right-lateral active faults that accommodate extrusion of material around the eastern Himalayan syntaxis.

Empirical global relationships between fault length and earthquake magnitude allow us to estimate maximum magnitudes for the active faults in each of these domains. The lengths of these structures imply that most are capable of generating events greater than Mw 7.0. However, the historical and instrumental records show that smaller earthquakes are common during partial rupture of these faults. Each of the four megathrust segments are capable of producing an earthquake of Mw 8.5 or greater, but only one has done so in the period of historical record. Estimates of slip rates for the faults of the Shan-Sino domain and empirical relationships between fault length and magnitude suggest that recurrence intervals for complete rupture of these faults are typically several thousand years. Seismic moment release in this domain during the past century may have been greater the millennially averaged rate. In contrast, empirical relationships and historical seismicity show that ruptures of each segment of the Sunda megathrust and the Sagaing fault should rupture on average every several hundred years.

Our analysis of these active, seismogenic faults serve provide a foundation for more formal evaluations of seismic hazard, risk and exposure of the Myanmar region.

Acknowledgments

We have benefited greatly from discussions with Win Swe and other friends in Myanmar during our stay in Yangon. We also appreciate assistance from members of the Myanmar

Geosciences Society (MGS), the Department of Meteorology and Hydrology (DMH) of Myanmar since 2006.

References

Abe, K. and S. Noguchi (1983) Revision of magnitudes of large shallow earthquakes, 1897 – 1912, Phys. Earth Planet. Int. 33, 1-11.

Aier, I, K. Luirei, S.S. Bhakuni, G. T. Thong, G. C. Kothyari (2011) Geomorphic evolution of Medziphema intermontane basin and Quaternary deformation in the schuppen belt, Nagaland, NE India, Zeitschrift für Geomorphologie, 55(2), 247-265.

Alam, M., 1989. Geology and depositional history of Cenozoic sediments of the Bengal Basin of Bangladesh. Palaeogeography, Palaeoclimatology, Palaeoecology 69, 125–139.

Allen, T. I., K. D. Marano, P. S. Earle, and D. J. Wald (2009), PAGER-CAT: A composite earthquake catalog for calibrating global fatality models, Seismol. Res. Lett., 80, 57–62, doi:10.1785/gssrl.80.1.57.

Amante, C. and B. W. Eakins (2009) ETOPO1 1 Arc-Minute Global Relief Model: Procedures, Data Sources and Analysis. NOAA Technical Memorandum NESDIS NGDC-24, 19 pp, March 2009.

Ansary, M.A., Al-Hussaini, T.M.and Sharfuddin, M. (2000), Damage Assessment of July 22, 1999 Moheshkhali Earthquake, Bangladesh, Proc., PMC-2000, 8th ASCE Specialty Conference on Probabilistic Mechanics & Structural Reliability, Indiana, USA.

Armijo, R., P. Tapponnier, P., H. Tonglin (1989), Late Cenozoic right-lateral strike-slip faulting in southern Tibet. J. Geophys. Res. 94, 2787 – 2838.

Banerjee, P., R. Bürgmann, B. Nagarajan, and E. Apel (2008), Intraplate deformation of the Indian subcontinent, Geophys. Res. Lett., 35, L18301, doi:10.1029/2008GL035468.

Bender, F. (1983), Geology of Burma, 293, Gebruder Borntraeger, Berlin.

Berger, P., et al., (1983), Assam–Arakan basin: Schlumberger Well Evaluation Conference India, 1134–1170.

Bertrand, G., et al. (1998), The Singu basalts (Myanmar): New constraints for the amount of recent offset on the Sagaing Fault, C. R. Acad. Sci., Ser. IIa, 327, 479–484.

Blaser, L., F. Krüger, M. Ohrnberger & F. Scherbaum (2010), Scaling relations of earthquake source parameter estimates with special focus on subduction environment, Bull. seism. Soc. Am., 100(6), 2914–2926.

Brown C (1929), The Rangoon earthquakes of September and December 1927. Rec Geol. Surv. India LXII p.258.

Brown C (1932), A note on the Swa earthquake of August 8th, 1929. Rec Geol. Surv. India LXVI p.244.

Brown, C. (1917), The Burma earthquake of May 1912, Memoirs of the Geological Survey of India, 42(1), 1–147.

Brown, C.J., P. Leicester, and H.L. Chhibber (1931), A preliminary note on the Pegu earthquake of May 5th, 1930, Rec. Geol. Surv. India, 65, 221–284.

Brown, J.C. and P. Leicester (1933), The Pyu earthquake of 3rd and 4th December, 1930 and subsequent Burma earthquakes up to January 1932. Memoirs of the Geological Survey of India, 42, 1-140.

Brune, J. N., J. Curray, L. Dorman, R. Raitt (1992), A proposed super-thick sedimentary basin, Bay of Bengal, Geophys. Res. Lett., 12, 565–568.

Brunnschweiler, R. O. (1966), On the geology of the Indo-Burma ranges, J. Geol. Soc. Aust., 13, 127–194.

Bureau of Geology and Mineral Resources of Yunnan (1993). Geological map of Yunnan, scale 1:500,000.

Bustin, A. M. M., R. D. Hyndman, H. Kao, and J. F. Cassidy (2007), Evidence for underthrusting beneath the Queen Charlotte margin, British Columbia, from teleseismic receiver function analysis, Geophys. J. Int., 171, 1198–1211, doi:10.1111/j.1365-246X.2007.03583.x.

Chang, Z.F., G. Chen and J.Q. Yu (2011), Geological evidence of Activity Along the Dayyingjiang fault since late Pleistocene, Seismology and Geology, 33(4), 877 – 888. DOI: 10.3969/j.issn.0253-4967.2011.04.012 (Chinese with English abstract).

Chang, Z.F., X.W. An, Y.F. Zhang (2012). Study on late-Quaternary Activity and Displacement of drainage systems along the Wanding fault. Seismology and Geology, 34(2), 228 – 239. doi:10.3969/j.issn.0253-4967.2012.02.00.

Chen Q F ed-in-chief (2002). Earthquake Cases in China (1995–1996). Seismological Press, Beijing, 1–488 (in Chinese).

Chhibber H.L., 1934, Geology of Burma: London, McMillan, 538 p.

Chlieh, M., et al. (2007), Coseismic slip and afterslip of the great (Mw 9.15) Sumatra-Andaman earthquake of 2004, Bull. Seismol. Soc. Am., 97, S152–S173, doi:10.1785/0120050631.

Chlieh, M., J. P. Avouac, K. Sieh, D. H. Natawidjaja, and J. Galetzka (2008), Heterogeneous coupling of the Sumatran megathrust constrained by geodetic and paleogeodetic measurements, J. Geophys. Res., 113, B05305, doi:10.1029/2007JB004981.

Clark, M. K., and R. Bilham (2008), Miocene rise of the Shillong Plateau and the beginning of the end for the Eastern Himalaya, Earth Planet. Sci. Lett., 269, 336–350.

Coates, D.A., A.K.M.K. Alam (1990), The Mymensingh Terrace: evidence of Holocene deformation in the delta of the Brahmaputra river, central Bangladesh. Geol. Soc. Amer. Bull. 22, 310 Abstracts with Program.

Compilation Group of China Seismic Intensity Zoning Map SSB (1979): Atlas of Chinese Earthquake Isoseismals, Seismological Press, Beijing. (in Chinese).

Cummins, P. R. (2007), The potential for giant tsunamigenic earthquakes in the northern Bay of Bengal, Nature, 449, 75–78.

Curiale, J.A., G.H. Covington, A.H.M. Shamsuddin, J.A. Morelos, and A.K.M. Shamsuddin (2002), Origin of petroleum in Bangladesh: AAPG Bulletin, 86(4), 625-652.

Curray, J. R. (2005), Tectonics and history of the Andaman Sea region, J. Asian Earth Sci., 25, 187–228.

Curray, J. R., F. J. Emmel, D. G. Moore (2003), The Bengal fan: morphology, geometry, stratigraphy, history and processes, Mar. Pet. Geol., 19, 1191–1223.

Curray, J. R., (1991), Possible greenschist metamorphism at the base of a 22-km sedimentary section, Bay of Bengal, Geology, 19, 1097–1100.

Curray, J.R., D.G. Moore, L.A. Lawver, F.J. Emmel, R.W. Raitt, M. Henry & R. Kieckhefer (1979). Tectonics of the Andaman Sea and Burma, Am. Assoc. Petrol. Geol. Mem., 29, 189–198.

Curray, J.R., F.J. Emmel, D.G. Moore, R.W. Raitt (1982). Structure, tectonics and geological history of the northeastern Indian Ocean. In: Nairn, A.E.M., Stehli, F.G. (Eds.), The Ocean Basins and Margins. The Indian Ocean, vol. 6. Plenum Press, New York, pp. 399–450.

Dahlen, F. A., J. Suppe, and D. Davis (1984), Mechanics of fold-and-thrust belts and accretionary wedges: Cohesive Coulomb Theory, J. Geophys. Res., 89(B12), 10087–10101, doi:10.1029/JB089iB12p10087.

Daryono, M., D.H. Natawidjaja, K. Sieh, (2012), Twin-Surface Ruptures of the March 2007 M > 6 Earthquake Doublet on the Sumatran Fault, Bull. Seismol. Soc. Am., 102(6), 2356-2367, doi: 10.1785/0120110220.

Dasgupta, S., et al. (2003), The geometry of the Burmese-Andaman subducting lithosphere, J. Seismol., 7, 155–174.

Davis, D., J. Suppe, and F. A. Dahlen (1983), Mechanics of fold-and-thrust belts and accretionary wedges, J. Geophys. Res., 88(B2), 1153–1172, doi:10.1029/JB088iB02p01153.

DeMets, C., R.G. Gordon, and D.F. Argus (2010), Geologically current plate motions, Geophys. J. Int., 181(1), 1-80, doi: 10.1111/j.1365-246X.2009.04491.x.

Densmore, A. L., M. A. Ellis, Y. Li, R. Zhou, G. S. Hancock, and N. Richardson (2007), Active tectonics of the Beichuan and Pengguan faults at the eastern margin of the Tibetan Plateau, Tectonics, 26, TC4005, doi:10.1029/2006TC001987.

Engdahl, E.R. & A. Villaseñor (2002), Global Seismicity: 1900–1999, International Handbook of Earthquake and Engineering Seismology, v. 81A, Elsevier Science Ltd., Amsterdam, The Netherlands, 665–690.

Fitch, T. J. (1972), Plate convergence, transcurrent faults, and internal deformation adjacent to southeast Asia and the western Pacific, J. Geophys. Res., 77, 4432–4457.

Frankel, K.L. et al. (2008), Active tectonics of the eastern California shear zone, in Field Guide to Plutons, Volcanoes, Reefs, Dinosaurs, and Possible Glaciation in Selected Areas of Arizona, California, and Nevada, Geol. Soc. Am. Field Guide, 11, pp. 43–81, eds E.M. Duebendorfer & E.I. Smith, Geological Society of America, Boulder , CO , doi:10.1130/2008.fld011(03).

Gahalaut VK, Kundu B, Laishram SS, Catherine JK, Kumar A, Devchandra M, Tiwari RP, Chadha RK, Samanta SK, Ambikapathy A, Mahesh P, Bansal A, Narsaiah M (2013) Aseismic plate boundary in the Indo-Burmese wedge, northwest Sunda Arc. Geology 41:235–238. doi:10.1130/G33771.1.

Gomberg, J., P. Bodin, W. Savage, and M. E. Jackson (1995), Landslide faults and tectonic faults, Analogs?—The slumgullion earthflow, Colorado, Geology, 23, 41–44.

Goodbred, S.L. Jr., S.A. Kuehl (1999), Holocene and modern sediment budget for the Ganges–Brahmaputra river system: evidence for highstand dispersal to flood-plain, shelf, and deep-sea depocenters. Geology 27, 559–562.

Guo, S.M., H.F. Xiang, X.W. Xu et al., (1999a) The preliminary study on late Quatrnary activity of Dayingjiang fault zone, western Yunnan Province. In: Institute of Geology, CEA(ed). Research on Active fault (7). Seismological Press, Beijing (in Chinese).

Guo, S.M., Y. Wang, F.J. Ji., (1999b) Tectonic mechanism of moderate-strong swarms in Yunnan's Simao-Pu'er region. J. Seism. Res., 22(2), 105-115 (in Chinese with English abstract).

Gupta, H. and V. Gahalaut (2009), Is the Northern Bay of Bengal Tsunamigenic? Bull. Seism. Soc. Am., 99(6), 3496–3501.

Gutenberg, B. and C.F. Richter (1954), Seismicity of the earth and Associate Phenomena, Princeton University Press, Princeton.

Guzman-Speziale, M., and J. F. Ni (1993), The opening of the Andaman Sea: Where is the short-term displacement being taken up, Geophys. Res. Lett., 20, 2949– 2952.

Halsted, E. P. (1841), Report on the Island of Chedooba, J. Asiatic Soc. Bengal, 114, New Series No. 27, 419–436.

Heuret, A., S. Lallemand, F. Funiciello, C. Piromallo, and C. Faccenna (2011), Physical characteristics of subduction interface type seismogenic zones revisited, Geochem. Geophys. Geosyst., 12, Q01004, doi:10.1029/2010GC003230.

Hla Maung (1987), Transcurrent movements in the Burma-Andaman Sea region, Geology, 15, 911 –912.

Hsu, Y.-J., S.-B. Yu, T.-R. Song, T. Bacolcol, (2012). Plate coupling along the Manila subduction zone between Taiwan and northern Luzon, J. Asian Earth Sci. 51(2), 98-108.

Huang, X.M., Y. Du, S.B. Shu and F.R. Xie (2010). Study of the Late Quaternary Slip Rate Along the Northern Segment on the south branch of the Longling-Ruili fault. Earthquake Research in China, 24(4), 456-466.

Hurukawa, N., and P. Maung Maung (2011), Two seismic gaps on the Sagaing Fault, Myanmar, derived from relocation of historical earthquakes since 1918, Geophys. Res. Lett., 38, L01310, doi:10.1029/2010GL046099.

Hutchinson, C. S.(1989), Geological Evolution of SE Asia, Oxford Monographs on Geology and Geophysics, 3, 368, Clarendon, Oxford, England.

Jade, S., M. Mukul, I. A. Parvez, M. B. Ananda, P. D. Kumar, and V. K. Gaur (2002), Estimates of coseismic displacement and post-seismic deformation using Global Positioning System geodesy for the Bhuj earthquake of 26 January 2001, Curr. Sci., 82, 748–752.

Jarvis, A., H.I. Reuter, A. Nelson, E. Guevara, (2008), Hole-filled SRTM for the globe Version 4, available from the CGIAR-CSI SRTM 90m Database (http://srtm.csi.cgiar.org).

Johnson, S. Y., and N. Alam (1991), Sedimentation and tectonics of the Sylhet Trough, Bangladesh, Geol. Soc. Am. Bull., 103, 1512–1527.

Kent, W.N., R.G. Hickman & U. Dasgupta (2002), Application of a ramp/flat-fault model to interpretation of the Naga thrust and possible implications for petroleum exploration along the Naga thrust front, AAPG Bull., 86, 2023–2045.

Khan, M.S.H., B. Parkash, S. Kumar (2005), Soil-landform development of a part of the fold belt along the eastern coast of Bangladesh. Geomorphology 71, 310-327.

Kreemer, C., W.E. Holt, and A.J. Haines (2003), An integrated global model of present-day plate motions and plate boundary deformation. Geophys. J. Int., 154: 8–34. doi: 10.1046/j.1365-246X.2003.01917.x.

Kumar, A., M. Sanoujam, L. Sunil, T. Dolendro (2011), Active Deformations at the Churachandpur Mao Fault (CMF) in Indo Burma Ranges: Multidisciplinary Evidences, Int. J. Geosci, 2, 597-609, doi:10.4236/ijg.2011.24062.

Lacassin, R., A. Replumaz, and P. H. Leloup (1998), Hairpin river loops and slip-sense inversion on southeast Asian strike-slip faults, Geology, 26, 703–706.

Lai, K.Y., Y.G. Chen, D.Đ. Lâm (2012) Pliocene to present morphotectonics of the Dien Bien Phu fault in northwest Vietnam. Geomorphology, 173-174, 52-68. DOI:10.1016/j.geomorph.2012.05.026.

Le Dain, A. Y., P. Tapponnier, and P. Molnar (1984), Active faulting and tectonics of Burma and surrounding regions, J. Geophys. Res., 89, 453–472.

Lei, J., G. Zhang, F. Xie, Y. Li, Y. Su, L. Liu, H. Ma and J. Zhang, (2012), Relocation of the 10 March 2011 Yingjiang, China, earthquake sequence and its tectonic implications, Earthq Sci, 25, 103-110. doi:10.1007/s11589-012-0836-4.

Leloup, P.H., P. Tapponnier, and R. Lacassin, (2007), Discussion on the role of the Red River shear zone, Yunnan and Vietnam, in the continental extrusion of SE Asia. J. Geol. Soc., 164: 1253–1260.

Li, C., R. van der Hilst, A. S. Meltzer, and E. R. Engdahl (2008), Subduction of the Indian lithosphere beneath the Tibetan Plateau and Burma, Earth Planet. Sci. Lett., 274, 157–168, doi:10.1016/j.epsl.2008.07.016.

Lienkaemper, J. J., G. Borchardt, *and* M. Lisowski *(*1991*),* Historic creep rate and potential for seismic slip along the Hayward Fault, California*,* J. Geophys. Res.*, 96(*B11*),* 18261–18283*, doi:*10.1029/91JB01589*.*

Lu, X. and L.Q. Zhou, (2011), Accurate location of the 2007 Ms 6.4 Ning'er, Yunnan, earthquake sequence, Seism. Geol., 33(3), 560-567. doi:10.3969/j.issn.0253-4967.2011.03.006.

Mallet, F. R. (1878), The Mud volcanoes of Ramri and Cheduba, Geol. Surv. India Rec., 11, part 2, 188–207.

Martin, S., and W. Szeliga (2010), A catalog of felt intensity data for 570 earthquakes in India from 1636 to 2009, Bull. Seismol. Soc. Am., 100(2), 562–569.

Mathur, L. P., and P. Evans (1964), Oil in India: 22nd Session International Geological Congress Proceedings, p. 7–52.

Maurin, T., and C. Rangin (2009), Structure and kinematics of the Indo-Burmese Wedge: Recent and fast growth of the outer wedge, Tectonics, 28, TC2010, doi:10.1029/2008TC002276.

Maurin, T., F. Masson, C. Rangin, U. T. Min, and P. Collard (2010), First Global Positioning System results in northern Myanmar: Constant and localized slip rate along the Sagaing fault, Geology, 38(7), 591–594, doi:10.1130/G30872.1.

Mazzotti, S., H. Dragert, J. Henton, M. Schmidt, R. Hyndman, T. James, Y. Lu and M. Craymer (2003), Current tectonics of northern Cascadia from a decade of GPS measurements. J. Geophys. Res. 108(B12): doi: 10.1029/2003JB002653. issn: 0148-0227.

McCaffrey, R., (2009), The tectonic framework of the Sumatran subduction zone, Annual Reviews of Earth and Planetary Sciences, 37, 345-366,

Meltzner, A. J., K. Sieh, M. Abrams, D. C. Agnew, K. W. Hudnut, J.-P. Avouac, and D. H. Natawidjaja (2006), Uplift and subsidence associated with the great Aceh-Andaman earthquake of 2004, J. Geophys. Res., 111, B02407, doi:10.1029/2005JB003891.

Milne, J. (1911). A Catalogue of Destructive Earthquakes A. D. 7 to A. D. 1899, BAAS, London.

Mitchell, A.H.G., (1977), Tectonic settings for emplacement of southeast Asian tin granites. Geological Society of Malaysia, Bulletin 6, 123–140.

Morgan, J. P., and W. Mclntire (1959), Quaternary Geology of the Bengal Basin, East Pakistan and India: Bull. Geol. Soc. America, 70, 319-342.

Morino M., A.S.M. M. Kamalb, D. Muslimc, R.E. Alid, M.A. Kamald, Z. Rahmane, F. Kanekoa (2011) Seismic event of the Dauki Fault in 16th century confirmed by trench investigation at Gabrakhari Village, Haluaghat, Mymensingh, Bangladesh, J. Asian Earth Sci., 42(2) 492-498.

Morley, C. K., M. Smith, A. Carter, P. Charusiri, and S. Chantraprasert (2007), Evolution of deformation styles at a major restraining bend, constraints from cooling histories, Mae Ping Fault zone, western Thailand, in Tectonics of Restraining and Releasing Bends, edited by D. Cunningham, and P. Mann, Geol. Soc. Spec. Publ., 290, 325–349.

Müller, R. D., W. R. Roest, J.-Y. Royer, L. M. Gahagan, and J. G. Sclater (1997), Digital isochrons of the world's ocean floor, J. Geophys. Res., 102(B2), 3211–3214, doi:10.1029/96JB01781.

Myint Thein, Kyaw Tint, Aye Ko Aung, (1981), On the lateral displacement of the Sagaing Fault. Georeports 1(1). University of Mandalay, Burma.

Ni, J. F., M. Guzman-Speziale, M. Bevis, W. E. Holt, T. C. Wallace, W. R. Seager, (1989), Accretionary tectonics of Burma and the three-dimensional geometry of the Burma subduction zone, Geology, 17, 68–71.

Nielsen, C., et al. (2004), From partial to full strain partitioning along the Indo-Burmese hyper-oblique subduction, Mar. Geol., 209, 303–327, doi:10.1016/j.margeo.2004.05.001.

Oldham, T. (1883), Catalogue of Indian Earthquakes, Mem. Geol. Surv. India, 19(3), 170 pp.

Pacheco, J.F. & L.R. Sykes, (1992). Seismic moment catalog of large shallow earthquakes, 1900 to 1989, Bull. seism. Soc. Am., 82, 1306–1349.

Pelayo, A. M., and D. A. Wiens (1989), Seismotectonics and relative plate motions in the Scotia Sea region, J. Geophys. Res., 94(B6), 7293–7320, doi:10.1029/JB094iB06p07293.

Peltzer, G., F. Crampe, S. Hensley, and P. Rosen (2001), Transient strain accumulation and fault interaction in the eastern California shear zone, Geology, 29, 975–978.

Penick, J. L., Jr. (1981) The New Madrid Earthquakes Rev. ed., Univ. of Mo. Press, Columbia.

Prawirodirdjo, L. and Y. Bock, (2004), Instantaneous global plate motion model from 12 years of continuous GPS observations, J. Geophys. Res., 109, B08405, doi:10.1029/2003JB002944.

Pubellier M. et al. (2008). Structural Map of Eastern Eurasia, Commission for the Geological Map of the World, 1:12.500.000 scale.

Ranga Rao, A., and M. K. Samanta, (1987), Structural style of the Naga overthrust belt and its implication on exploration: Bulletin of the Oil and Natural Gas Commission, v. 24, p. 69–109.

Rao, N. P., and Kalpna (2005), Deformation of the subducted Indian lithospheric slab in the Burmese arc, Geophys. Res. Lett., 32, L05301, doi:10.1029/2004GL022034.

Replumaz, A., (1999). Reconstruction de la zone de collision Inde-Asie. Étude centrée sur l'Indochine. PhD thesis, Université de Paris 7-IPG, Paris, 230 pp.

Richards, S., G. Lister, and B. Kennett (2007), A slab in depth: Three-dimensional geometry and evolution of the Indo-Australian plate, Geochem. Geophys. Geosyst., 8, Q12003, doi:10.1029/2007GC001657.

Rudolf, B. and U. Schneider (2005): Calculation of Gridded Precipitation Data for the Global Land-Surface using in-situ Gauge Observations, Proceedings of the 2nd Workshop of the International Precipitation Working Group IPWG, Monterey October 2004, EUMETSAT, ISBN 92-9110-070-6, ISSN 1727-432X, 231-247.

Satyabala, S. P. (1998), Subduction in the Indo-Burma region: Is it still active? Geophys. Res. Lett., 25, 3189–3192.

Sella, G. F., T. H. Dixon, and A. Mao (2002), REVEL: A model for recent plate velocities from space geodesy, J. Geophys. Res., 107(B4), 2081, doi:10.1029/2000JB000033.

Shen, Z.-K., J. Lu, M. Wang, and R. Burgmann (2005), Contemporary crustal deformation around the southeast borderland of the Tibetan Plateau, J. Geophys. Res., 110, B11409, doi:10.1029/2004JB003421.

Shishikura, M., et al. (2009), Geomorphological evidence of great Holocene earthquakes of western Myanmar, Proceedings of the International Workshop on Tsunami and Storm Surge Hazard Assessment and Management for Bangladesh, CDMP, 35–40.

Shyu, J. B. H., K. Sieh, Y.-G. Chen, and C.-S. Liu (2005), Neotectonic architecture of Taiwan and its implications for future large earthquakes, J. Geophys. Res., 110, B08402, doi:10.1029/2004JB003251.

Sieh, K., and D. Natawidjaja (2000), Neotectonics of the Sumatran fault, Indonesia, J. Geophys. Res., 105(B12), 28295–28326, doi:10.1029/2000JB900120.

Simons, W. J. F., et al. (2007), A decade of GPS in Southeast Asia: Resolving Sundaland motion and boundaries, J. Geophys. Res., 112, B06420, doi:10.1029/2005JB003868.

Smith, G., L. McNeill, T. J. Henstock, and J. Bull (2012), The structure and fault activity of the Makran accretionary prism, J. Geophys. Res., 117, B07407, doi:10.1029/2012JB009312.

Socquet, A., and M. Pubellier (2005), Cenozoic deformation in western Yunnan (China-Myanmar border), J. Asian Earth Sci., 24, 495–515.

Socquet, A., C. Vigny, N. Chamot-Rooke, W. Simons, C. Rangin, and B. Ambrosius (2006), India and Sunda plates motion and deformation along their boundary in Myanmar determined by GPS, J. Geophys. Res., 111, B05406, doi:10.1029/2005JB003877.

Soe Thura Tun, Saw Ngwe Khaing, Y. Wang, Myo Thant, Nyunt Htay, Yin Myo, Min Htwe, Than Myint, K. Sieh (2013) Surface Ruptures of the 2011 Tarlay Earthquake and Their Relationship to the Active Tectonics of Eastern Myanmar, in preparation.

Steckler, M.S., Akhter, S.H. & Seeber, L., (2008), Collision of the Ganges–Brahmaputra Delta with the Burma Arc: implications for earthquake hazard, Earth planet Sci. Lett., 273, 367–378.

Steckler et al. (2012), GPS Velocities and Structure Across the Burma Accretionary Prism and Shillong Anticline in Bangladesh, American Geophysical Union, Fall Meeting 2012, abstract # T51F-2667

Stein, R. S., Barka, A. A. and Dieterich, J. H. (1997), Progressive failure on the North Anatolian fault since 1939 by earthquake stress triggering. Geophysical Journal International, 128: 594–604. doi: 10.1111/j.1365-246X.1997.tb05321.x

Strasser, F.O., M.C. Arango and J.J. Bommer (2010), Scaling of the source dimensions of interface and intraslab subduction-zone earthquakes with moment magnitude, Seism. Res. Lett., 81(6), 941–950.

Stuart, M. (1920), The Srimangal earthquake of 8th July 1918, Memoirs of the Geological Survey of India, 46(1).

Szeliga, W., et al. (2010), Intensity, magnitude, location, and attenuation in India for felt earthquakes since 1762, Bull. Seismol. Soc. Am., 100(2), 570–584.

Tapponnier, P., G. Peltzer, A.Y. Le Dain, R. Armijo & P. Cobbold (1982), Propagating extrusion tectonics in Asia: new insights from simple experiments with plasticine, Geology, 10, 611–616.

Than Tin Aung, K. Satake, Y. Okamura, M. Shishikura, Win Swe, Hla Saw, Tint Lwin Swe, Soe Thura Tun, and Thura Aung (2008), Geologic evidence for three great earthquakes in the past 3400?years off Myanmar, J. Earthquake Tsunami, 2, 259–265.

Tsutsumi, H., and T. Sato (2009), Tectonic geomorphology of the southernmost Sagaing Fault and surface rupture associated with the May 1930 Pegu (Bago) earthquake, Myanmar, Bull. Seismol. Soc. Am., 99, 2155–2168, doi:10.1785/0120080113.

Uddin, A., and N. Lundberg (1999), A paleo-Brahmaputra? Subsurface lithofacies analysis of Miocene deltaic sediments in the Himalyan-Bengal system, Bangladesh, Sediment. Geol., 123, 239–254.

Verma, R. K., and M. Mukhopadhyay (1977), An analysis of the gravity field in northeastern India, Tectonophysics, 42, 283–317.

Vigny, C., A. Socquet, C. Rangin, N. Chamot-Rooke, M. Pubellier, M. Bouin, G. Bertrand, and M. Becker (2003), Present-day crustal deformation around Sagaing fault, Myanmar, J. Geophys. Res., 108(B11), 2533, doi:10.1029/2002JB001999.

Wang, E. and B. C. Burchfiel, (1997), Interpretation of Cenozoic tectonics in the right-lateral accomodation zone between the Ailao Shan shear zone and the eastern Himalayan syntaxis, Int. Geol. Rev., 39, 191–219

Wang, E., B. C. Burchfiel, L. H. Royden, L. Chen, J. Chen, W. Li, (1998), Late Cenozoic Xianshuihe-Xiaojiang and Red River fault systems of southwestern Sichuan and central Yunnan, China, Spec. Pap. Geol. Soc. Am., 327, 108.

Wang, G., J. Wan, E. Wang, D. Zheng, and F. Li (2008), Late Cenozoic to recent transtensional deformation across the Southern part of the Gaoligong shear zone between the Indian plate and SE margin of the Tibetan Plateau and its tectonic origin, Tectonophysics, 460, 1–20, doi:10.1016/j.tecto.2008.04.007.

Wang, H., Z.J. Qiang, Z.Z. Yuan, Y.L. Wang, H. Zhang, X. Zhao, (1991), The Distribution of seismic intensities and surface rupture in the Lancang-Gengma (Yunnan Province, China) earthquakes of November 6, 1988. Acta Seismologica Sinica, 13(3), 344 – 353. (in Chinese with English abstract).

Wang, J.N., Y.L. Wang, X.W. An, X.D. Yang (2006), Analysis of Latest Activity on NE-segment of West Branch of Nantinghe Fault, Journal of seismological research, 29(3), 264 – 268.

Wang, Y., E. Wang, Z. Shen, M. Wang, W. Gan, X. Qian, G. Meng, T. Li, W. Tao, Y. Yang, J. Cheng, and P. Li (2008), GPS-constrained inversion of present-day slip rates along major faults of the Sichuan-Yunnan region, China, Sci. China D, 51, 1267–1283.

Wang, Y. K, Sieh, Soe Min, Saw Ngwe Khaing, Soe Thura Tun (2009), Smoking gun of the May-1912 Burma earthquake? Neotectonics of the Kyaukkyan fault system, Eastern Burma (Myanmar). American Geophysical Union, Fall Meeting 2009, abstract #T33B-1912.

Wang, Y., Sieh, K., Aung, T., Min, S., Khaing, S. N. and Tun, S. T. (2011), Earthquakes and slip rate of the southern Sagaing fault: insights from an offset ancient fort wall, lower Burma (Myanmar). Geophysical Journal International, 185:49–64. doi:10.1111/j.1365-246X.2010.04918.x

Wang, Y. et al. (2013a), Permanent upper plate deformation in western Myanmar during the great 1762 earthquake: Implications for neotectonic behavior of the northern Sunda megathrust, J. Geophys. Res. Solid Earth, 118, doi:10.1002/jgrb.50121.

Wang, Y., Y.N. Lin, M. Simons, Soe Thura Tun (2013b) Shallow rupture of the 2011 Tarlay earthquake (Mw 6.8), Eastern Myanmar. BSSA, in review.

Wells, D.L. & K.J. Coppersmith (1994), New empirical relationships among magnitude, rupture length, rupture width, rupture area, and surface displacement, Bull. seism. Soc. Am., 84(4), 974–1002.

Wesnousky, S. (2006), Predicting the endpoints of earthquake ruptures, Nature, 444, 358–360, doi:10.1038/nature05275.

Wesnousky, S. (2008), Displacement and geometrical characteristics of earthquake surface ruptures: Issues and implications for seismic-hazard analysis and the process of earthquake rupture, Bull. Seismol. Soc. Am., 98, 1609–1632, doi:10.1785/0120070111.

Win Swe, (1970), Rift-features at the Sagaing-Tagaung ridge, in Proc. 5th Burma Research Congress, Rangoon.

Win Swe, C. Thacpaw, Nay Thaung Thaung, Kyaw Nyunt (1972), Geology of part of the Chindwin basin of the central belt, Burma, Department of Geology, Arts and Science University, Mandalay. 34p.

Win Swe, (2006), Earthquake hazard potentials in Myanmar: a science to public welfare outlook, in Symp. Tectonics, Seismotectonics, and Earthquake Hazard Mitigation and Management of Myanmar, Yangon, Abstract.

Xie, Y.S. and M.B. Tsai (Chief Eds). (1983), Compilation of historical materials of Chinese Earthquakes, Vol. X, Science Press, Beijing (in Chinese).

Yeats, R. S., K. Sieh, and C. R. Allen, (1997), The Geology of Earthquakes, Oxford Univ. Press, New York.

Yu, W.X., T.J. Cai, X.Y. Hou, (1991), Deformation zone of M = 7.6 Lancang earthquake, Seismology and Geology, 13(4), 343- 352 (in Chinese with English abstract).

Zhu Y.X., P. Li, J.W. Ren (1994), Activity of Nandinghe fault zone and its paleoearthquake events, Earthquake Research in China, 10(4), 347-356. (in Chinese with English abstract)

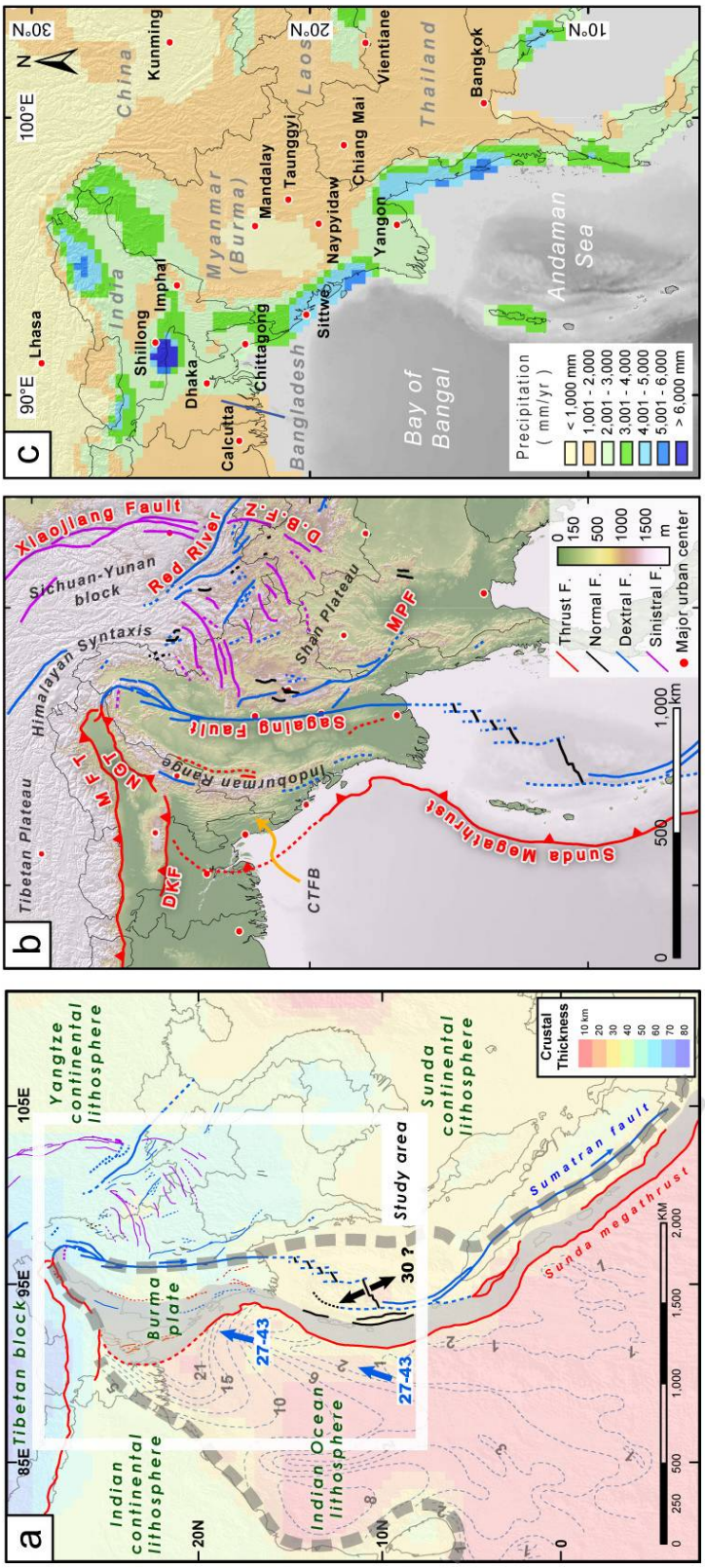
a
Tibetan block
Yangtze continental lithosphere
Sunda continental lithosphere
Indian continental lithosphere
Indian Ocean lithosphere
Burma plate
Study area
30 ?
27-43
27-43
Sumatran fault
Sunda megathrust
Crustal Thickness
b
Tibetan Plateau
Himalayan Syntaxis
Sichuan-Yunan block
Xiaojiang Fault
Red River F.
D.B.T.
Shan Plateau
MPF
Sagaing Fault
Indoburman Range
MBT
DKF
CTFB
Sunda Megathrust
Thrust F.
Normal F.
Dextral F.
Sinistral F.
Major urban center
c
Lhasa
Kunming
China
India
Shillong
Imphal
Dhaka
Calcutta
Chittagong
Bangladesh
Myanmar (Burma)
Mandalay
Taunggyi
Laos
Vientiane
Sittwe
Naypyidaw
Chiang Mai
Thailand
Bangkok
Yangon
Andaman Sea
Bay of Bangal
Precipitation (mm/yr)
< 1,000 mm
1,001 - 2,000
2,001 - 3,000
3,001 - 4,000
4,001 - 5,000
5,001 - 6,000
> 6,000 mm

Figure 1 Major tectonic elements of the Myanmar region and the extreme variation in rainfall that influence the preservation of tectonic landforms. (a) Crustal thickness associated with the major plates and tectonic blocks of the region. The pale-blue arrow shows the direction of Indian plate motion relative to Sunda plate (e.g., Socquet et al., 2006). The black arrow shows the opening direction of the Central Andaman spreading center. The velocity is in mm/yr. (b) Two major fault systems accommodate the northward translation of the Indian plate into Eurasia. These are the northern extension of the Sunda megathrust and the Sagaing fault system, which form the western and eastern margin of the Burma Plate. Conjugate right- and left-lateral faults of the Shan plateau and southern China accommodate southwestward extrusion of the Sichuan-Yunnan block around the eastern Himalayan syntaxis. (c) Extreme variations in annual rainfall across the region result in extreme variations in preservation of tectonic landforms. The precipitation data is from GPCC global data (Rudolf and Schneider, 2005).

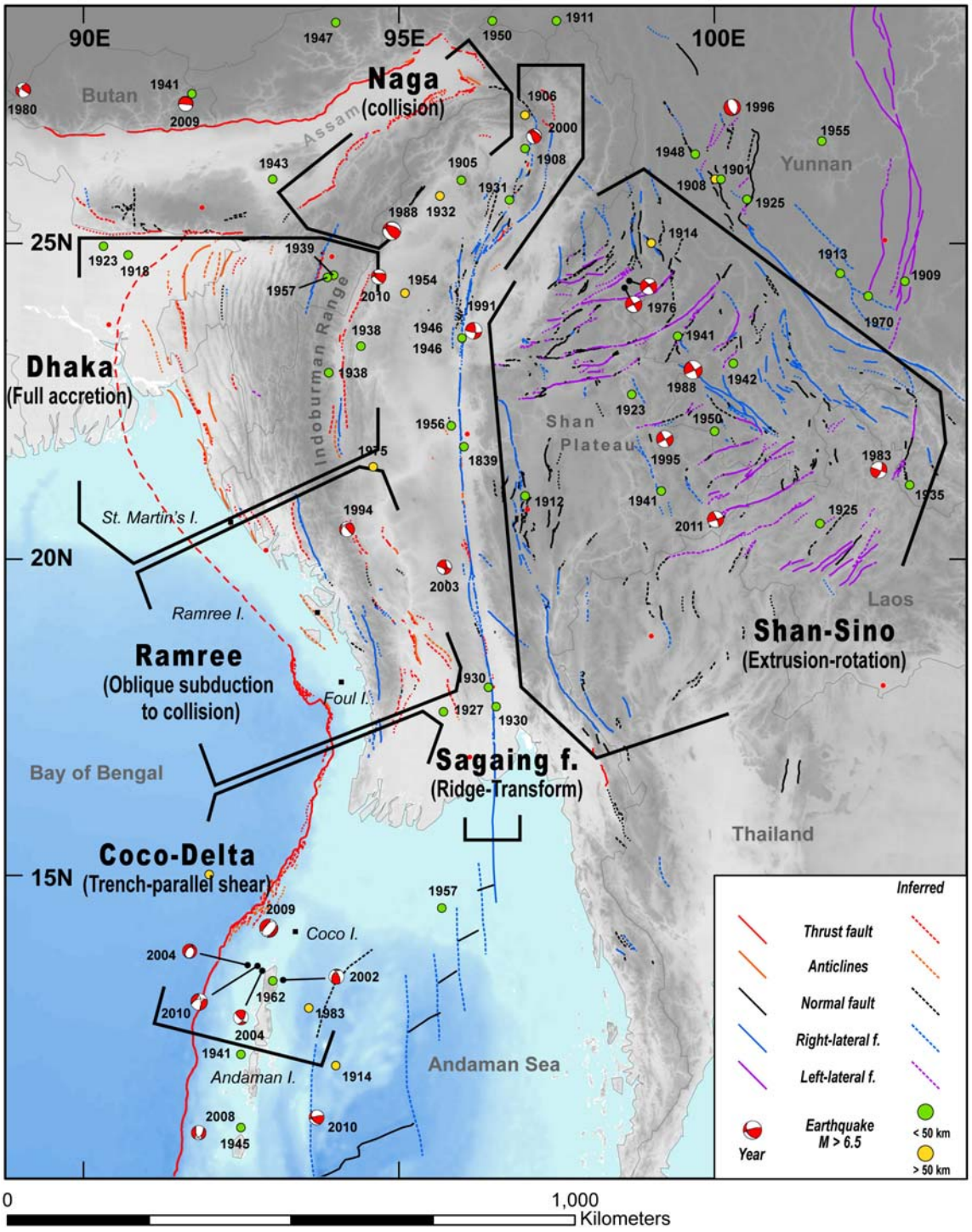

Figure 2 Simplified neotectonic map of the Myanmar region. Black lines encompass the six neotectonic domains that we have defined. Green and Yellow dots show epicenters of the major 20th-century earthquakes (source: Engdahl and Villaseñor, 2002). Red and white beachballs are focal mechanisms of significant modern earthquakes (source: GCMT database since 1976). A more detailed, high-resolution map, from which is this figure was derived, appears in the Appendix 1 Fig. S2.

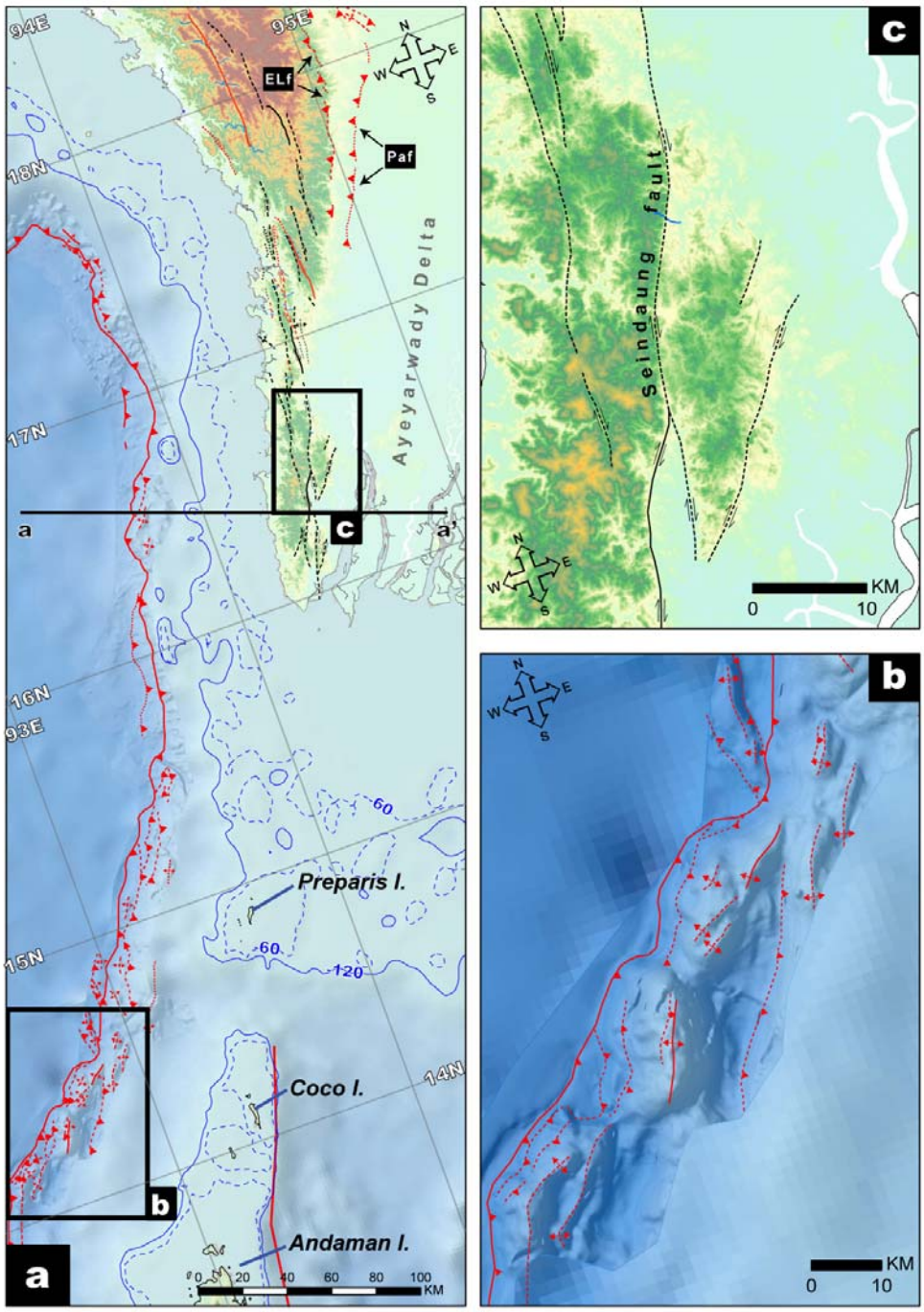

Figure 3 (a) Major active faults within the Coco-Delta domain. (b) Structures along the deformation front include a series of anticlinal structures very close to the trench. Detailed inset bathymetry is from Nielsen et al. (2004). (c) Seindaung fault and other dextral-slip faults along the eastern flank of the southern Indoburman range. Although these faults are clearly expressed in the topography, we cannot identify any obvious young offset features.

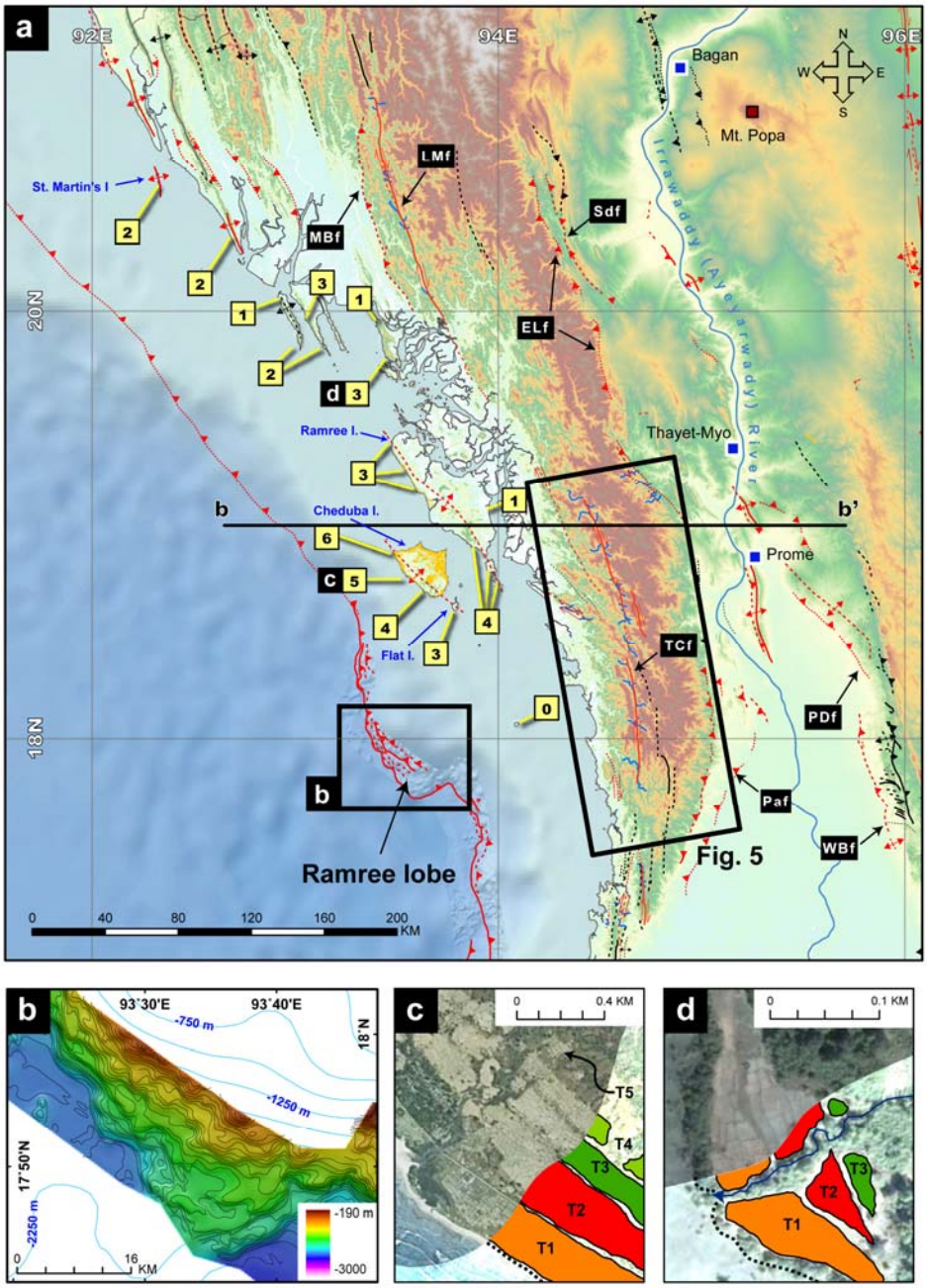

Figure 4 (a) Major active faults within the Ramree domain (Name abbreviations in black boxes). Numbers in yellow boxes indicate number of marine terraces visible in high-resolution satellite imagery. (b) Detailed bathymetry of the Ramree lobe shows clear geomorphic expression of imbricated faults and anticlines, which imply active shortening near the deformation front. (c) Marine terraces on the western side of Cheduba Island (colored patches) from satellite imagery. (d) Nested alluvial fan surfaces north of Ramree Island show episodic uplift during the seaward growth of the fan.

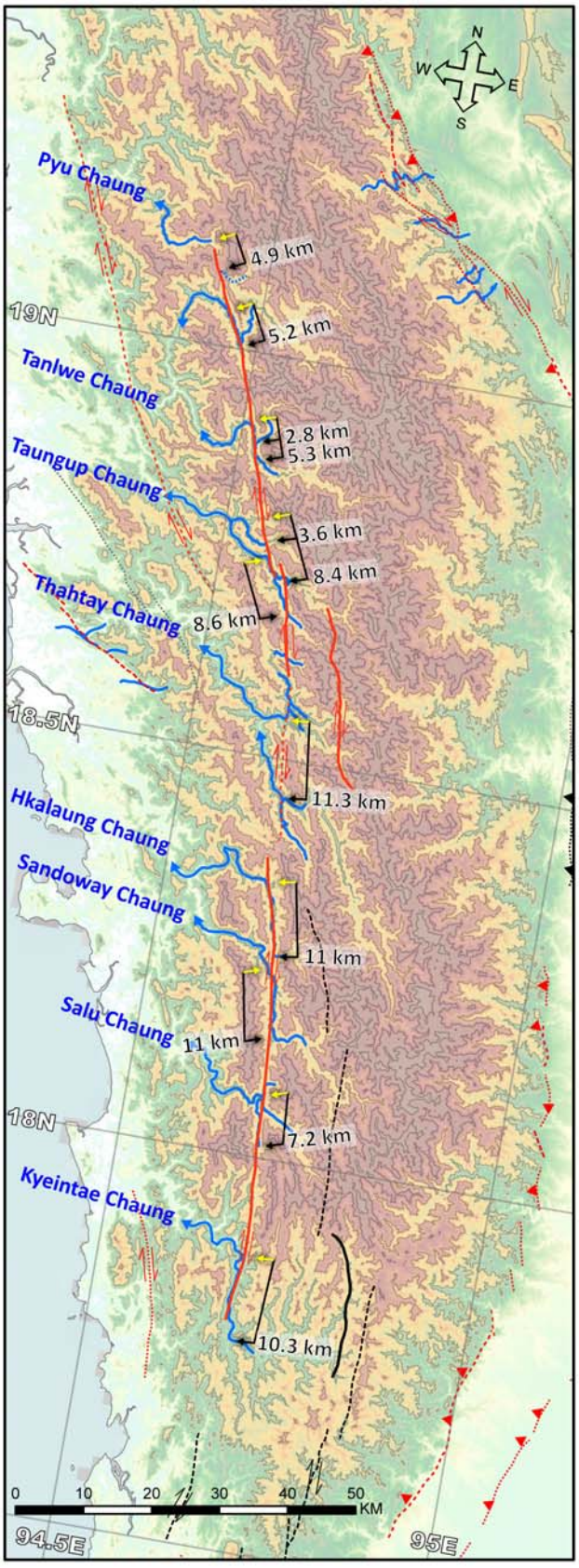

Figure 5 Right-lateral offset of river channels along the Thahtay Chaung fault, within the Indoburman Range. The maximum geomorphic offset is about 10.3 km, close to the southern limit of the fault.

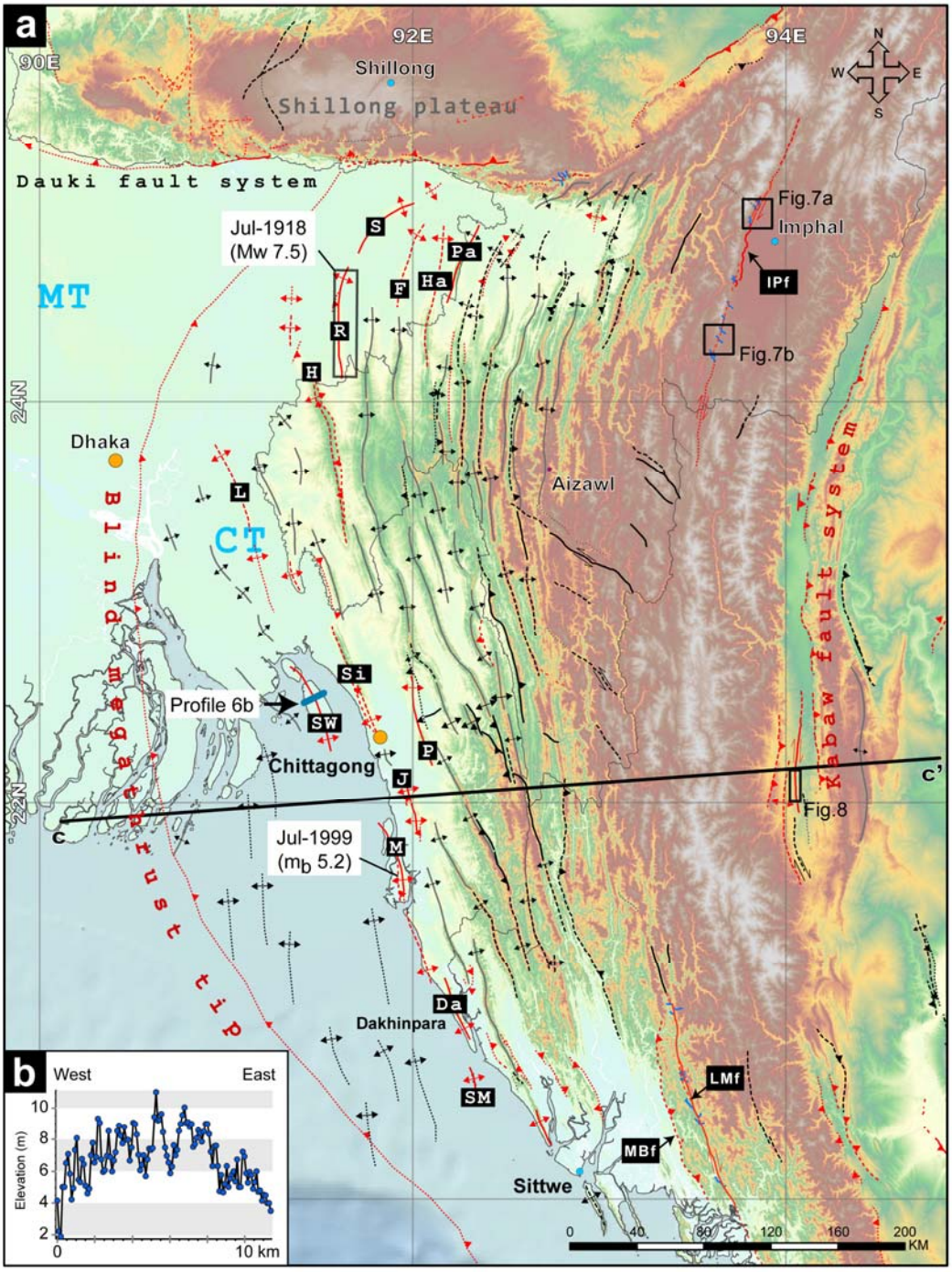

Figure 6 (a) Active faults and anticlines of the Dhaka domain superimposed on SRTM topography. Most of the active anticlines lie within 120 km of the deformation front. CT = Comilla Tract, MT = Madhupur tract. White boxes contain the dates and magnitudes of earthquakes mentioned in the text. (b) Profile from SRTM topography of Sandwip Island. Cross-section CC' appears in Figure 19.

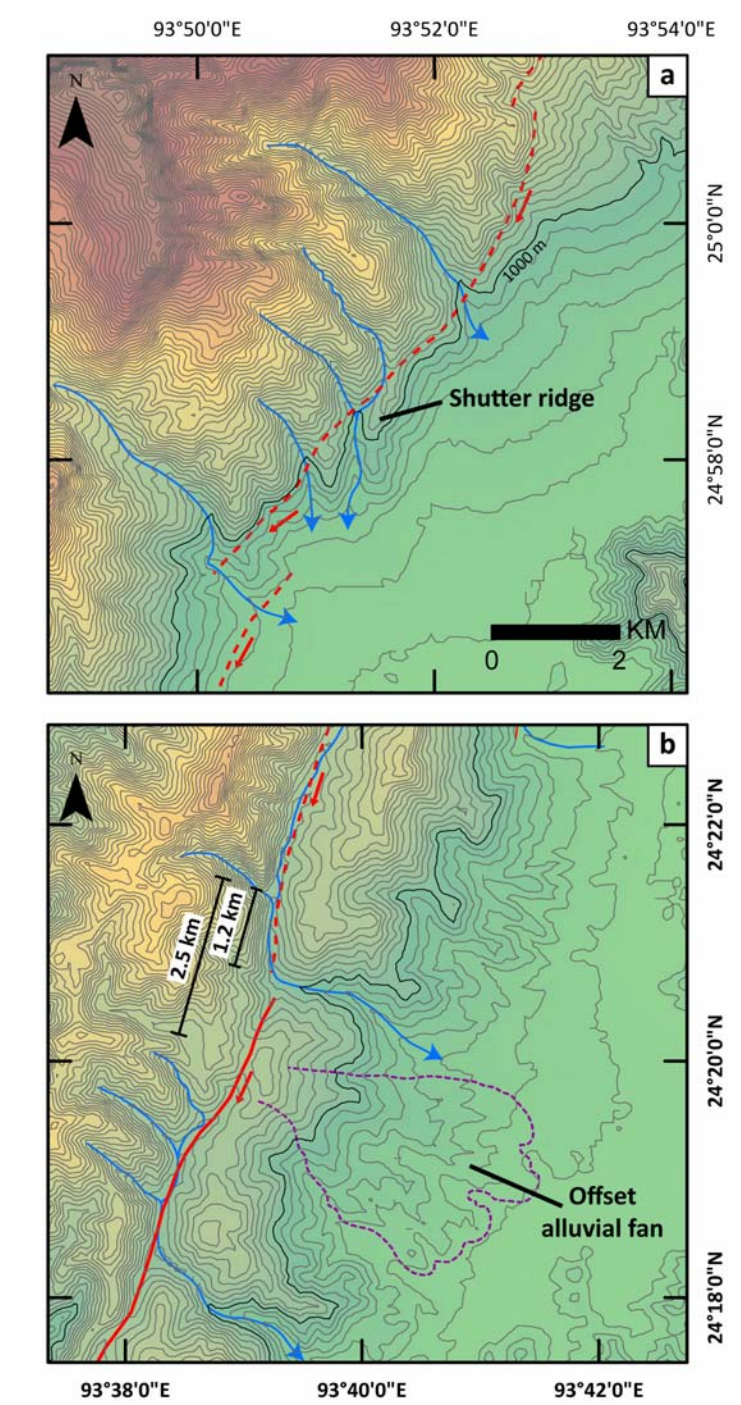

Figure 7 Geomorphological features of the Churachandpur-Mao fault at two different locations reflect clear dextral motions along the fault. (a) Clear right-lateral channel deflections on the 25-meter contour map from SRTM topography along the northwestern margin of the Imphal basin. (b) Eroded and beheaded alluvial fan and nearest plausible source basin about 2.5 krn to the northeast along the fault.

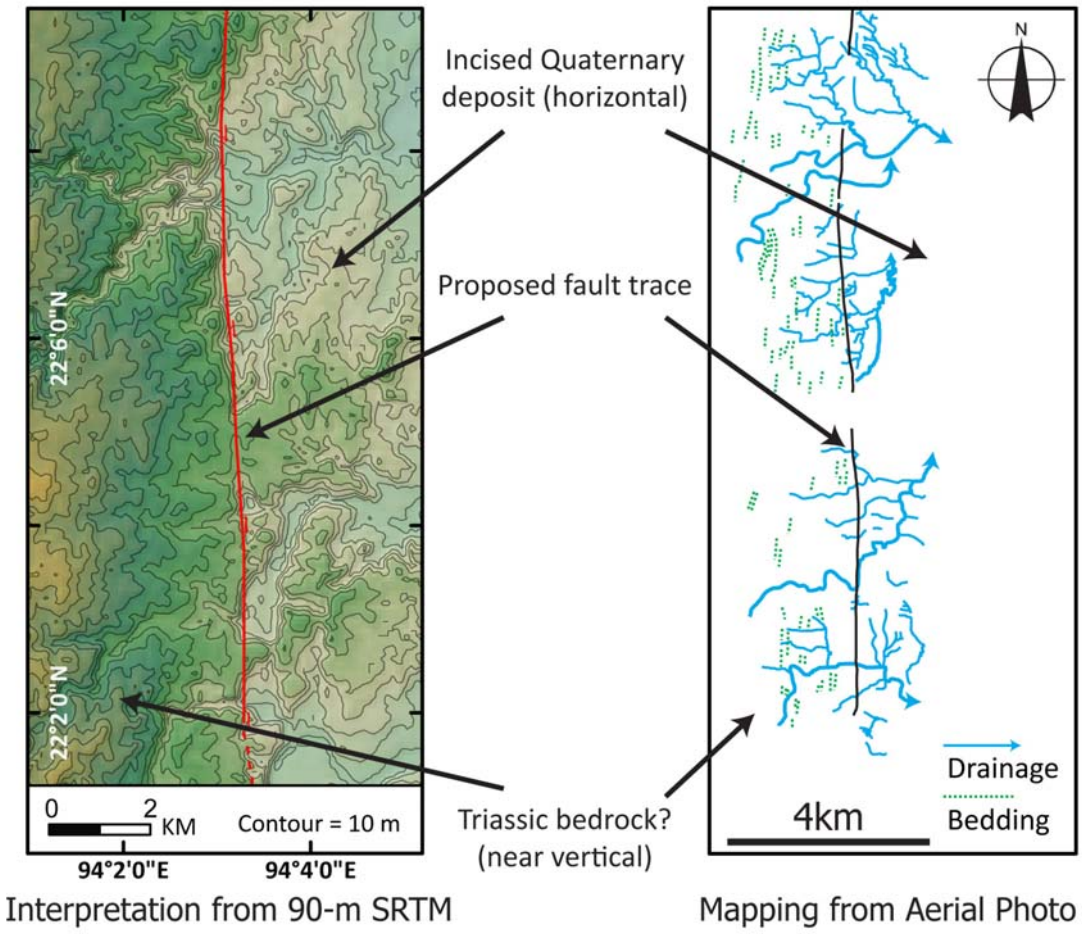

Figure 8 Fault and drainage map in the southern part of the Kabaw valley shows no young offset features along a strike-slip element of the fault.

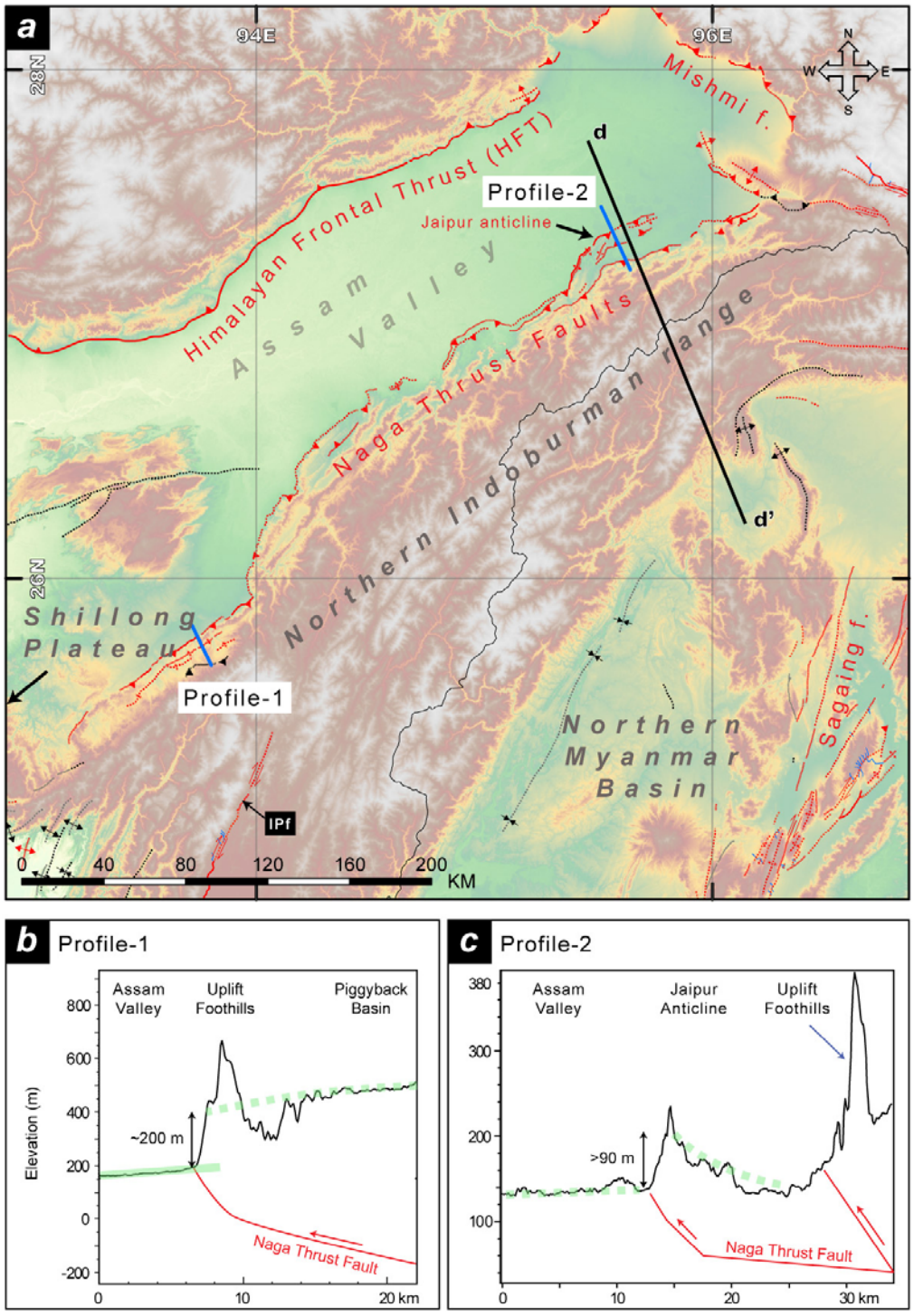

Figure 9 Map and cross sections of the Naga thrust fault system. (a) Map of traces of the fault visible in SRTM imagery shows three distinct lobes along its ~400-km length. The geomorphic profiles in (b) and (c) show the thrust fault system deforms late-Quaternary depositional surfaces and offsets them vertically by more than 90 m. Cross section DD' appears in Figure 19. The scale at depth is not equal to the scale of topographic profiles.

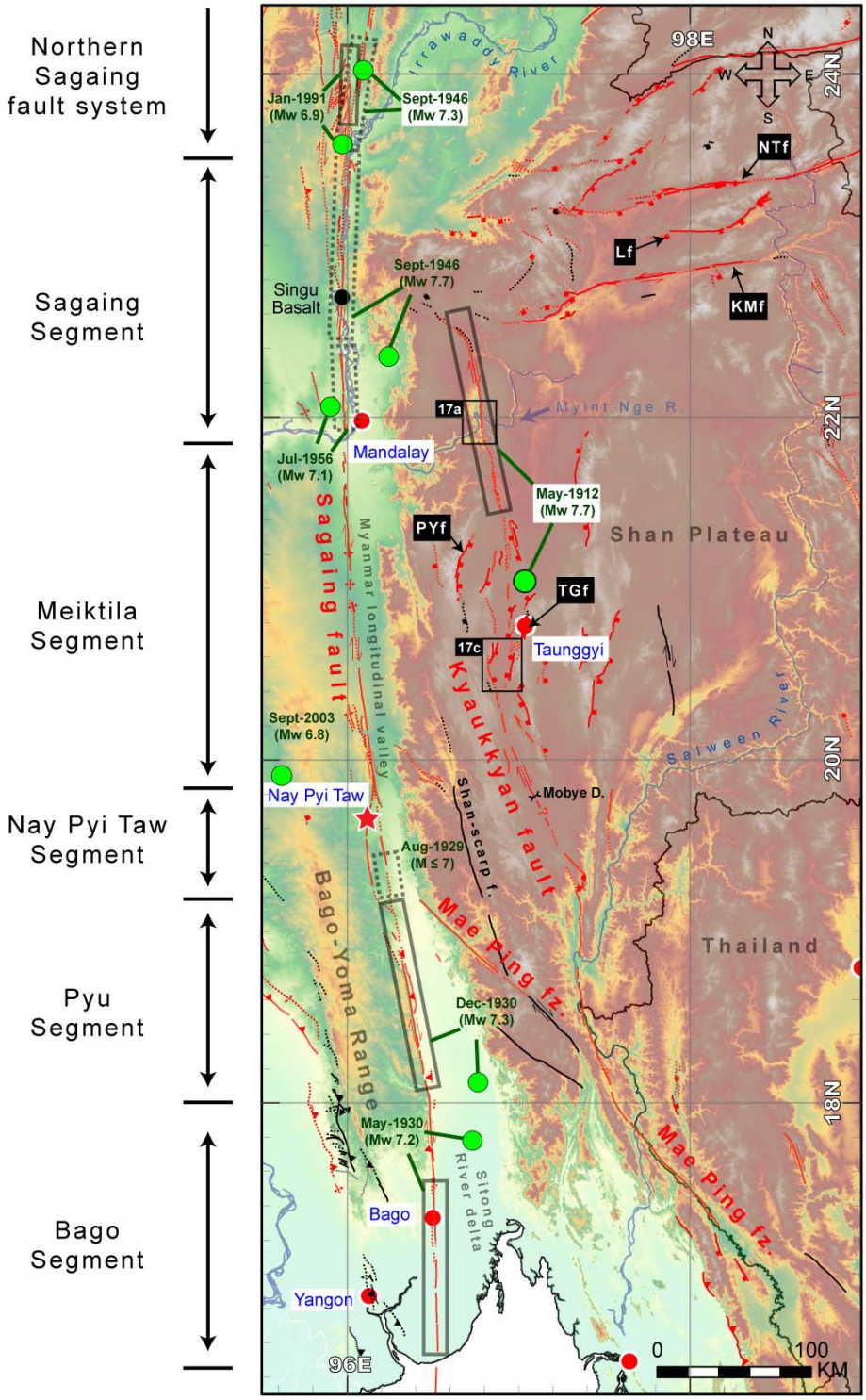

Figure 10 Fault segments and historical earthquakes along the central and southern parts of the Sagaing fault. Green dots show relocated epicenters from Hurukawa and Phyo Maung Maung (2011). Dashed and solid gray boxes surround segments of the fault that ruptured in historical events.

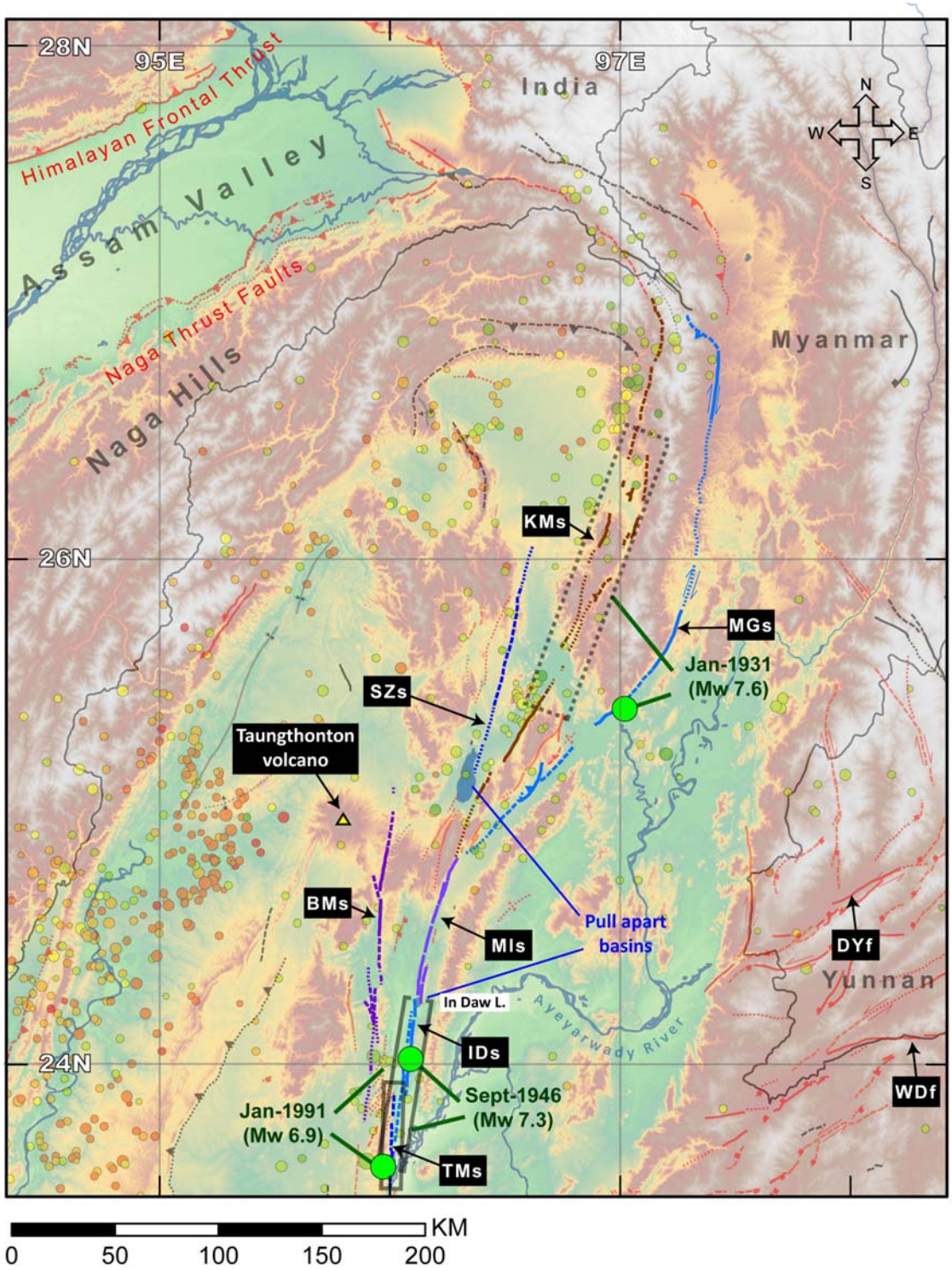

Figure 11 Fault segments of the northern Sagaing fault, differentiated by purple, blue and brown colors. Lettering in black boxes show the abbreviated names of the segments. Green dots are relocated epicenters of major earthquakes from Hurukawa and Phyo Maung Maung (2011). Gray boxes show inferred rupture patches during these earthquakes.

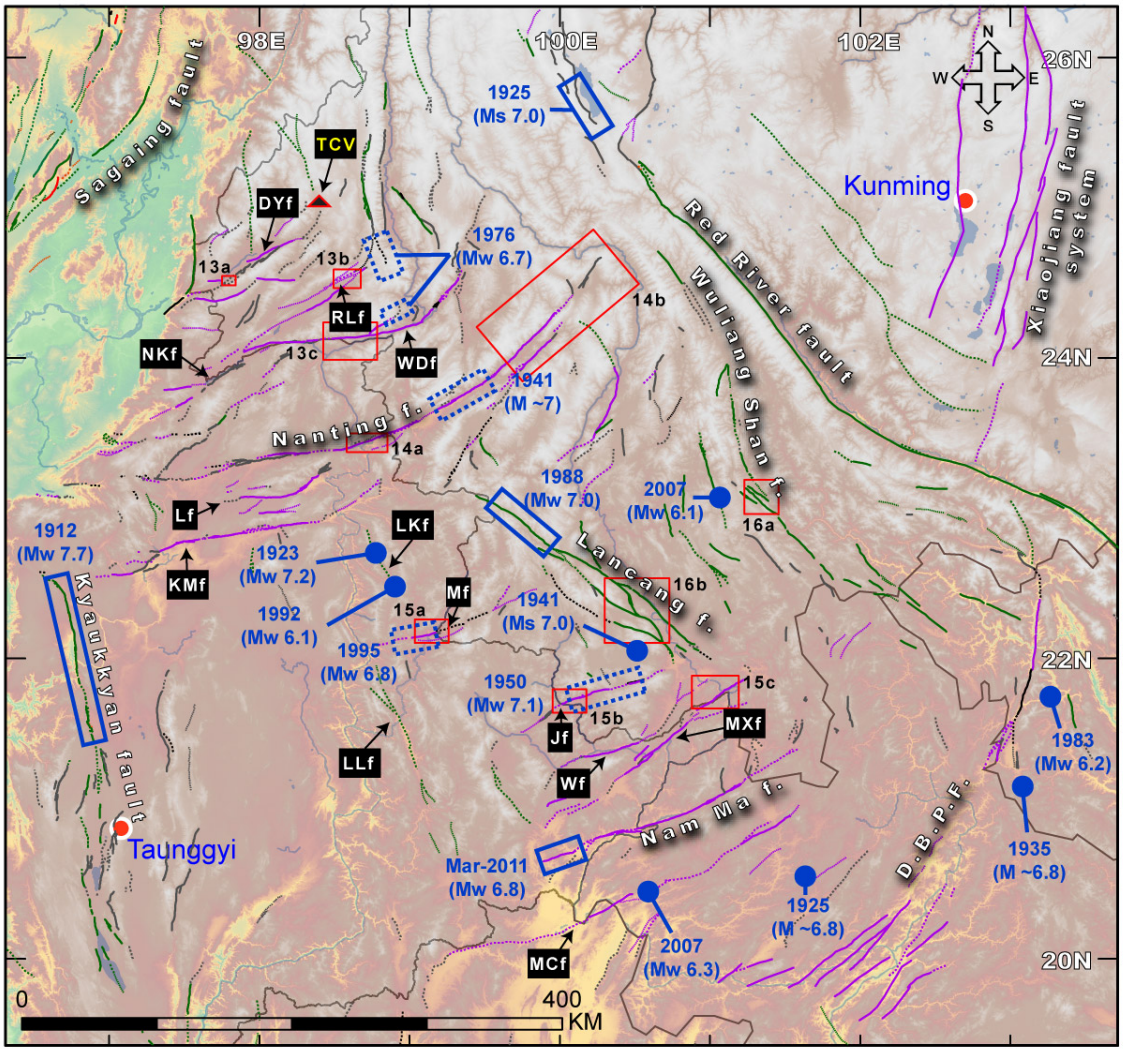

Figure 12 Active faults and associated historical earthquakes within the Shan-Sino domain. Purple = left-lateral faults. Green = right-lateral faults. Gray = normal faults. Blue dots and boxes show locations of earthquake and ruptures of the past century. Red boxes are the locations of coming up figures. TCV = Tengchong Volcano; DYf = Da Yingjiang fault; RLf = Ruili fault; WDf = Wanding fault; NKf = Namkham fault; Lf = Lashio fault; KMf = Kyaukme fault; LKf = Loi Kwi fault; Mf = Menglian fault; LLf = Loi Lung fault; Jf = Jinghong fault; Wf = Wan Ha fault; MXf = Mengxing fault.

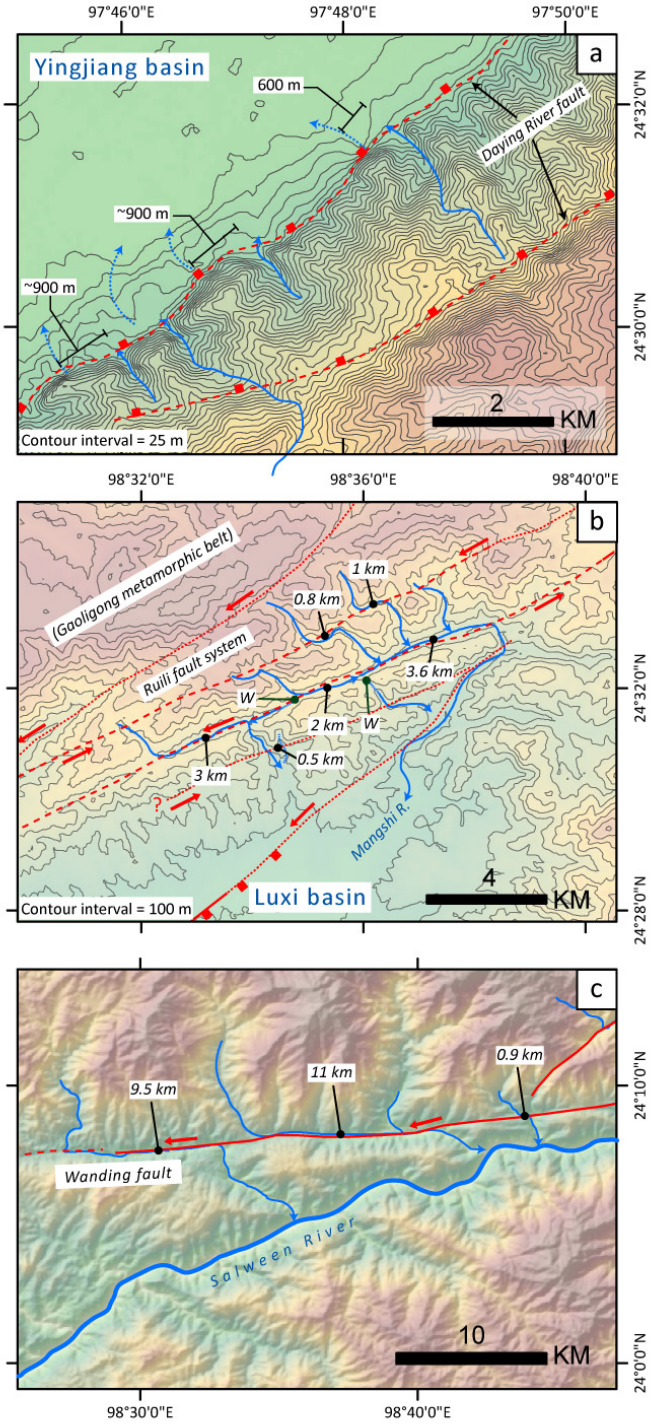

Figure 13 Selected examples of the geomorphological expression of active faults of the Shan-Sino domain, from SRTM topography and LANDSAT imagery. Blue lines = streams. Red lines = fault traces. (a) The Daying River fault appears as a trace with large vertical displacements within the mountain range and a trace with left-lateral displacements at the mountainfront. (b) Offsets along multiple strands of the left-lateral Ruili fault total 10 to 11 km. W = wind gap. (c) Matches of tributaries of the Salween River suggest left-lateral offsets of ~11 km along the Wanding fault.

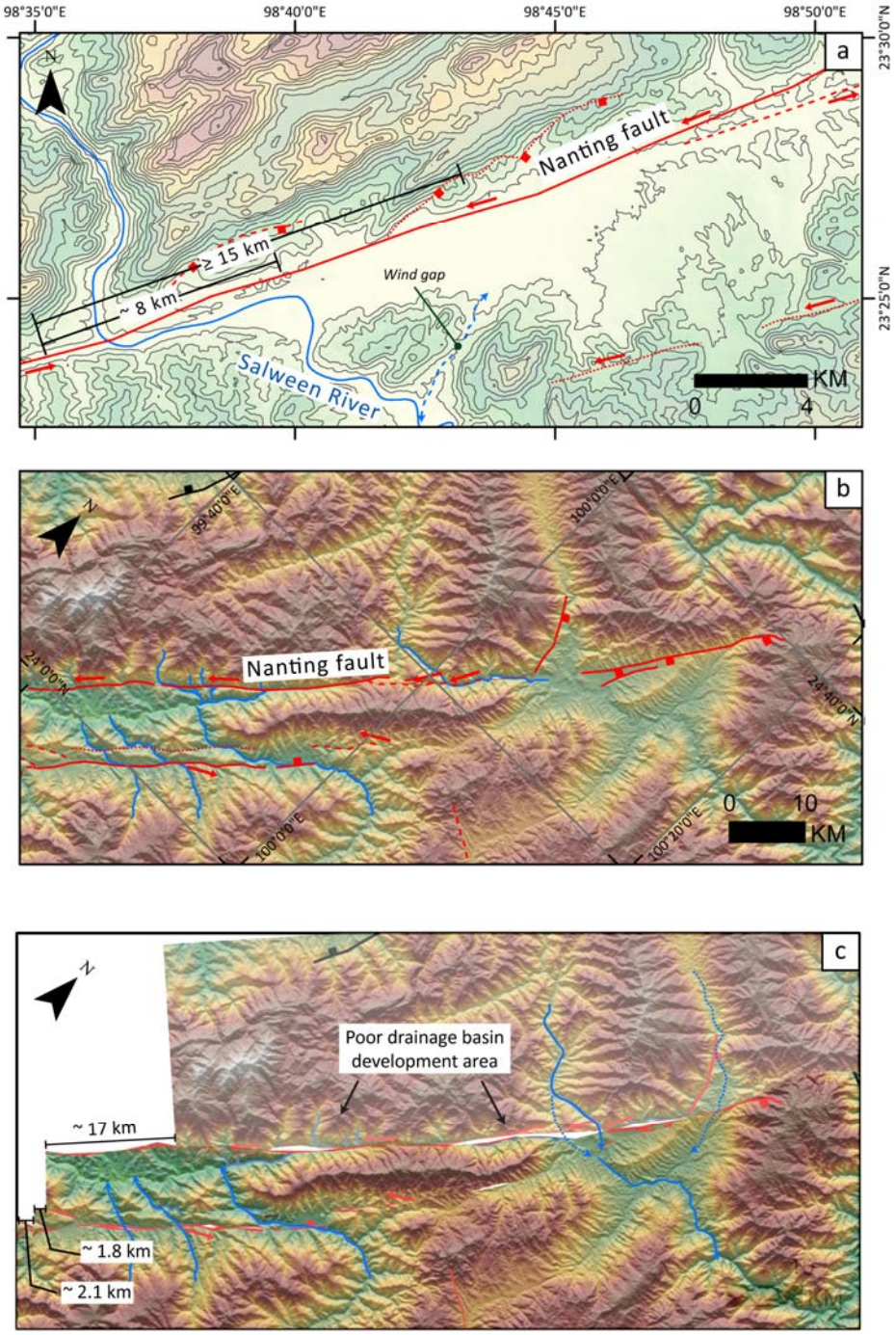

Figure 14 Tectonic geomorphological expressions of select locations along the Nanting fault. Conventions same as in previous figures. (a) Plausible 15-km offset along the central part of the Nanting fault, based upon recognition of a wind gap between the fault and the Salween River. (b and c) Current and restored stream-channel patterns along the northeastern reach of the Nanting fault suggest a 20-km offset.

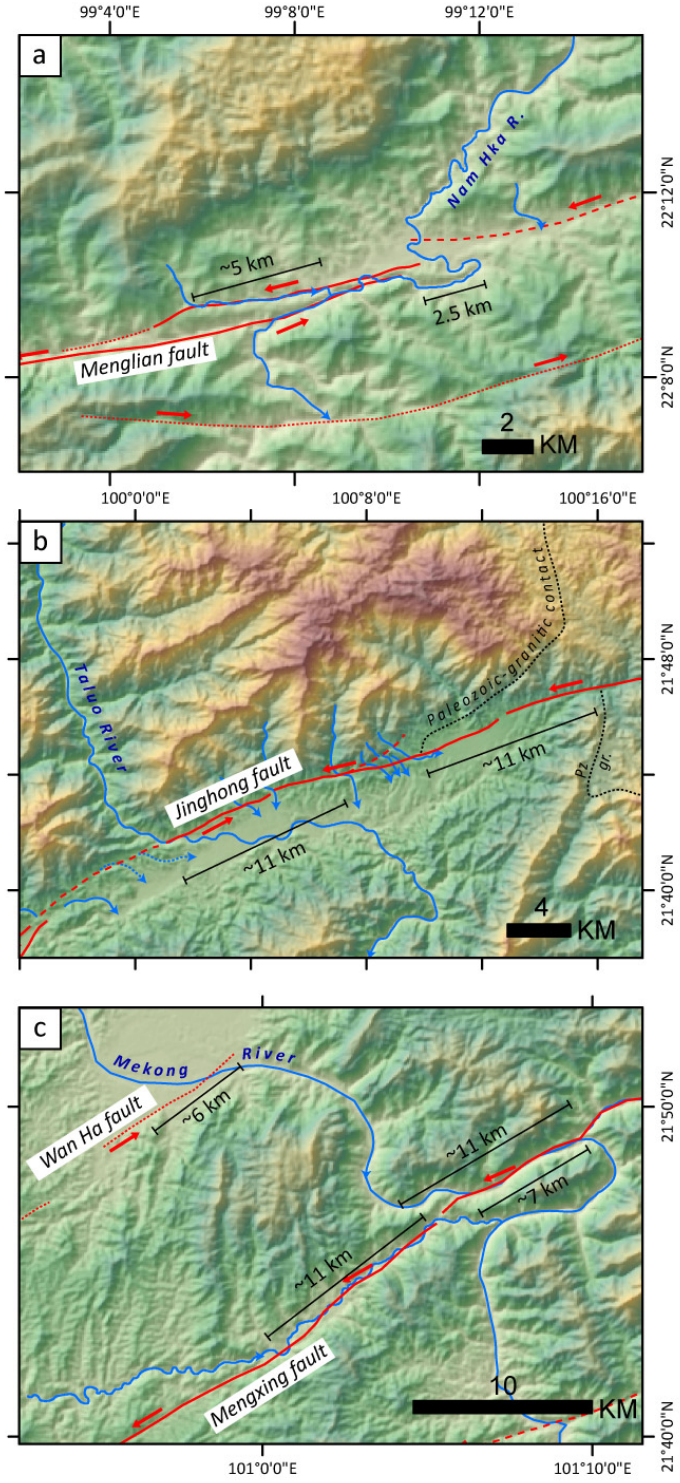

Figure 15 Tectonic geomorphological expressions of the Menglian, Jinghong and Mengxing faults. (a) Deflections of the Nam Hka River and a tributary imply 2.5- and 5-km left-lateral offsets along the Menlian fault. (b) Deflections of the Taluo river imply an 11 km left-lateral offset along the Jinghong fault, which roughly matches the 11 km left-lateral offset of a bedrock contact. (c) Left-lateral deflections of the Mekong river and a tributary imply an 11-km offset by the Menxing fault.

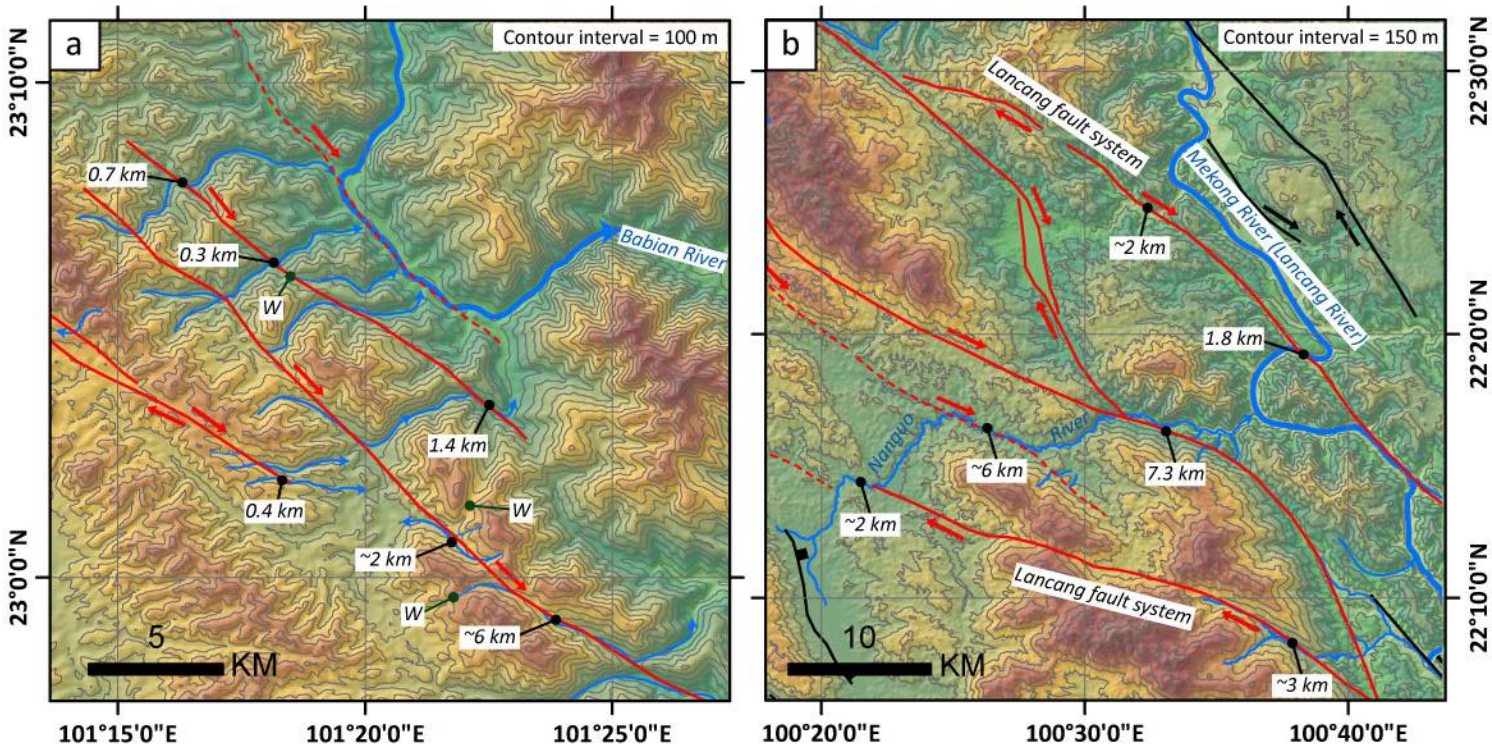

Figure 16 Tectonic geomorphology along parts of the right-lateral Wuliang Shan fault and Lancang fault system. (a) Maximum deflections of drainages across the Wuliang Shan fault zone is about 6 km here. (b) Deflections of the Nanguo river across a complicated set of faults suggests ~ 17 km of dextral offset across the Lancang fault system here.

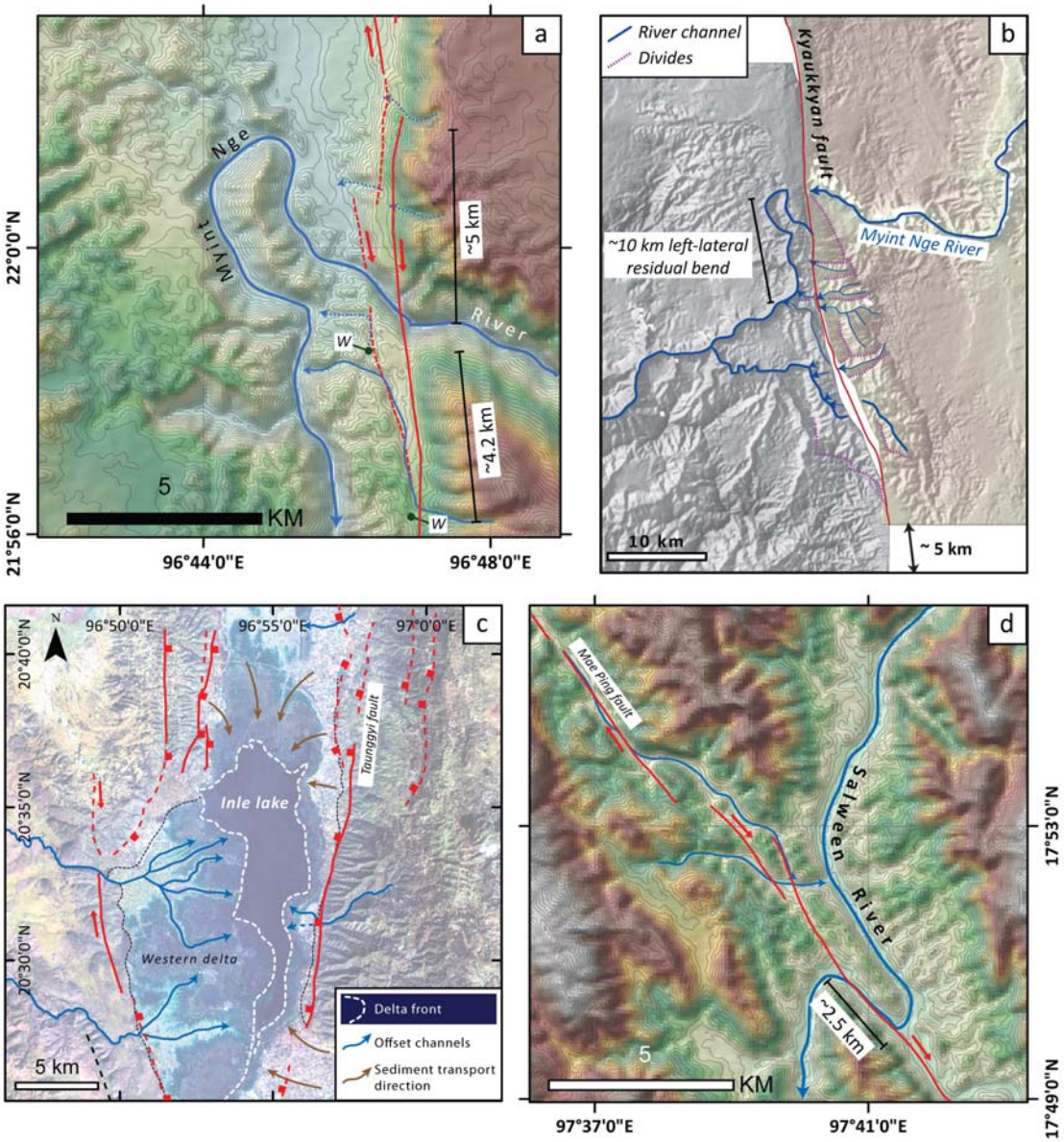

Figure 17 Geomorphological expression of particularly informative parts of the right-lateral Kyaukkyan fault system. (a) The hairpin geometry of the Myint Nge river channel, along the northern reach of the Kyaukkyan fault shows clear evidence for normal and dextral displacement along the fault. (b) Restoration of a 5-km recent right-lateral component of slip leaves a remaining, earlier 10-km left-lateral bend. (c) LANDSAT imagery of the Inle lake region showing the complex geometry of Taunggyi normal fault. (d) The Mae Ping fault zone offsets the Salween river channel and tributaries about 2.5 km.

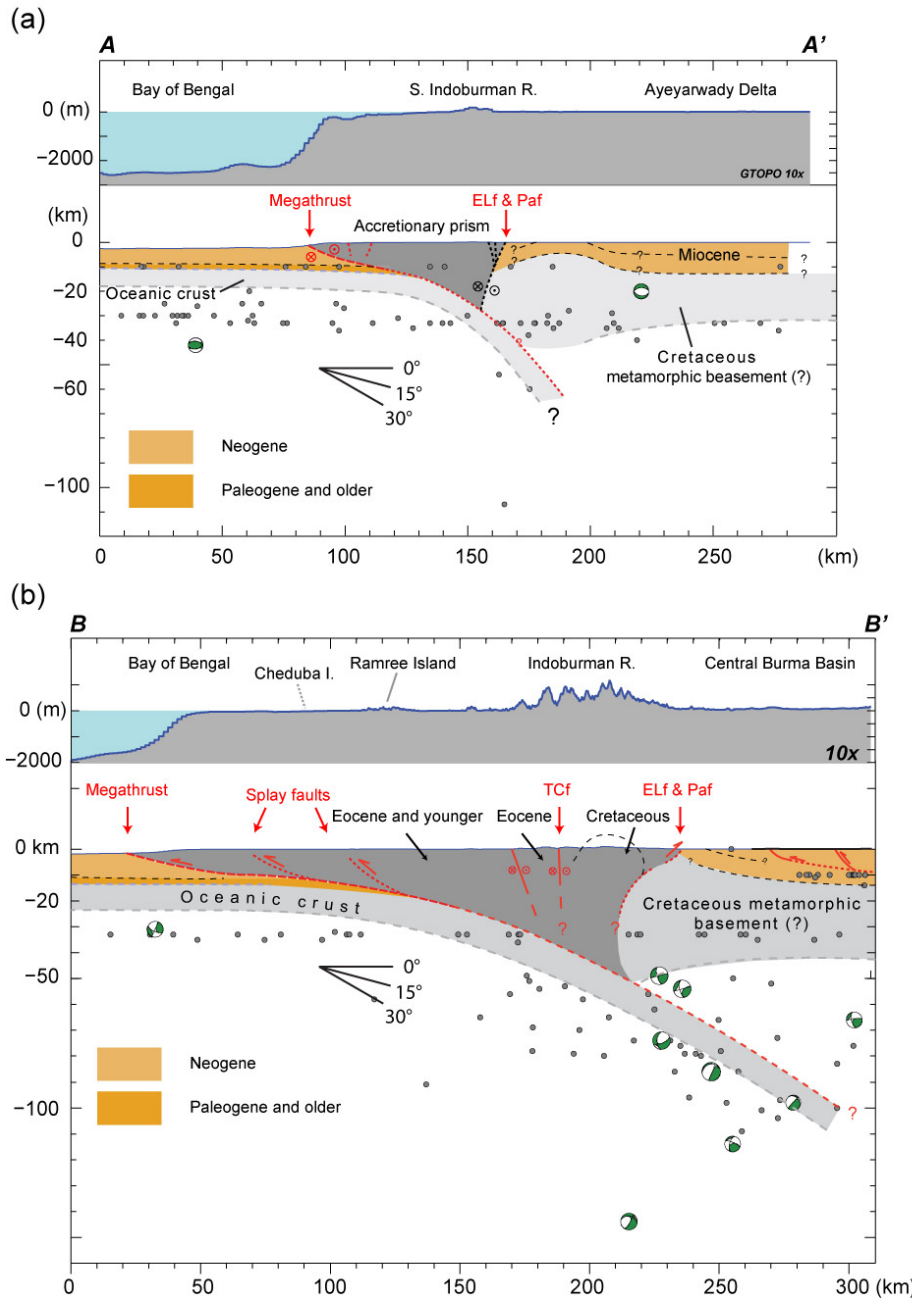

Figure 18 Schematic cross sections through two domains of the northern Sunda megathrust show the geometry of the megathrust and hangingwall structures. Grey dots the hypocenter locations from NEIC catalog since 1976. Green and white focal mechanisms are from GCMT database. (a) The megathrust along the Coco-Delta domain dips moderately and has secondary active structures near the deformation front. See Figure 3 map for profile location. (b) The megathrust along the Ramree domain dips shallowly and is associated with splay thrust faults and strike-slip faults within the hangingwall block. See Figure 4 map for location of the profile.

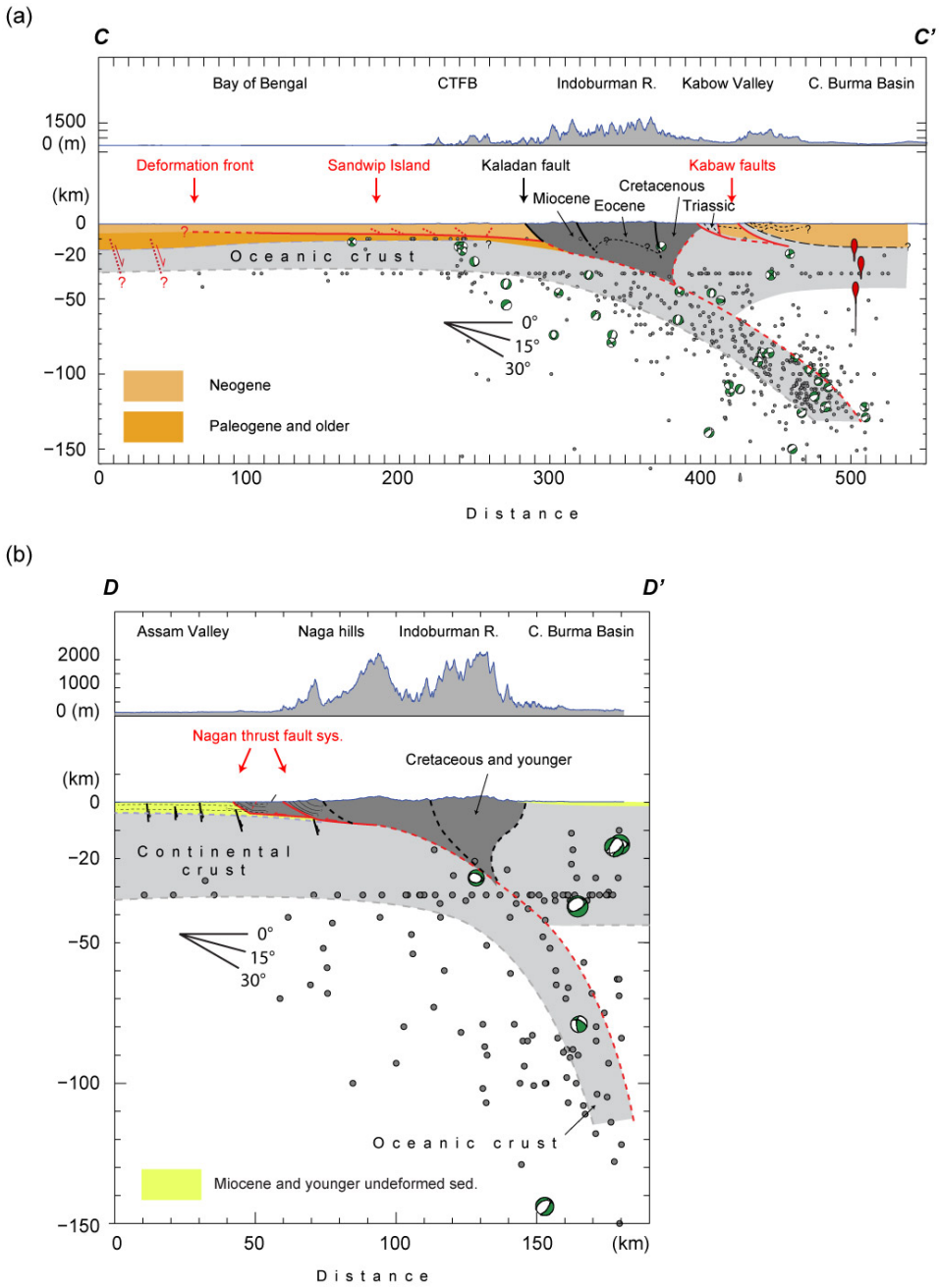

Figure 19 Schematic cross sections through two domains of the northern Sunda megathrust show the geometry of the megathrust and hangingwall structures. Symbols as in Figure 18. (a) The megathrust along the Dhaka domain dips very shallowly and has secondary active thrust faults within 120 km of the deformation front. See Figure 6 map for profile location. (b) The megathrust along the Naga domain dips moderately and juxtaposes continental against continental crust, but still has an attached subducting slab of Indian-plate oceanic crust. See Figure 9 map for profile location.

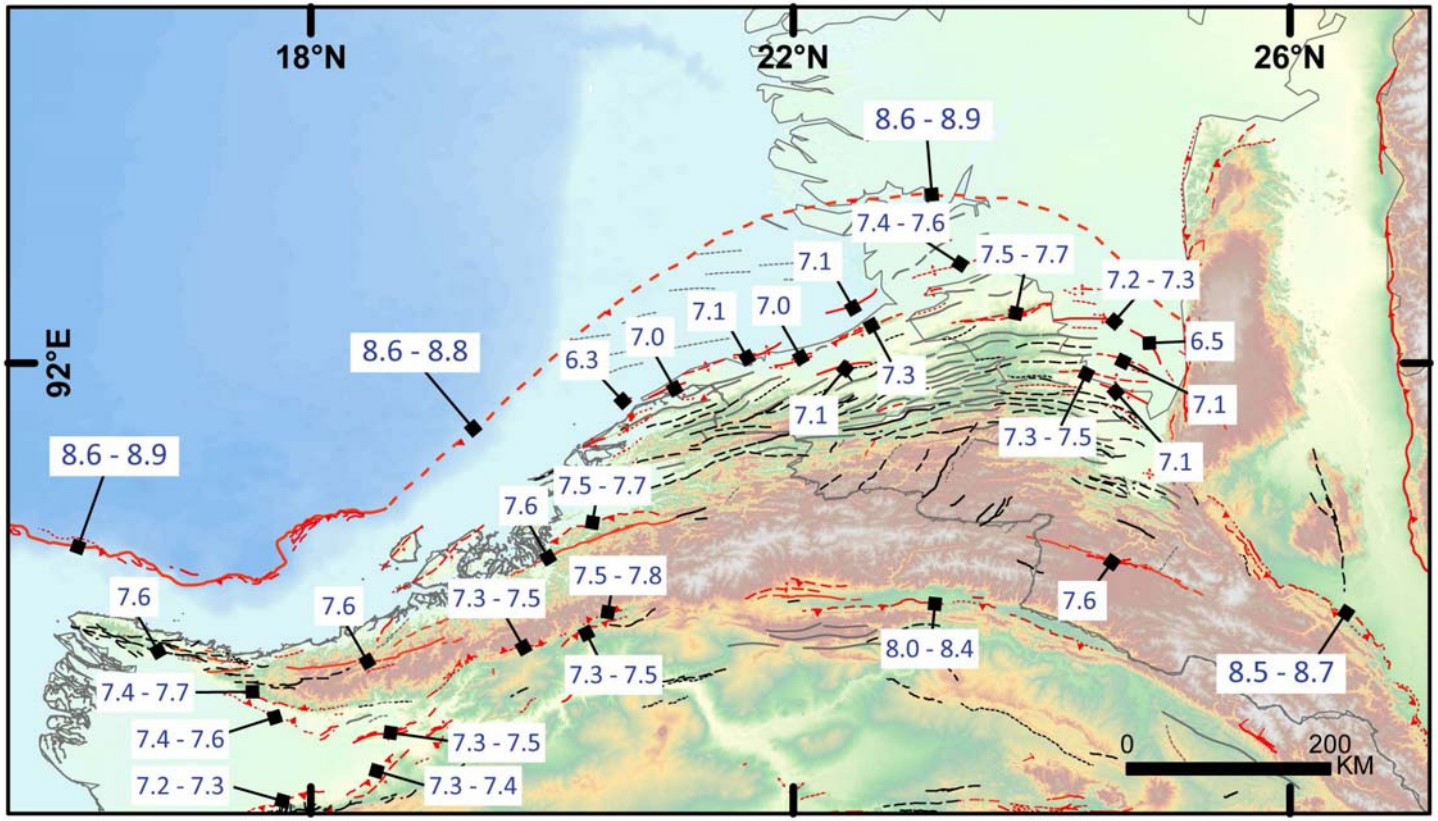

Figure 20. Map of potential maximum earthquake magnitudes (Mw) associated with shallow active faults of the four domains of the northern Sunda megathrust and Indoburman range. Blue numbers show earthquake magnitudes assuming complete rupture of each fault along its entire strike length. Red lines show the active structures mapped from digital elevation model and satellite imagery. Black lines show structures that we interpret to be inactive.

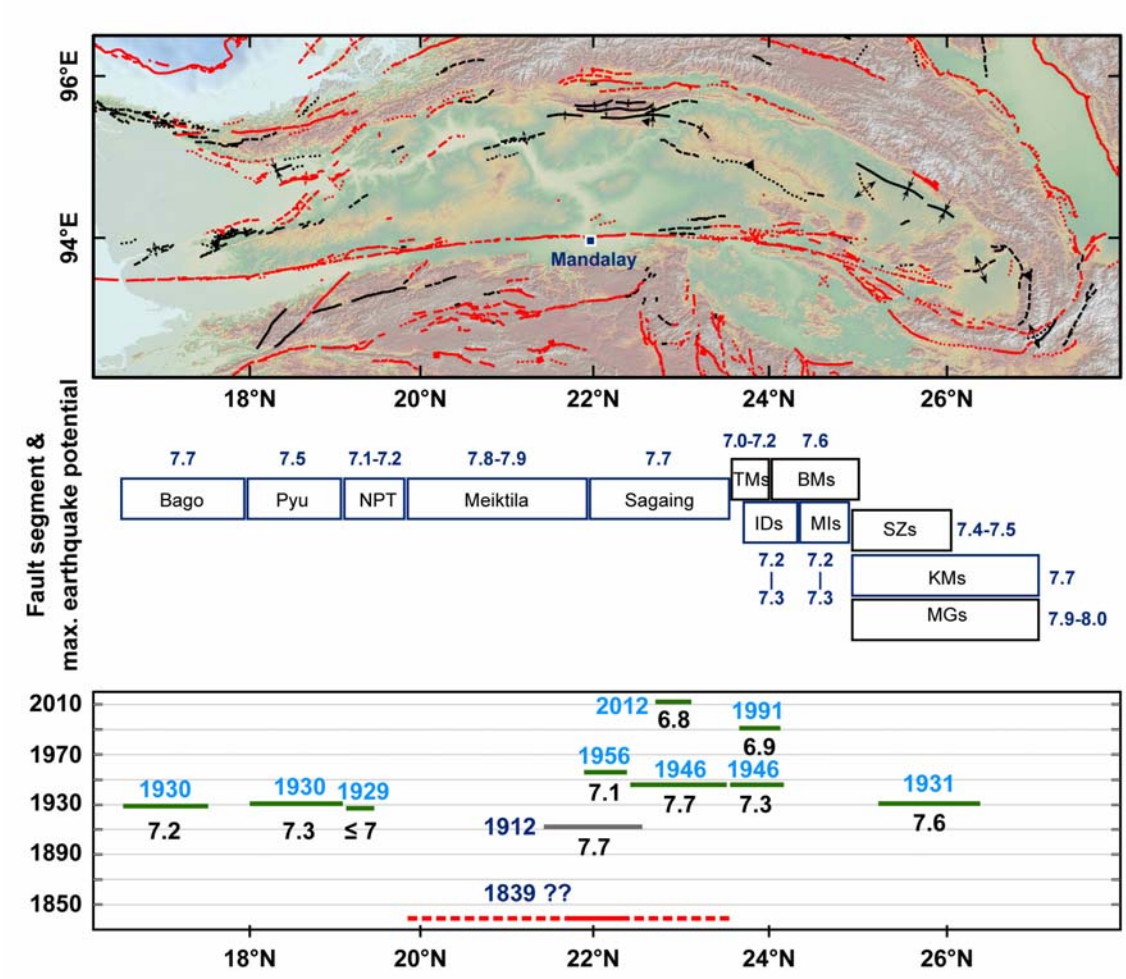

Figure 21 Map and chart of potential maximum earthquake magnitudes (Mw) associated with named segments of the Sagaing fault. Ruptures of the past century appear in the lower box

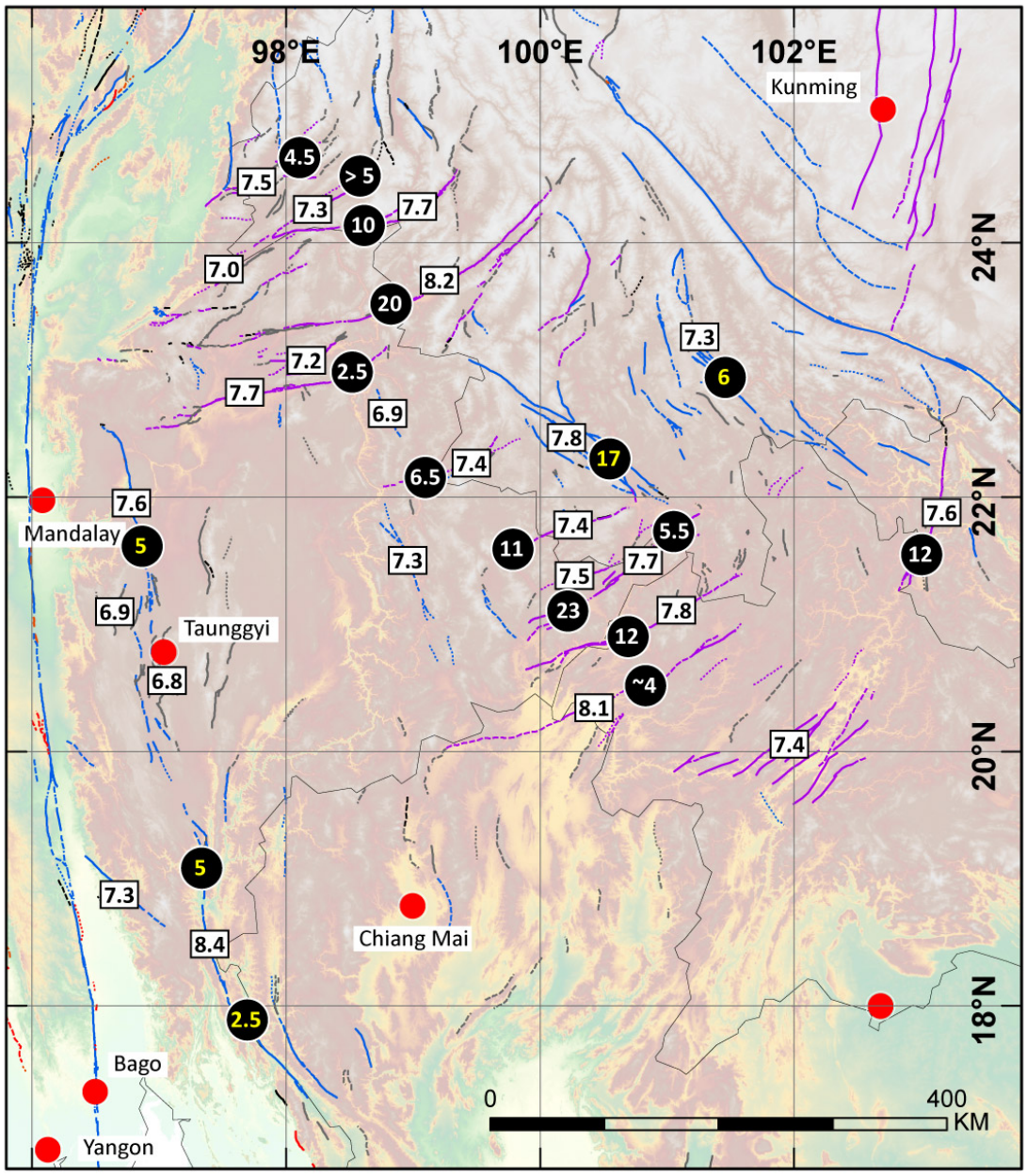

Figure 22 Map of total geomorphological evident offset (black dots) and potential maximum earthquake magnitudes (Mw) (White rectangles) associated with named faults of the Shan-Sino domain. The maximum earthquake magnitudes are based on the assumption that each fault will rupture along its entire length. Purple, blue and gray lines represent left-lateral, right-lateral and normal faults, respectively.

Table 1. Significant earthquakes within the study area since the late-19th century

Date (YYYY-MM-DD)	Lat	Lon	M	M_{type} ‡	Location	Type of records	Reference
Indoburman Range and central Burma basin							
1762/4/2	19	93.5	> 8.5	M_{fault}	Sunda megathrust	Int + G	H; O; W1
1858/3/23	19.3	95	7.7	M_{int}	Central Burma basin	Int	O; A&D;
1906/6/24	15	92	7.3	M_{unk}	Near megathrust	S	A
1918/7/8	24.5	91	7.5	Mw	Bangladesh	Int + S	S; E&V
1927/12/17	17.5	95.5	~ 6?	M	North of Yangon	Int	Brown, 1929
1943/10/23	26	93	7.1	Mw	Assam Valley	S	E&V
Sagaing fault							
1839/3/23	22	96	> 7	M	Near Mandalay	Int	O
1929/8/8	19.2	96.2	~7	M	Near Taungoo	Int	B2
1930/5/5	17.78	96.73	7.2	Mw	Bago	Int + S	Brown et al., 1931; E&V; H&P
1930/12/3	18.12	96.76	7.3	Mw	Pyu	Int + S	Brown et al., 1933; E&V; H&P
1931/1/27	25.41	97.02	7.6	Mw	Kamaing	Int + S	Chhibber, 1934; E&V; H&P
1946/9/12	24.02	96.09	7.3	Mw	Sagaing fault	S	E&V; H&P
1946/9/12	22.35	96.24	7.7	Mw	Sagaing fault	S	E&V; H&P
1956/7/16	22.06	95.9	7.1	Mw	Sagaing	S + Int	E&V; H&P

Table 1. (Continue)

Date (YYYY-MM-DD)	Lat	Lon	M	M_{type} ‡	Location	Type of records	Reference
1991/1/5	23.59	95.97	6.9	Mw	Tagaung	S	E&V; H&P; GCMT
2003/9/21	19.91	95.63	6.6	Mw	Taungdwingyi	S	E&V; H&P; GCMT
2012/11/11	22.755	95.708	6.8	Mw	Singu	S + G	NEIC; GCMT;
Shan-Sino domain							
1912/5/23	21	97	7.7	Mw	Kyaukkyan fault	Int + S	Brown, 1917; E&V
1923/6/22	22.589	98.681	7.2	Mw	Eastern Myanmar	S	E&V
1925/12/22	20.538	101.667	6.8	M_{unk}	Mae Chan fault ?	S	A
1935/11/1	21.148	103.082	6.8	M_{unk}	close to DBPF	S	E&V
1941/5/16	23.7	99.4	6.9	Ms	Nanting fault	S + Int + G	Lee and Wang, 1978; GNSIZM, 1979; E&V
1941/12/26*	21.08 ?	99.14 ?	7	Ms	Yunnan-Myanmar	Int + S	GNSIZM, 1979; E&V
1942/2/1	23.1	100.3	6.8	M_{unk}	Yunnan	Int + S	X; A
1950/2/2	21.758	99.97	7.1	Mw	Jinghong fault ?	Int + S	X; A
1976/5/29	24.509	98.913	6.7	Mw	Yunnan	Int + S	GNSIZM, 1979; A; GCMT
1976/5/29	24.52	98.502	6.6	Mw	Yunnan	Int + S	GNSIZM, 1979; A; GCMT
1983/6/24	21.721	103.265	6.2	Mw	close to DBPF	Int + S	Trieu et al., 2008; A; GCMT
1988/11/6	22.869	99.571	7	Mw	Lancang fault	Int + S + G	Yu et al., 1991; A; GCMT

Table 1. (Continue)

Date (YYYY-MM-DD)	Lat	Lon	M	M_{type} ‡	Location	Type of records	Reference
1992/4/23	22.422	98.887	6.1	Mw	Myanmar	S	A; GCMT
1992/4/23	22.41	98.821	6.1	Mw	Myanmar	S	A; GCMT
1995/7/11	21.89	99.22	6.8	Mw	Myanmar-Yunnan, Menglian fault ?	Int + S	Chen et al., 2002; A; GCMT
2007/3/10	24.727	97.597	5.5	Mw	Myanmar-Yunnan, Daying River fault	S	NEIC; GCMT; Lei et al., 2012
2007/6/2	23.02	101.01	6.1	Mw	Yunnan, Wuliang Shan fault	S	A; GCMT
2007/5/16	20.47	100.69	6.3	Mw	Laos, Mae Chan fault	S	A; GCMT
2011/3/24	20.62	100.02	6.8	Mw	Myanmar, Nam Ma fault	S + G	Wang et al., 2013b; GCMT

‡ M_{fault}: calculated from the fault slip model; M_{int}: Calculated from the seismic intensity record; M_{unk}: Instrument record, with unknow type of magnitude. **M:** speculation from the intensity records in history

$ Type of records: **Int:** Intensity; **S:** Instrument; **G:** Ground deformation

***** The epicenter location is inconsistence to the isoseismal map

Reference: **A:** Allen et al., 2009; **A&D:** Ambraseys and Douglas, 2004**; E&V:** Engdahl and Villaseñor, 2002; **H:** Halsted, 1842; **H&P:** Hurukawa and Phyo Maung Maung, 2011; **O:** Oldham, 1883; **S:** Stuart, 1920; **W1**: Wang et al., 2013; **X:** Xie and Tasi, 1983;

Table 2. Summary of maximum fault offset in the Sino-Shan domain fault system.

Fault name	Fault length (KM)	Fault type[a]	Location[b]		Type of offset	Max. offset (KM)	Ref.[c]	Note
			Lon	Lat				
Daying River Fault	135	L + N	97.95	24.65	River channel	4		Min. offset
Huna Fault	60	L + N	97.65	24.38	River channel	5		
Manda fault	> 30	L	98.09	24.52	Ridge crest	4.5		
Ruili fault (Eastern)	100	L + N	98.57	24.43	River channel	≤13		> 5 km
Ruili fault (Western)	40	L + N	97.76	23.98		> 1.7		
Namkham fault	60	L + N	97.47	23.79	River channel	> 0.6		
Wanding fault	170	L	98.63	24.14	Salween River system	10 ± 1	LAC	
Nanting fault	380	L	100.17	24.52	Ridge crests & rivers	20		
Lashio fault	85	L	97.99	23.07	Ridge crest & basin	6.5?		> 2.5 km
Kyaukme fault	> 200	L	98.13	22.88	River channel	2.5		
Menglian fault	120	L	99.53	22.32	River channel	5.5 ± 0.5		
Jinghong fault	110	L	100.05	21.7	River channel	~11		
Wan Ha fault	140	L	100.18	21.34	Nam Loi River	5.5 ± 0.5	LAC	
Mengxing fault	180	L	100.63	21.38	Nam Loi River	23.5 ± 0.5	LAC	
Nam Ma fault	215	L	100.58	20.88	Mekong River	13 ± 1	LAC	
Mae Chan fault	310	L	100.71	20.508	Ridge crest and channels	~4		
Dien Bien Phu fault	150	L	103.15	20.02	River channel	12.5	LAI	Single fault
Dien Bien Phu fault	~110	L	101.6	19.9	Mekong River	< 60		Multi. faults
Wiliang Shan Fault	~400	R	101.4	22.98	Mekong River sys.	~6		
Lancang fault	210	R	100.52	22.28	Nanguo River	~17		
Northern Kyaukkyan	~160	R	99.77	21.99	Myint Nge River	~5		

a. N = Normal fault; L = Left-lateral fault; R = Right-lateral fault;
b. The location is roughly the center point of the offset feature along the fault
c. LAC = Lacassin et al., 1998; LAI = Lai et al., 2012

Table 3. Scaling relationships for fault length and magnitude that used in this study.

Equation	Reference	Note
Reverse/Thrust fault		
Mw = 4.16 + 1.75 * log10(L)	Blaser et al., 2010	
M = 5.00 + 1.22 * log10(SRL)	Wells and Coppersmith, 1994	
M = 4.49 + 1.49 * log10(RLD)	Wells and Coppersmith, 1994	For blind structure
Mw = 4.868 + 1.392 * log10(L)	Strasser et al., 2010	For subduction interface
Normal fault		
Mw = 3.67 + 1.92 * log10(L)	Blaser et al., 2010	
M = 4.86 + 1.32 * log10(SRL)	Wells and Coppersmith, 1994	
M = 4.34 + 1.54 * log10(RLD)	Wells and Coppersmith, 1994	For blind structure
Strike-slip fault		
Mw = 4.20 + 1.56 * log10(L)	Blaser et al., 2010	
M = 5.16 +1.12 * log10(SRL)	Wells and Coppersmith, 1994	
M = 4.33 +1.49 * log10(RLD)	Wells and Coppersmith, 1994	For blind structure

Table 4. Proposed Major Seismic Structures of Myanmar and surrounding countries.

Code	Name	Type‡	Length (km)	Slip rate mm/yr	Strike	Dip	$M_{W\&C}$ [length]	M_{Blaser} [length]	$M_{Strasser}$ [length]	Last known earthquake		
										Year	M	Partial / Entire
Coco-Delta domain												
	Sunda megathrust (Coco-delta section)	SS + R	480	8 to 28 [A]	N20E	20	8.3	**8.9**	**8.6**			
Paf	Pathein fault	R	95	< 12[B]	N20E	45	**7.4**	**7.6**				
Elf[S]	East-limb fault (Southern section)	R	100	< 12[B]	N20E	45	**7.4**	**7.7**				
	Seidaung fault	SS	>160	< 5 ?	N20E	90	**7.6**	**7.6**				
Ramree domain												
	Sunda megathrust (Ramree section)	R	450	< 23[B]	N35W	16	8.2	**8.8**	**8.6**	1762	8.5 to 8.8	Entire
WBf	Weest Bogo-Yoma fault	R	65	> 0.4[c]	N20W	45	**7.2**	**7.3**		1927?	~6?	Partial?
PDf	Paungde Fault	R	70	> 0.4[c]	N45W	45	**7.3**	**7.4**				
MBf	Minbya Fault	R	105	--	N20W	45	**7.5**	**7.7**				
LMf	Laymyo Fault	SS	175	~ 0.6[D]	N20W	90	**7.7**	**7.6**				
TCf	Thahtay Chaung fault	SS	>150	~ 2[D]	N15W	90	**7.6**	**7.6**				
Elf[C]	East-Limb fault (central section)	R	60	< 9[B]	N45W	45	**7.2**	**7.3**				
Elf[N]	East-Limb fault (northern section)	R	~120	< 9[B]	N25W	45	**7.5**	**7.8**				
Sdf	Sidoktaya Fault	R	70	< 9[B]	N25W	45	**7.3**	**7.4**				
PTf	Pato fault	R	30	--	N45W	45	**6.8**	**6.7**		1858?	7.7	Entire?
Pyf	Pyay fault	R	80	--	N15W	45	**7.3**	**7.5**				

Table 4. Proposed Major Seismic Structures of Myanmar and surrounding countries (Continued).

Code	Name	Type‡	Length (km)	Slip rate mm/yr	Strike	Dip	$M_{W\&C}$ [length]	M_{Blaser} [length]	$M_{Strasser}$ [length]	Last known earthquake		
										Year	M	Partial / Entire
Dahaka and Naga domains												
	Blinded Sunda megathrust (Dhaka section)	R	520	> 6[A]	N15W	5	8.3	**8.9**	**8.6**			
IPf	Churachandpur-Mao fault	SS	≧170	16[E]	N10E	90	**7.6**	**7.6**				
	Kabaw fault	R	~280	< 9[B]	N-S	45	**8.0**	**8.4**				
SM	St. Martin's Island	A	>16	1 to 3[F]	N10W	--	**6.3**	**6.3**				
Da	Dakshin Nila	A	40	1 to 3[F]	N30W	--	**6.9**	**7.0**				
M	Maheshkhali	A	50	1 to 3[F]	N20W	--	**7.0**	**7.1**		1999	5.2	Partial
J	Jaldi	A	40	1 to 3[F]	N20W	--	**6.9**	**7.0**				
P	Patiya	A	50	1 to 3[F]	N20W	--	**7.0**	**7.1**				
Si	Sitakund	A	65	1 to 3[F]	N25W	--	**7.2**	**7.3**				
SW	Sandwip	A	50	1 to 3[F]	N25W	--	**7.0**	**7.1**				
L	Lalmai	A	90	1 to 3[F]	N15W	--	**7.4**	**7.6**				
H	Habiganj	A	105	1 to 3[F]	N15W	--	**7.5**	**7.7**				
R	Rashidpur	A	62	1 to 3[F]	N5W	--	**7.2**	**7.3**		1918	7.5	Entire
S	Sylhet	A	22	1 to 3[F]	N70E	--	**6.5**	**6.5**				
F	Fenchunganj	A	45	1 to 3[F]	N10W	--	**7.0**	**7.1**				
Ha	Hararganj	A	80	1 to 3[F]	N15W	--	**7.3**	**7.5**				
Pa	Patharia	A	46	1 to 3[F]	N15W	--	**7.0**	**7.1**				
	Naga thrust fault	R	400	< 5[G]	N48E	23	8.2	**8.7**	**8.5**			

Table 4. Proposed Major Seismic Structures of Myanmar and surrounding countries (Continued).

Code	Name	Type[‡]	Length (km)	Slip rate mm/yr	Strike	Dip	$M_{W\&C}$ [length]	M_{Blaser} [length]	$M_{Strasser}$ [length]	Last known earthquake		
										Year	M	Partial / Entire
Sagaing domain												
	Bago	SS	>170	18[H]	N-S	90	**7.7**	**7.7**		1930	7.2	Partial
	Pyu	SS	130	18[H]	N10W	90	**7.5**	**7.5**		1930	7.3	Entire
	Nay Pyi Taw	SS	70	18[H]	N10W	90	**7.2**	**7.1**		1929	~7	Partial
	Meiktila	SS	220	18[H]	N5W	90	**7.8**	**7.9**		1839?		Entire?
	Sagaing	SS	180	18[H]	N-S	90	**7.7**	**7.7**		1946/1956	7.6/7.0	Partial
BMs	Ban Mauk	SS	150	<< 20[I]	N5E	90	**7.6**	**7.6**				
TMs	Tawma	SS	60	<< 20[I]	N-S	90	**7.2**	**7.0**		1991	6.9	Entire
IDs	In Daw	SS	80	~20[I]	N10E	90	**7.3**	**7.2**		1946	7.3	Entire
Mls	Mawlu	SS	90	~20[I]	N10E	90	**7.3**	**7.2**				
Szs	Shaduzup	SS	120	< 20[I]	N10E	90	**7.5**	**7.4**				
Kms	Kamaing	SS	170	~20[I]	N15W	90	**7.7**	**7.7**		1931	7.5	Partial?
Mgs	Mogang	SS	260	< 20[I]	N10W	90	**7.9**	**8.0**				
Shan-Sino domain												
DYf	Daying River Fault	SS + N	135	1.4 ± 0.2[J]	N50E	90	**7.5**	**7.5**		2007	5.5	Partial
	Huna Fault	SS + N	60	~1[K]	N70E	90	**7.2**	**7.0**				
	Manda fault	SS	> 30	~0.9[K]	E-W	90	**6.8**	**6.5**				
RLf	Ruili fault (Eastern)	SS + N	100	~2[L]	N50E	90	**7.4**	**7.3**				
RLf	Ruili fault (Western)	SS + N	40	< 2[L]	N50E	90	**7.0**	**6.7**				

Table 4. Proposed Major Seismic Structures of Myanmar and surrounding countries (Continued).

Code	Name	Type‡	Length (km)	Slip rate mm/yr	Strike	Dip	$M_{W\&C}$ [length]	M_{Blaser} [length]	$M_{Strasser}$ [length]	Last known earthquake		
										Year	M	Partial / Entire
NKf	Namkham fault	SS + N	60	?	N50E	90	**7.2**	**7.0**				
Wdf	Wanding fault	SS	170	~2[M]	N40E - E-W	90	**7.7**	**7.7**				
NTf	Nanting fault	SS	380	4.2[K]	N50E-N80E	90	**8.0**	**8.2**		1941	7	Partial
Lf	Lashio fault	SS	85	1.3[K]	E-W	90	**7.3**	**7.2**				
KMf	Kyaukme fault	SS	165	~0.5[K]	N80E	90	**7.6**	**7.7**				
Mf	Menglian fault	SS	120	~1[K]	N70E	90	**7.5**	**7.4**		1995	6.8	Partial
Jf	Jinghong fault	SS	110	~2.2[K]	N70E	90	**7.4**	**7.4**		1950	7.1	Partial
Wf	Wan Ha fualt	SS	140	~1[K]	N70E	90	**7.6**	**7.5**				
MXf	Mengxing fault	SS	180	~4.8K	N50E	90	**7.7**	**7.7**				
MNf	Nam Ma fault	SS	215	~2.6[K]	N70E	90	**7.8**	**7.8**		2011	6.8	Partial
MCf	Mae Chan fault	SS	310	~1[K]	N70E	90	**8.0**	**8.1**		2007	6.3	Partial
DBPf-V	Dien Bien Phu fault (Vietnam segment)	SS	150	2.5[K]	N10E	90	**7.6**	**7.6**		1935/1983	6.8/6.2	Partial
DBPf-M	Dien Bien Phu fault (Mekong segment)	SS	110	2.5[K]	N45E	90	**7.4**	**7.4**				
LKf	Loi Kwi fault	SS	50	~0.8[K]	N25W	90	**7.1**	**6.9**		1992	6.1	Partial
LLf	Loi Lung fault	SS	95	~0.7[K]	N20W	90	**7.4**	**7.3**				

Table 4. Proposed Major Seismic Structures of Myanmar and surrounding countries (Continued).

Code	Name	Type‡	Length (km)	Slip rate mm/yr	Strike	Dip	$M_{W\&C}$ [length]	M_{Blaser} [length]	$M_{Strasser}$ [length]	Last known earthquake		
										Year	M	Partial / Entire
KKF	Kyaukkyan fault (Myint Nge segment)	SS	160	~1[K]	N10W	90	**7.6**	**7.6**		1912	7.7	Entire
PYf	Pingdaya fault	SS	50	--	N10E	60	**7.1**	**6.9**				
TGf	Taunggyi fault	SS	45	--	N10E	60	**7.0**	**6.8**				
KKF	Kyaukkyan fault (Salween segment)	SS	480	~1[K]	N10W	90	**8.2**	**8.4**				
WLSf	Wuliang Shan fault zone	SS	105[#]	> 1.2[K]	N10W-N50W	90	**7.4**	**7.4**		2007	6.1	Partial
LCf	Lancang fault	SS	200	> 3.4[K]	N50W	90	**7.7**	**7.8**		1988	7	Partial
MPf	Mae Ping fault	SS	100	~0.5[K]	N45W	90	**7.4**	**7.3**				

‡ R: Reverse fault; N: Normal fault; SS: Strike-slip fault; A: Anticline with unknown type of blind faulting.
# The longest dextral fault trace within the Wuliang Shan fault zone.
A: The rate is estimated from the Indian, the Burma and the Sunda plate motion vectors (See Appendix-1 Table S1).
B: Inferred from the Socquet et al., 2006.
C: We assume the age of 30-m high uplift surface is ~100 ka.
D: We assume the strike slip begin to active in 5 Ma.
E: The rate is from Gahalaut et al., 2013.
F: speculate from the anticline uplift rates in this region.
G: speculate from the uncertainity of geodetic analysis.
H: Slip rate is from Vigny et al., 2003.
I: Slip rate is from Maurin et al., 2010.
J: Average fault slip rate is from Chang et al., 2011.
K: Rate = maximum offset / 5 Ma. We assume the fault slip began in 5 Ma, based on the regional tectonic history.
L: Average fault slip rate is from Huang et al., 2010.
M: Average fault slip rate is from Chang et al., 2012.